



Industria Textilă

ISSN 1222-5347 (179-238)

4/2014

Revistă cotate ISI și inclusă în Master Journal List a Institutului pentru Știința Informării din Philadelphia – S.U.A., începând cu vol. 58, nr. 1/2007/

ISI rated magazine, included in the ISI Master Journal List of the Institute of Science Information, Philadelphia, USA, starting with vol. 58, no. 1/2007

Editată în 6 nr./an, indexată și recenzată în:

Edited in 6 issues per year, indexed and abstracted in:

Science Citation Index Expanded (SciSearch®), Materials Science Citation Index®, Journal Citation Reports/Science Edition, World Textile Abstracts, Chemical Abstracts, VINITI, Scopus, Toga FIZ tehnik

COLEGIUL DE REDACȚIE:

Dr. ing. EMILIA VISILEANU
cerc. șt. pr. I – EDITOR ȘEF
Institutul Național de Cercetare-Dezvoltare
pentru Textile și Pielărie – București

Dr. ing. CARMEN GHIȚULEASA
cerc. șt. pr. I
Institutul Național de Cercetare-Dezvoltare
pentru Textile și Pielărie – București

Prof. dr. GELU ONOSE
cerc. șt. pr. I
Universitatea de Medicină și Farmacie
„Carol Davila” – București

Prof. dr. GEBHARDT RAINER
Saxon Textile Research Institute – Germania

Prof. dr. ing. CRIȘAN POPESCU
Institutul German de Cercetare a Lăinii – Aachen

Prof. dr. ing. PADMA S. VANKAR
Facility for Ecological and Analytical Testing
Indian Institute of Technology – India

Prof. dr. SEYED A. HOSSEINI RAVANDI
Isfahan University of Technology – Iran

Dr. FRANK MEISTER
TITK – Germania

Prof. dr. ing. ERHAN ÖNER
Marmara University – Istanbul

Dr. ing. FAMING WANG
Soochow University – China
University of Alberta – Canada

Prof. univ. dr. ing. CARMEN LOGHIN
Universitatea Tehnică „Ghe. Asachi” – Iași

Ing. MARIANA VOICU
Ministerul Economiei

Prof. dr.
LUCIAN CONSTANTIN HANGANU
Universitatea Tehnică „Ghe. Asachi” – Iași

Prof. ing. ARISTIDE DODU
cerc. șt. pr. I
Membru de onoare al Academiei de Științe
Tehnice din România

Prof. univ. dr. DOINA I. POPESCU
Academia de Studii Economice – București

KADİR BİLİŞİK

Studiul comportamentului la alunecare și aderență al țesăturilor,
folosind metoda rezistenței la smulgere 181–189

**DAWID STAWSKI, FRANK SIMON, DOROTA ZIELIŃSKA,
STEFAN POŁOWIŃSKI, MICHAŁ PUCHALSKI**
Aplicarea tehnologiei de depunere strat cu strat pe materiale
textile tricotate 190–199

SI CHEN, HAI-RU LONG
Studiul proprietăților de comprimare ale compozitelor poliuretanic,
din tricouri din urzeală distanțate, utilizate ca materiale de amortizare.
Partea I. Experiment 200–205

**ANDREI SEBASTIAN ARDELEANU, EFTALEA CĂRPUȘ, RĂZVAN SCARLAT,
EMILIA VISILEANU, CARMEN MIHAI, ALEXANDRA ENE**
Estimarea proprietăților ESD ale materialelor textile cu structură bistrat 206–212

**ANGELA CEREMPEI, ABRAMIUC DANKO, CRIȘAN POPESCU,
RODICA MUREȘAN, AUGUSTIN MUREȘAN**
Materiale textile tratate cu emulsie antimicrobiană de îngrijire a pielii,
optimizată prin modelare matematică 213–219

**NEBOJŠA RISTIĆ, ANITA TARBUK, ANA MARIJA GRANCARIĆ,
IVANKA RISTIĆ, MIODRAG ŠMELCEROVIĆ**
Fenomene de interfață și capacitatea de vopsire cu coloranți reactivi
a bumbacului cationizat 220–227

B. YEŞİM BÜYÜKAKINCI, NİHAL SÖKMEN, ERHAN ÖNER
Îmbunătățirea capacității de vopsire a fibrelor poliolefinice
prin încălzirea cu microunde 228–232

PEI CHU, REN-CHENG TANG
Vopsirea cu coloranți acizi și cationici a amestecului fibros
din nailon și nailon modificat chimic 233–238

DOCUMENTARE 189, 219

Recunoscută în România, în domeniul Științelor ingineresti, de către
Consiliul Național al Cercetării Științifice din Învățământul Superior
(C.N.C.S.I.S.), în grupa A /

Acknowledged in Romania, in the engineering sciences domain,
by the National Council of the Scientific Research from the Higher Education
(CNCSIS), in group A

Contents

KADİR BİLİŞİK	Analysis and stick-slip properties of woven fabric in pull-out method	181
IDAWID STAWSKI FRANK SIMON DOROTA ZIELIŃSKA STEFAN POŁOWIŃSKI MICHAŁ PUCHALSKI	Application of the layer-by-layer technique for knitted fabrics	190
SI CHEN HAI-RU LONG	Investigation on compression properties of polyurethane-based warp-knitted spacer fabric composites for cushioning applications. Part I. Experiment	200
ANDREI SEBASTIAN ARDELEANU EFTALEA CĂRPUȘ RĂZVAN SCARLAT EMILIA VISILEANU CARMEN MIHAI ALEXANDRA ENE	ESD properties assessment of fabrics with bilayer structure	206
ANGELA CEREMPEI ABRAMIUC DANKO CRIȘAN POPESCU RODICA MUREȘAN AUGUSTIN MUREȘAN	Textile materials treated with antimicrobial skin care emulsion optimized by mathematical modelling	213
NEBOJŠA RISTIĆ ANITA TARBUK ANA MARIJA GRANCARIĆ IVANKA RISTIĆ MIODRAG ŠMELCEROVIĆ	Interface phenomena and dyeability with reactive dyes of cationized cotton	220
B. YEŞİM BÜYÜKAKINCI NİHAL SÖKMEN ERHAN ÖNER	Improving the dyeability of polyolefin fibres by microwave heating	228
PEI CHU REN-CHENG TANG	Acid and cationic dyeing of nylon/cationic dyeable nylon mixture	233
DOCUMENTARE	Documentation	189, 219

Referenții articolelor publicate în acest număr al revistei **INDUSTRIA TEXTILĂ**/
Scientific reviewers for the papers published in this number:

Cerc. șt. gr. II dr. ing. / *Senior researcher dr. eng.* IULIANA DUMITRESCU
Cerc. șt. gr. III dr. ing. / *Senior researcher dr. eng.* ALINA POPESCU
Cerc. șt. gr. III dr. ing. / *Senior researcher dr. eng.* ANA-MARIA MOCIOIU
Cerc. șt. gr. III ing. / *Senior researcher eng.* DOINA TOMA
Ing. / *Eng.* CONSTANȚA HULEA

COLECTIVUL DE REDACȚIE

Redactor șef: Marius Iordănescu

Redactor: Elena Bălțătescu

Grafician: Florin Prisecaru

e-mail: marius.iordanescu@certex.ro

Analysis and stick-slip properties of woven fabric in pull-out method

KADIR BİLİŞİK

REZUMAT – ABSTRACT

Studiul comportamentului la alunecare și aderență al țesăturilor, folosind metoda rezistenței la smulgere

În lucrare sunt analizate forțele de frecare la alunecare și de aderență ale țesăturilor paraaramidice înguste. În acest scop, a fost efectuat un test de rezistență la smulgere pentru țesăturile paraaramidice Twaron®. S-a constatat că forța de frecare la alunecare și aderența, precum și forța de retragere cumulativă depind de desimea țesăturii, de numărul de fire trase din țesătură și de dimensiunile mostrei de țesătură. În urma testului de rezistență la smulgere, s-a evidențiat faptul că forțele de frecare la alunecare și de aderență sunt mai mari în cazul firelor multiple, decât în cazul firelor simple. Totodată, folosind testele de rezistență la smulgere ale firelor simple și multiple, s-a observat că forțele de frecare la alunecare și de aderență au fost, în general, mai mari în cazul țesăturilor înguste CT 716, cu desime mare, decât în cazul țesăturilor înguste CT 714, cu desime mică. Pe de altă parte, s-a demonstrat că nivelul forțelor de frecare la alunecare și de aderență este influențat de numărul punctelor de legătură din țesătură, iar forța de retragere cumulativă depinde de modul de reacție a structurii țesăturii.

Cuvinte-cheie: fire simple, fire multiple, rezistență la smulgere, forță de frecare la alunecare, aderență, forță de retragere cumulativă, punct de legătură, dispozitiv de fixare pentru testul rezistenței la smulgere

Analysis and stick-slip properties of woven fabric in pull-out method

The study was conducted to understand the stick-slip properties of narrow para-aramid woven fabrics. For this reason, pull-out test was conducted on para-aramid Twaron® woven fabrics. It was found that stick-slip force and accumulative retraction force depend on fabric density, the number of pulled ends in the fabric and fabric sample dimensions. Stick-slip forces in the multiple yarn pull-out test were higher than those of the single yarn pull-out test. Stick-slip forces in single and multiple yarn pull-out tests in the dense narrow CT 716 fabric were generally higher than those of the loose narrow CT 714 fabric. On the other hand, the amount of stick-slip force was related to the number of interlacement points in the fabric whereas the amount of accumulative retraction force was related to fabric structural response.

Key-words: single yarn, multiple yarn, pull-outs, stick-slip force, accumulative retraction force, interlacement point, pull-out fixture

Ballistic fabrics with higher pull-out force have been shown to perform favourably in impact loading [1]. Yarn pull-out was defined as one end of the yarn pulled out from the fabric structure by the motion of the penetrator. The force required to pull the yarn from the fabric structure was the sum of the frictional forces between the yarn sets at all intersecting points [1], [2]. The three distinct modes of fabric failure observed in slow penetration tests were yarn pull-out, local yarn rupture and remote yarn failure [3], [4]. Ballistic performance depends upon friction, material properties such as elastic modulus and strength of the yarn, fabric structure and multiple plies and far field boundary conditions [5], [6]. The tribological behaviour of woven fabric made from yarns of different linear densities was compared with the friction properties of their constituent yarns using different surface treatments. It was found that fabrics with high friction and the lowest effective moduli dissipated larger amounts of energy relative to fabrics with lower friction [7].

The fabric maximum pull-out forces in para-aramid fabric structures have been investigated with regards to their ballistic performance. It was found that stitched ballistic layered structures showed high pull-

out force which enhanced the ballistic resistance of the structures [8]. The fabric displacement stage and crimp extension stage in single and multiple yarn ends pull-out have been investigated. It was concluded that the fabric displacement stage could be utilized to determine fabric shear behaviour and the crimp extension stage could be used to explain the fabric failure under tensile loads [9]. The stick-slip phenomenon has been identified in nature and textile materials [10], and even everyday life. The stick-slip phenomenon was considered during single and multiple yarn ends pull-out in fabric [9]. As seen in literature, the friction in the stick-slip stage of pull-out in fabric structure was an important energy absorption mechanism for soft ballistic [11]. Therefore, the aim of this study was to understand the behaviour of the stick-slip stage of para-aramid single woven fabric under single and multiple yarn pull-outs.

EXPERIMENTAL PART

Para-aramid fibre and woven fabrics

The woven fabric was constructed with para-aramid type of fibres (Twaron® of Teijin, Japan). The fibre and fabric properties are presented in table 1 and table 2. Two types of fabrics were used. These were

Table 1

PROPERTIES OF HIGH MODULUS PARA-ARAMID TWARON FIBRES						
Fibre type	Fibre diameter, μm	Fibre density, g/cm^3	Tensile strength, GPa	Tensile modulus, GPa	Elongation at break, %	Decomposition point, $^{\circ}\text{C}$
Twaron CT [®] , Teijin	12	1.45	3.2	115	2.9	550

Table 2

PROPERTIES OF HIGH MODULUS PARA-ARAMID TWARON FABRICS										
Fabric type	Weave type	Yarn linear density, tex		Density/ per cm		Weight, g/m^2	Crimp, %		Thickness, mm	Treatment
		warp	filling	warp	filling		warp	filling		
Twaron CT [®] 714	Plain	110	110	8.5	8.5	190	1.38	1.98	0.30	Water repellent
Twaron CT [®] 716	Plain	110	110	12.2	12.2	280	6.36	1.96	0.40	Water repellent

Twaron CT[®] 716 (CT 716) and Twaron CT[®] 714 (CT 714). They were both plain weave and the warp and filling yarn linear densities were 110 tex. The warp and filling densities of the CT 716 and CT 714 fabrics were 12.2 ends/cm and 8.5 ends/cm, respectively. The weights of the fabric unit areas were 280 g/m^2 and 190 g/m^2 , respectively. Water repellent treatment was also applied to both fabrics. Crimp measurement was performed using a Tautex digital instrument (James H. Heal Co., UK) according to ISO 7211-3. Fabric thickness measurement was performed using an R&B cloth thickness tester (James H. Heal Co., UK) based on ISO 5084. Fabric weight measurement was performed based on ISO 6348. The fabric's initial angle between warp and weft was measured by an optical microscope (Olympus SZ61-TR).

Pull-out tests

Pull-out tests were conducted to determine the yarn-to-yarn friction on single or multiple yarn ends in the frayed edge of the plain fabric structure. For this reason, a pull-out fixture was developed. Figure 1 shows the fixture and the pull-out test carried out in the testing instrument. Fabric from both edges was clamped. In this set-up, the fabric stick-slip stage was defined as "the end of one yarn set (either warp or weft) passes through from each of the consecutive intersecting points in the fabric during single or multiple yarn pull-out after the maximum pull-out force stage completed". Figure 2 shows the schematic views of the fixture and pull-out test during the stick-slip stage. In addition, "the pulled yarn end in the fabric is released from each yarn which is normal to the pulled yarn direction in where the response of the remaining part of the pulled yarn in the fabric is defined as the accumulative retraction force". Fabric crimp interchange during the pull-out test was ignored. The residual tension on the fabric due to clamped fabric edges was also ignored. The yarn slippages and yarn flattening

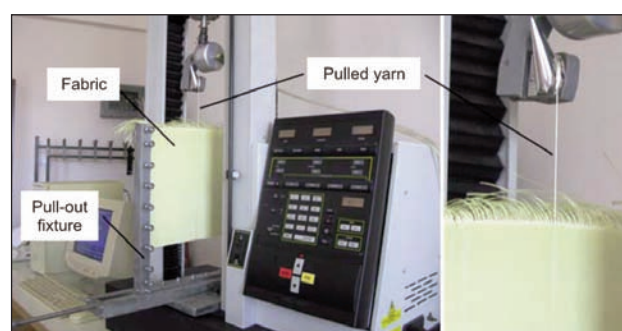


Fig. 1. Pull-out fixture with fabric on the tensile testing instruments

in warp and weft directions in the fabric interlacement regions were not considered for simplification purposes. The testing instrument used was the Instron 4411 and the testing speed was 100 mm/minute. Fabric dimensions for performing the pull-out test were prepared as a fabric width of 110 mm for the total sample dimension, and 50 mm for the sample dimension in the fixture. Fabric sample lengths ranged from 50 mm, 150 mm to 300 mm for warp directional pull-out test, whereas fabric sample lengths ranged from 50 mm, 100 mm to 300 mm for weft directional pull-out test. The pull-out direction was in the warp and weft directions of the fabrics. The frayed yarn length of the sample was 150 mm and the total edge length holding the sample in the fixture edge was 60 mm. In the single yarn pull-out test, only one yarn was pulled from the middle of the fabric sample. In the multiple yarn pull-out test, 2, 3, 4 and 5 yarns were pulled from the middle of each fabric sample. The Instron 4411 pull head draws individual yarn ends from the frayed edge of the single fabric. The force-displacement curve data obtained from single and multiple pull-outs were analyzed by MATLAB based algorithm [12]. Using the algorithm, the stick-slip forces and accumulative retraction forces were calculated.

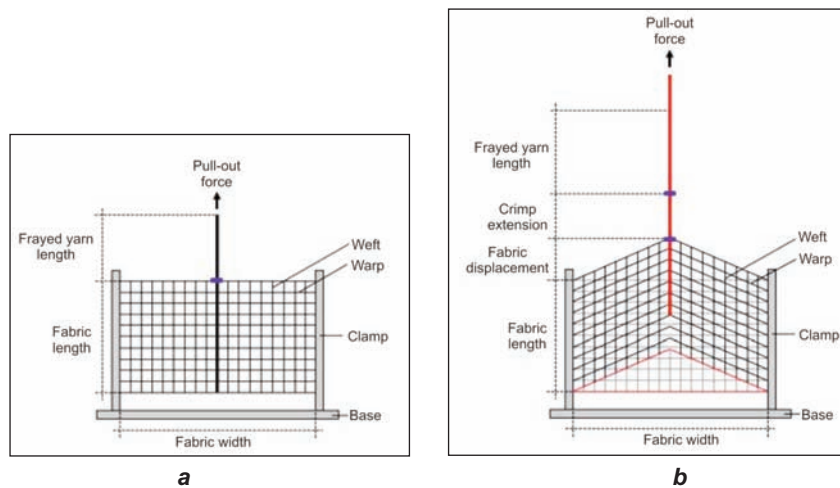


Fig. 2. Schematic views of the fabric and yarn positions measured during pull-out test: a – fabric position before pull-out test; b – stick-slip stage of fabric position during pull-out test

RESULTS AND DISCUSSIONS

Stick-slip stage in the yarn pull-out

Single and multiple yarn pull-out tests on CT 716 (dense fabric) and CT 714 (loose fabric) samples were carried out. Single and multiple yarn pull-out force-displacement curves were obtained. In the yarn pull-out force-displacement curve, the stick-slip stages of the kinetic friction part, which was from the beginning of the maximum pull-out force to the end of the yarn pull-out test, were considered. The curve in the kinetic region has one maximum and one minimum for each two crossing points where from maximum to minimum (one minima) is called stick-slip and from minimum to maximum (one maxima) is called accumulative retraction force due to fabric structure. Figure 3 shows the stick-slip stages of the single yarn pull-out force-displacement curve in where the 6 meso-cells of para-aramid fabric in the bottom of the fabric edge (fig. 3 a) and at the centre of the fabric (fig. 3 b) were considered to investigate the stick-slip stage of the single and multiple yarn pull-out force-displacements. The end of the stick-slip stage at the top of the fabric edge is also shown in figure 3 c. One meso cell is composed of one stick region and one slip region as shown in figure 4. In the stick

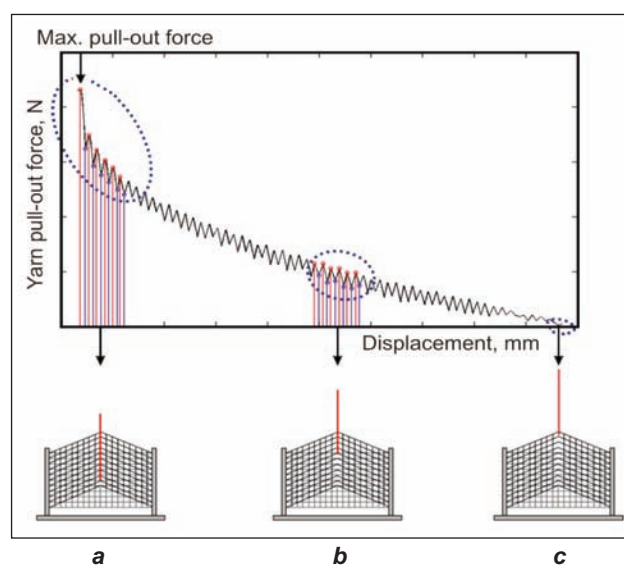


Fig. 3. Stick-slip stage of single yarn pull-out force-displacement curves of para-aramid fabric: a – the number of the meso-cells in the beginning of stick-slip stage at the bottom of the fabric edge; b – the number of meso-cells in the middle of the stick-slip stage at the centre of the fabric; c – the end of the stick-slip stage at the top of the fabric edge (fabric width: 50 mm, fabric length: 300 mm)

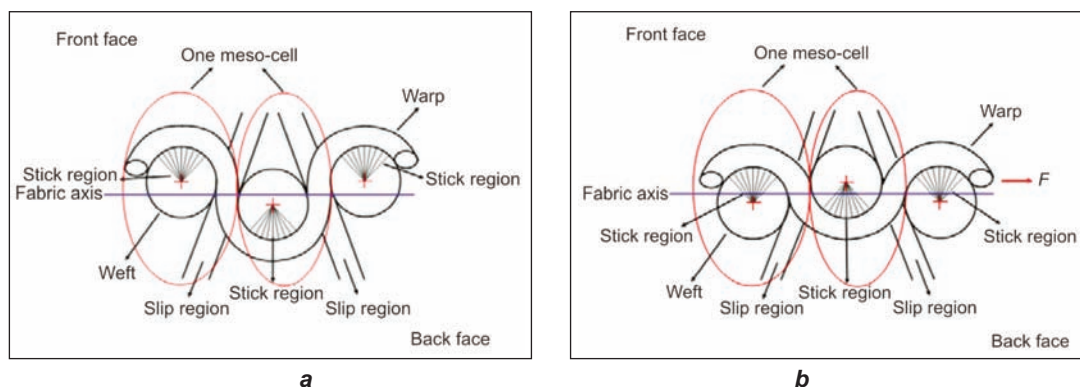


Fig. 4. The schematic views of slip-stick stage in the meso-cells of para-aramid fabric structures: a – before pull-out force is applied; b – after pull-out force is applied

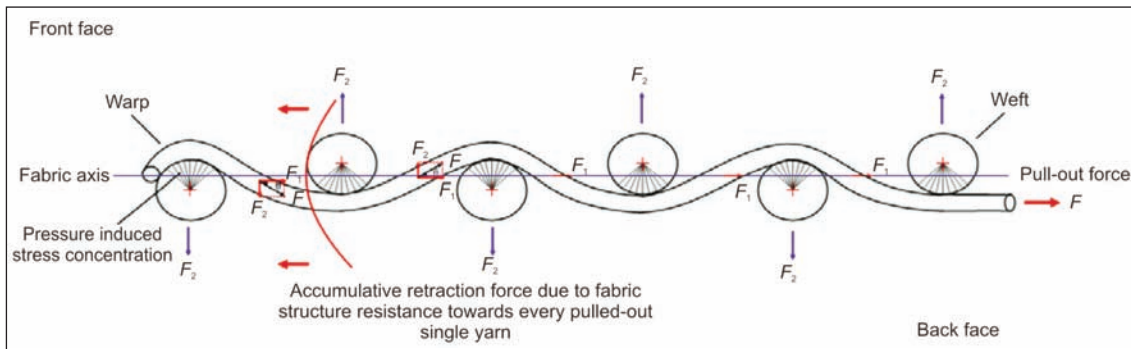


Fig. 5. The schematical views of pull-out force components in slip-stick stage of the para-aramid fabric

region, there is pressure between the warp and weft yarns either in the front face or back face of the fabric during the pulling of the warp or weft yarns as shown schematically in figure 5. In the slip region, there is pressure between the warp and weft yarns where the warp is crossed during the pulling of the warp yarn as shown in figure 5. The amount of pressure is proportional, as given in the following relationships (1) and (2):

$$F_1 = \cos \theta \cdot F \quad (1)$$

$$F_2 = \sin \theta \cdot F \quad (2)$$

where:

F is the pull-out force;

θ – the initial crossing angle;

F_1 – the in-plane direction pull-out force component;

F_2 – the out-of-plane direction pull-out force component.

The initial crossing angle (θ) depends on directional fabric density and directional crimp ratio. Under the pull-out force on warp yarn, fabric displacement and crimp extension stages occurred first [9]. This causes straightening of the pulled warp yarn and θ is decreased from its initial value. The measured average initial θ values for CT 716 and CT 714 fabrics were 10.37 degree and 4.41 degree, respectively. If we use equations (1) and (2), we get:

$$F_1 = 0.984 \cdot F \text{ and } F_2 = 0.175 \cdot F, \text{ for CT 716} \quad (3)$$

$$F_1 = 0.996 \cdot F \text{ and } F_2 = 0.087 \cdot F, \text{ for CT 714} \quad (4)$$

As seen in the relations, the out-of-plane direction pull-out force F_2 was very small and the in-plane direction pull-out force F_1 was very high for both fabric structures. In the stick regions, the in-plane direction pull-out force component F_1 is most likely to main force to generate pressure on the yarn in the fabric structure. In slip regions, out-of-plane direction pull-out force component F_2 is most likely to force to generate pressure on the crossing part of the yarn in the fabric structure as shown in figure 4 and figure 5. However, more research is required to define the yarn pressure in the slip region of the fabric during pull-out.

When we look at the meso-cells in the stick-slip stages of the single yarn pull-out force-displacement

curve in figure 3, there is an exponential function which has periodic decrease and increase lines. It is most likely that the decreasing line corresponds to each stick-slip region ($S_k - S_p$) whereas the increasing line corresponds to each accumulative retraction force by fabric structure, A_r . After the maximum pull-out force stage was completed, the first decreasing line occurred due to the 1st yarn stick-slip region. When the 1st yarn (warp) was released from the fabric structure, the first increasing line occurred due to accumulative retraction force by fabric structure coming from the remaining 5 yarns in the end of the pulled yarn (weft) as shown in figure 5. When the pull-out phenomena was repeated, the second decreasing line occurred due to the 2nd yarn stick-slip region. Immediately afterwards, the 2nd yarn was released from the fabric structure and the second increasing line occurred due to accumulative retraction force by the fabric structure coming from the remaining 4 yarns in the end of the pulled yarn. This phenomenon was repeated until the 6th yarn was released from the pulled yarn.

Stick-slip force in single yarn pull-out

The warp and weft directional stick-slip force and accumulative retraction force obtained from the single yarn pull-out force-displacement curve of CT 716 and CT 714 fabrics for 6 meso-cells. Figure 6 a, b shows the relationship between warp directional stick-slip force and the number of meso-cells in the single yarn pull-out test of CT 716 and CT 714 fabrics, respectively. Figure 7 a, b shows the relationship between weft directional stick-slip force and the number of meso-cells in the single yarn pull-out test of CT 716 and CT 714 fabrics, respectively.

As seen in figures 6 a, b and 7 a, b, the warp and weft directional single yarn stick-slip forces in the MC-1 to the MC-6 of CT 716 and CT 714 fabrics in fabric edges decreased for various fabric lengths, whereas no significant differences were obtained in the MC-1 to the MC-6 of CT 716 and CT 714 fabrics in fabric centres. The warp and weft directional single yarn stick-slip forces in the MC-1 to MC-6 of CT 716 and CT 714 fabrics in fabric edge generally slightly increased when the fabric length increased due to the increasing number of crossing points. The warp

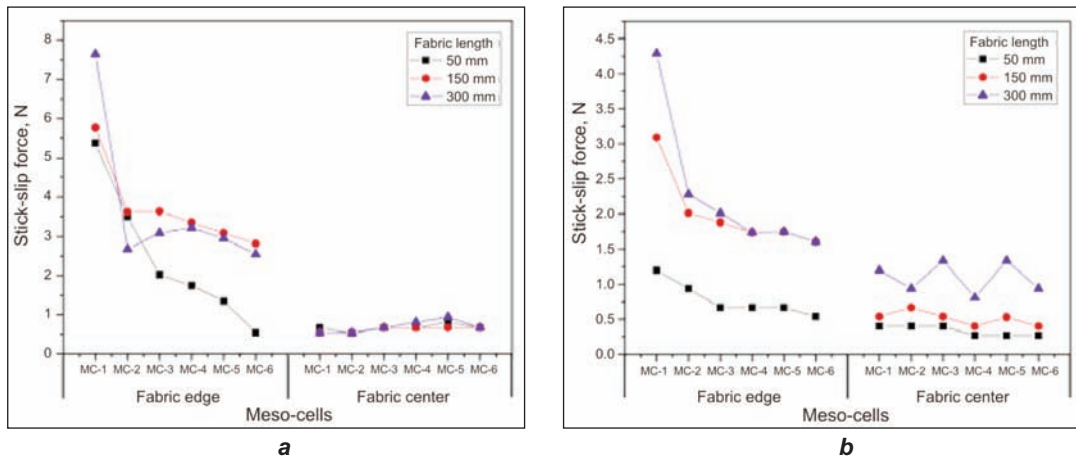


Fig. 6. Relationship between warp directional stick-slip force and the number of meso-cells in single yarn pull-out test of para-aramid fabric in the fabric edge and centre regions: a – CT 716 woven fabric; b – CT 714 woven fabric

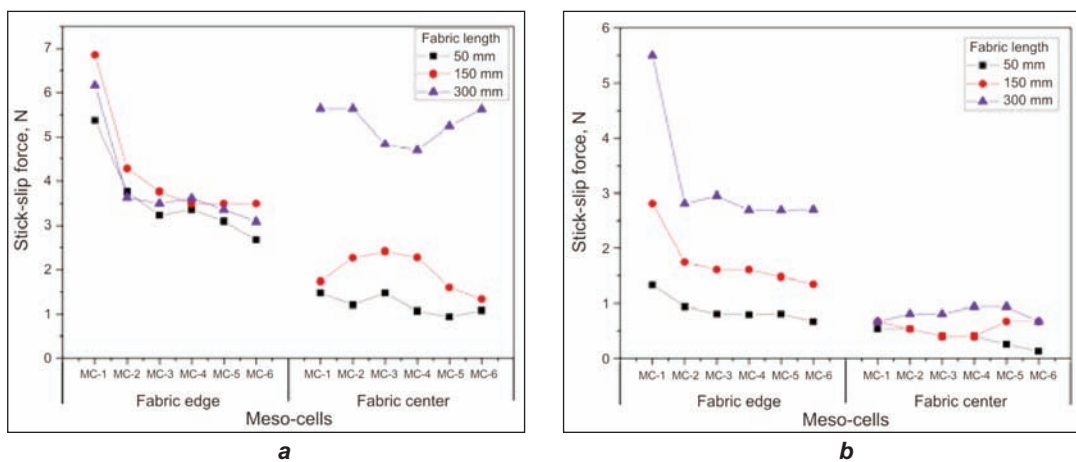


Fig. 7. Relationship between weft directional stick-slip force and the number of meso-cells in single yarn pull-out test of para-aramid fabric in the fabric edge and centre regions: a – CT 716 woven fabric; b – CT 714 woven fabric

and weft directional single yarn stick-slip forces in the MC-1 of CT 716 and CT 714 fabrics in the fabric edge were higher than those of the MC-6 of CT 716 and CT 714 fabrics due to the remaining crossing points in the fabric during pull-out. In addition, the warp and weft directional single yarn stick-slip forces in the MC-1 to MC-6 of CT 716 and CT 714 fabrics in the fabric edge were higher than those of the fabric centre. On the other hand, the warp and weft directional single yarn stick-slip forces in CT 716 fabrics were higher than those of CT 714 fabrics due to fabric density. Fabric length considerably affected the warp and weft directional stick-slip forces of dense CT 716 fabric and loose CT 714 fabric due to the increasing number of crossing points. The position of the meso-cells also affected the warp and weft directional stick-slip forces of CT 716 and CT 714 fabrics.

Accumulative retraction force due to fabric structure in single yarn pull-out

The accumulative retraction forces obtained from the warp and weft directional single yarn pull-out force-

displacement curves of CT 716 and CT 714 fabrics for 6 meso-cells in the fabric edge and fabric centre. Figure 8 a, b shows the relationship between warp directional accumulative retraction forces due to fabric structure and the number of meso-cells in the single yarn pull-out test of CT 716 and CT 714 fabrics, respectively. Figure 9 a, b shows the relationship between weft directional accumulative retraction forces due to fabric structure and the number of meso-cells in the single yarn pull-out test of CT 716 and CT 714 fabrics, respectively.

Although we did not find any significant differences in the warp and weft directional single yarn accumulative retraction forces of the MC-1 to MC-6 of various fabric lengths of CT 716 and CT 714 fabrics in the fabric edge and fabric centre regions, the weft directional single yarn accumulative retraction forces of CT 716 and CT 714 fabrics were slightly higher than those of the warp directional single yarn accumulative retraction forces of CT 716 and CT 714 fabrics. On the other hand, the warp and weft directional single yarn accumulative retraction forces of CT 716 and

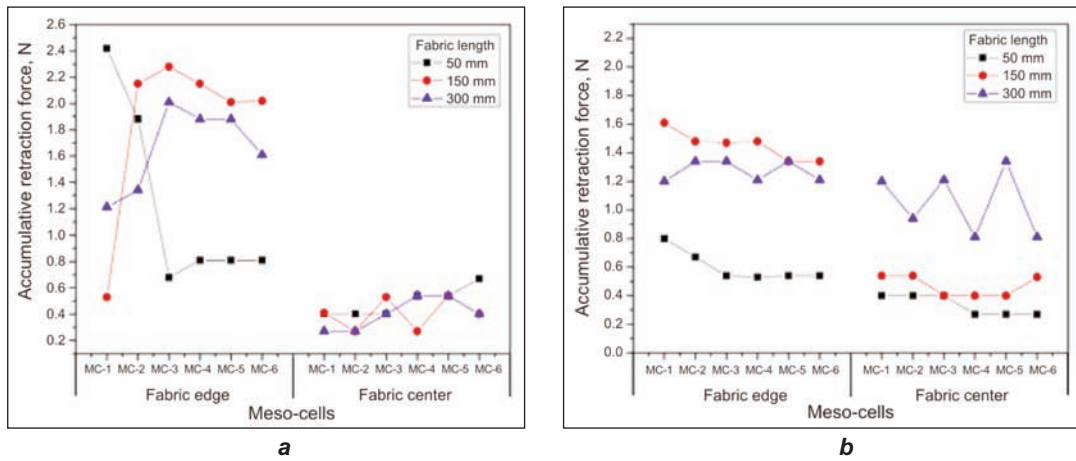


Fig. 8. Relationship between warp directional accumulative retraction force due to fabric structure and the number of meso-cells in single yarn pull-out test of para-aramid fabric in the fabric edge and centre regions: a – CT 716 woven fabric; b – CT 714 woven fabric

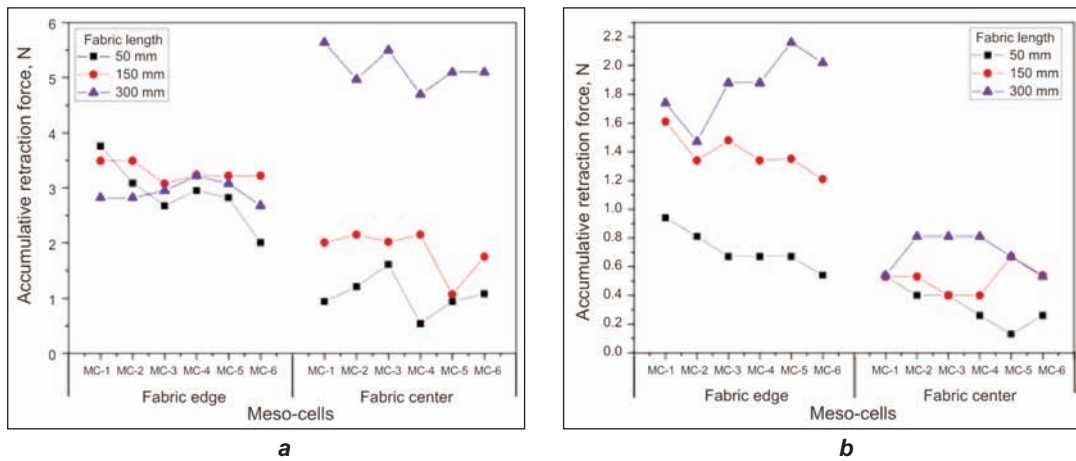


Fig. 9. Relationship between weft directional accumulative retraction force due to fabric structure and the number of meso-cells in single yarn pull-out test of para-aramid fabric in the fabric edge and centre regions: a – CT 716 woven fabric; b – CT 714 woven fabric

CT 714 fabrics in the fabric edge regions were higher than those of CT 716 and CT 714 fabrics in the fabric centre regions. In addition, the warp and weft directional single yarn accumulative retraction forces in CT 716 fabric were slightly higher than those of the CT 714 due to fabric density.

Stick-slip force in multiple yarn pull-out

The warp and weft directional stick-slip force and accumulative retraction force obtained from the multiple yarn pull-out force-displacement curves of CT 716 and CT 714 fabrics for 6 meso-cells. Figure 10 a, b shows the relationship between warp directional stick-slip force and the number of meso-cells in the multiple yarn pull-out test of CT 716 and CT 714 fabrics, respectively. Figure 11 a, b shows the relationship between weft directional stick-slip force and the number of meso-cells in the multiple yarn pull-out test of CT 716 and CT 714 fabrics, respectively.

As seen in figure 10 a, b and figure 11 a, b, the warp and weft directional multiple yarn stick-slip force in

the MC-1 to the MC-6 of CT 716 and CT 714 fabrics in fabric edges decreased sharply for various fabric lengths whereas, no significant differences were obtained in the MC-1 to the MC-6 of all fabric lengths in CT 716 and CT 714 fabrics in fabric centres. The warp and weft directional multiple yarn stick-slip force in the MC-1 of CT 716 and CT 714 fabrics in fabric edge was the highest, but the warp and weft directional multiple yarn stick-slip force in the MC-6 of CT 716 and CT 714 in fabric edge was the lowest. In addition, the warp and weft directional multiple yarn stick-slip forces in the MC-1 to MC-6 of CT 716 and CT 714 fabrics in the fabric edge were higher than those of the fabric centre. On the other hand, the warp and weft directional multiple yarn stick-slip forces in CT 716 fabric were higher than those of CT 714 fabric due to fabric density. The number of the pull-out ends and the position of the meso-cells affected the stick-slip forces of CT 716 and CT 714 fabrics. Also, fabric length considerably affected the multiple yarn stick-slip forces of the CT 716 and CT 714 fabrics.

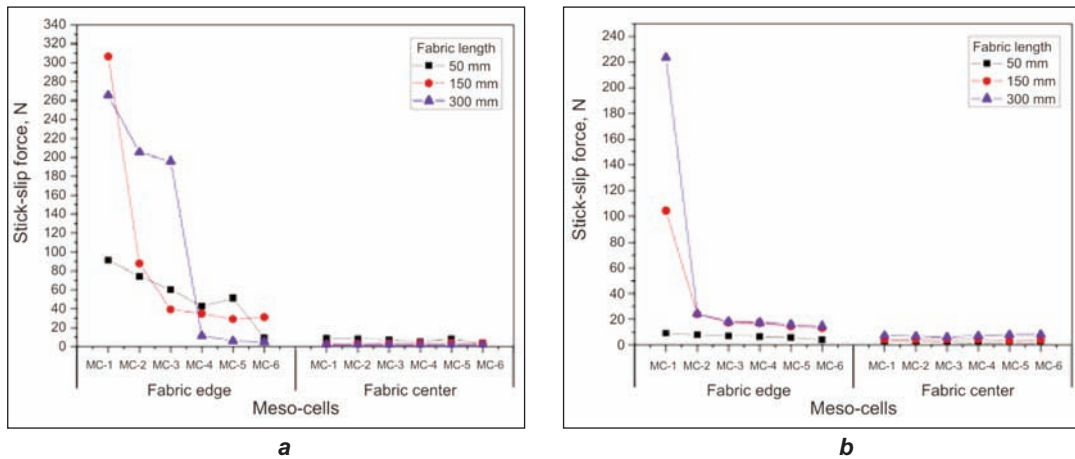


Fig. 10. Relationship between warp directional stick-slip force and the number of meso-cells in multiple yarn pull-out test of para-aramid fabric: *a* – CT 716 woven fabric (pulled yarn ends: 4); *b* – CT 714 woven fabric (pulled yarn ends: 5)

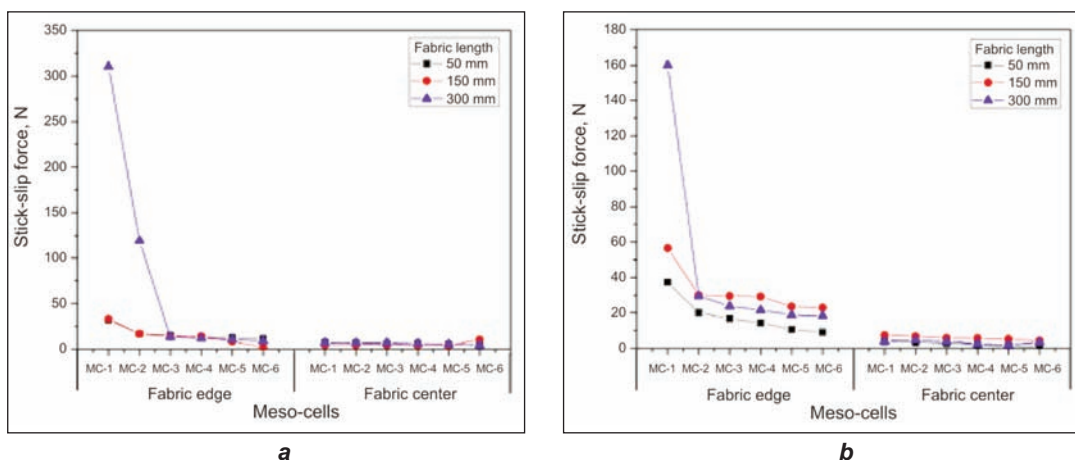


Fig. 11. Relationship between weft directional stick-slip force and the number of meso-cells in multiple yarn pull-out test of para-aramid fabric: *a* – CT716 woven fabric (pulled yarn ends: 4); *b* – CT714 woven fabric (pulled yarn ends: 5)

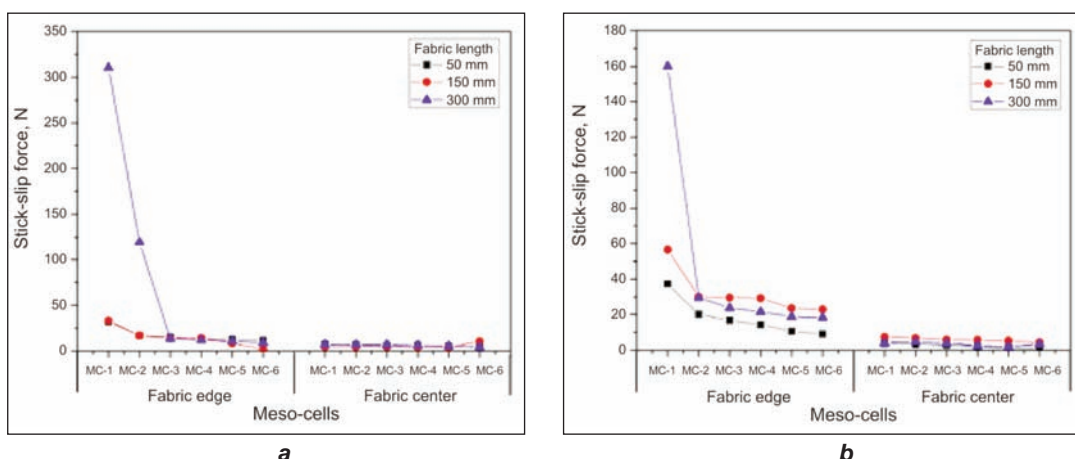


Fig. 12. Relationship between warp directional accumulative retraction force due to fabric structure and the number of meso-cells in multiple yarn pull-out test of para-aramid fabric: *a* – CT716 woven fabric (pulled yarn ends: 4); *b* – CT714 woven fabric (pulled yarn ends: 5)

Accumulative retraction force due to fabric structure in multiple yarn pull-out

The accumulative retraction forces obtained from the warp and weft directional multiple yarn pull-out force-

displacement curves of CT 716 and CT 714 fabrics for 6 meso-cells in the fabric edge and fabric centre. Figure 12 *a, b* shows the relationship between warp directional accumulative retraction forces due to fabric

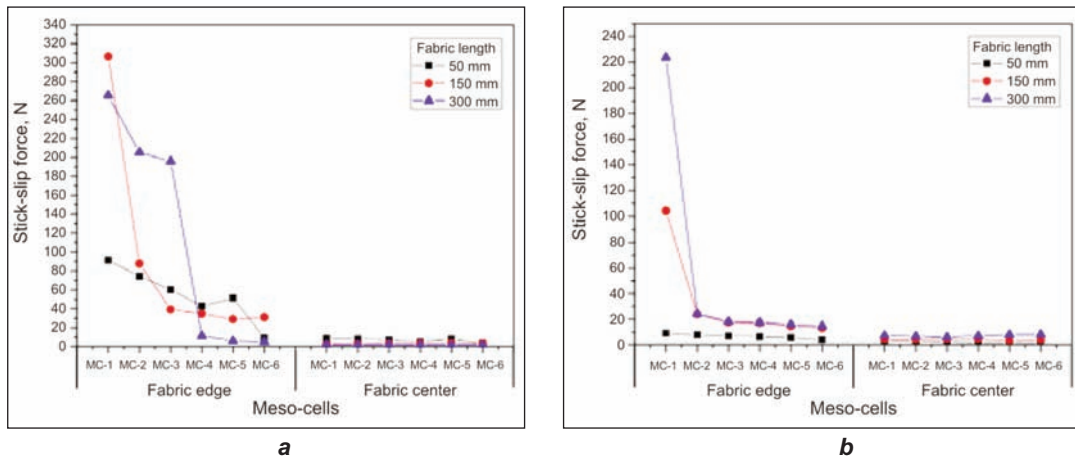


Fig. 13. Relationship between weft directional accumulative retraction force due to fabric structure and the number of meso-cells in multiple yarn pull-out test of para-aramid fabric: a – CT716 woven fabric (pulled yarn ends: 4); b – CT714 woven fabric (pulled yarn ends: 5)

structure and the number of meso-cells in the multiple yarn pull-out test of CT 716 and CT 714 fabrics, respectively. Figure 13 a, b shows the relationship between weft directional accumulative retraction forces due to fabric structure and the number of meso-cells in the multiple yarn pull-out test of CT 716 and CT 714 fabrics, respectively.

The warp directional multiple yarn accumulative retraction forces of CT 716 fabric in various fabric lengths were significantly higher than those of the weft directional multiple yarn accumulative retraction forces of CT 716 fabric, whereas the weft directional multiple yarn accumulative retraction forces of CT 714 fabric in various fabric lengths were significantly higher than those of the warp directional multiple yarn accumulative retraction forces of CT 714 fabric. On the other hand, the warp and weft directional multiple yarn accumulative retraction forces of CT 716 and CT 714 fabrics in the fabric edge regions were higher than those of the fabric centre regions. In addition, it was found that the multiple yarn accumulative retraction forces in various fabric lengths of CT 716 and CT 714 fabrics in fabric edge and centre regions were higher than those of the single yarn retraction forces of CT 716 and CT 714 fabrics.

CONCLUSIONS

It was found that the decreasing line in the single and multiple yarn pull-out force-displacement curves corresponds to each stick-slip region ($S_k - S_p$) whereas the increasing line in the single and multiple yarn

pull-out force-displacement curve corresponds to each accumulative retraction force by fabric structure (A_p). The warp and weft directional single and multiple yarn stick-slip forces in the MC-1 of CT 716 and CT 714 fabrics were generally higher than those of the MC-6 of CT 716 and CT 714 in the fabric edges. The MC-1 was found the most critical cell due to the starting point of the yarn pulling region and it was related to fabric boundary. The amount of stick-slip force and accumulative retraction force in multiple yarn pull-out were extremely nonlinear compared to that of the single yarn pull-out. On the other hand, the amount of stick-slip force was related to the number of interlacement points in the fabric, whereas the amount of accumulative retraction force was related to fabric structural response. In general, stick-slip force and accumulative retraction force depended on fabric density, the number of pulled yarn ends and fabric dimensions. The stick-slip force and accumulative retraction force of CT 716 and CT 714 fabrics obtained from the multiple yarn pull-out test were higher than those of the single yarn pull-out test. On the other hand, the stick-slip force of CT 716 was higher than those of CT 714 fabrics due to fabric density.

Future research should be conducted to find the analytical relation among stick-slip force, accumulative retraction force and yarn-fabric structural parameters. This could result in a multiaxially interlaced fabric with improved frictional properties which could be used in soft ballistic applications.

BIBLIOGRAPHY

- [1] Dong, Z., Sun, C. T. *Testing and modeling of yarn pull-out in plain Kevlar fabrics*. In: Composites. Part A: Applied Science and Manufacturing, 2009, vol. 40, issue 12, p. 1 863
- [2] Kirkwood, K. M., Kirkwood, J. E., Lee, Y. S., Ronald, G., Egres, J. R. *Yarn pull-out as a mechanism for dissipating impact energy in Kevlar KM-2 fabric*. Part I: *Quasi-static characterization of yarn pull-out*. In: Textile Research Journal, 2004, vol. 74, issue 10, p. 920
- [3] Erlich, D. C., Shockey, D. A., Simons, J. W. *Slow penetration of ballistic fabrics*. In: Textile Research Journal, 2003, vol. 73, issue 2, p. 179

- [4] Dulgheriu, I., Avădanei, M., Badea, S., Safta, I. *Experimental research on establishing the level of bullets protection for a ballistic protection structure*. In: Industria Textilă, 2012, vol. 63, issue 4, p. 198
- [5] Cheeseman, B. A., Bogetti, T. A. *Ballistic impact into fabric and compliant composite laminates*. In: Composite Structures, 2003, vol. 61, p. 161
- [6] Cunniff, P. M. *A semiempirical model for the ballistic impact performance of textile based personnel armor*. In: Textile Research Journal, 1996, vol. 66, issue 1, p. 45
- [7] Briscoe, B. J., Motamedi, F. *The ballistic impact characteristics of aramid fabrics. The influence of interface friction*. In: Wear, 1992, vol. 158, p. 229
- [8] Bilisik, K., Korkmaz, M. *Multilayered and multidirectional stitched aramid woven fabric structures: Experimental characterization of ballistic performance by considering yarn pull-out test*. In: Textile Research Journal, 2010, vol. 80, issue 16, p. 1 697
- [9] Bilisik, K. *Experimental determination of yarn pull-out properties of para-aramid (Kevlar®) woven fabric*. In: Journal of Industrial Textiles, 2012, vol. 41, issue 3, p. 201
- [10] Gupta, B. S. (ed.). *Friction in Textile Materials*. The Textile Institute, Woodhead Pub. Ltd., Cambridge, UK, 2008
- [11] Bilisik, K. *Stick-slip behavior of para-aramid fabric in yarn pull-out*. In: Textile Research Journal, 2013, vol. 83, issue 1, 2013, p. 13
- [12] MathWorks, *MATLAB R2008a, ver. 7*. Computer program, The MathWorks Inc., Natick, MA, USA, 2008

Author:

KADİR BİLİŞİK

Department of Textile Engineering

Faculty of Engineering

Erciyes University

38039 Talas-Kayseri, Turkey

e-mail: kadirbilisik@gmail.com; kbilisik@erciyes.edu.tr

DOCUMENTARE



MATERIALE VII DIN NANOFIBRE ȘI BACTERII

Oamenii de știință de la **Institutul Tehnologic din Massachusetts** au dezvoltat materiale hibride, care reprezintă o încrucișare între celule bacteriene vii și unele componente care nu sunt vii, cum ar fi nanoparticulele de aur sau punctele cuantice. Materialele vii, asemenea celulelor vii, au capacitatea de a răspunde mediului în care trăiesc, dar posedă și alte proprietăți, cum ar fi conductivitatea electrică și capacitatea de a emite lumină.

Echipa de cercetare, condusă de profesorul universitar de Timothy Lu, specialist în inginerie electrică și inginerie biologică, și-a început studiul cu bacteria *Escherichia coli*. Această bacterie a fost selectată datorită faptului că ea produce în mod normal o peliculă bio ce conține structuri de proteine, cunoscute sub numele de fibre „curli”, care ajută bacteriile să adere la diverse suprafețe.

Prin introducerea selectivă a peptidelor pe fibre, cercetătorii au făcut posibilă lipirea acestora de unele

elemente, cum ar fi nanoparticulele de aur, care au fost introduse în mediul lor. Fibrele obținute, acoperite cu particule de aur s-au transformat în nanofire de aur, care au permis peliculei bio să devină conductor electric. De asemenea, au fost produse pelicule bio acoperite cu puncte cuantice, reprezentate prin nanocristale compuse din materiale semiconductoare.

În cercetările efectuate, Lu și echipa sa au fost inspirați de structura unor materiale, cum ar fi osul, care conține atât elemente minerale, cât și celule vii, și care favorizează răspunsul la stimulii de mediu. Se preconizează ca, la finalizarea acestui studiu, noua tehnologie să poată fi utilizată în producția de materiale cu proprietăți de autovindecare, senzori de diagnosticare sau matrice pentru ingineria tisulară, baterii, celule solare etc.

Smarttextiles and nanotechnology, iunie 2014, p. 14

Application of the layer-by-layer technique for knitted fabrics

DAWID STAWSKI
FRANK SIMON

DOROTA ZIELIŃSKA
STEFAN POŁOWIŃSKI
MICHAŁ PUCHALSKI

REZUMAT – ABSTRACT

Aplicarea tehnologiei de depunere strat cu strat pe materiale textile tricotate

Polielectroliti încărcați cu sarcini electrice diferite, de tipul acidului (poli)acrilic și al clorhidratului de (poli)alilamină, au fost depuși pe un material textil tricotat, din polipropilenă, folosind metoda de depunere strat cu strat. Ca metode de analiză a procesului de modificare a proprietăților s-au folosit: spectroscopia în infraroșu cu transformată Fourier, spectroscopia de fotoelectroni cu raze X și microscopia electronică cu baleiaj. S-a constatat că efectele obținute în cazul materialelor tricotate sunt similare cu cele observate anterior, la materialele nețesute. Aplicarea straturilor de polielectroliti, prin metoda depunerii strat cu strat, modifică în mod semnificativ capacitatea de vopsire, hidrofilia și proprietățile electrostatice.

Cuvinte-cheie: tehnica depunerii strat cu strat, material tricotat polipropilenic, capacitate de vopsire, hidrofilie, proprietăți electrostatice

Application of the layer-by-layer technique for knitted fabrics

Oppositely charged polyelectrolytes such poly(acrylic acid) and poly(allylamine hydrochloride) have been deposited on a polypropylene knitted fabric by the layer-by-layer technique. The modification process was controlled by a series of tests like: Fourier transform infrared spectroscopy, X-ray photoelectron spectroscopy and scanning electron microscopy. It has been found that effects obtained for knitted fabric are very similar to those which were previously observed for nonwovens. The deposition of polyelectrolyte layers by the layer-by-layer method considerably modifies dyeability, hydrophilicity and electrostatic properties.

Key-words: layer-by-layer technique, polypropylene knitted fabric, dyeability, hydrophilicity, electrostatic properties

The main principle of the layer-by-layer (LbL) method consists in alternately depositing oppositely-charged layers of polyelectrolytes, which interact due to electrostatic forces. Films in the nanosize are deposited using dilute solutions (concentrations of several milligrams per millilitre). The coated material, which now possesses an external layer of a polyelectrolyte, can now adsorb next an oppositely charged layer. The strong electrostatic attraction is the dominant factor in the adsorption process. Multilayer structures may be composed of polyelectrolytes, charged molecular substances or colloidal materials. Adsorption times per layer vary from minutes for polyelectrolytes to hours for some colloids. Applying such modifications gives a possibility to obtain products that combine the properties of the main object with the superficial parameters of a new external layer.

Electrolyte or polyelectrolyte nanolayers can be deposited on various flat surfaces such as mica [1] – [2], glass [3] – [5], [7], quartz [8], gold [9], titanium [10], silicon [11] – [13], [15], pigment particles [16], polymeric membranes [15], [17], [18] or microspheres [19]. The deposition of polyelectrolyte layers on fibres, textile supports and textile materials is clearly in the initial stage.

The textile industry increasingly makes use of functional nanoparticles in order to achieve new or improved

properties of textile materials [20]. Changes in its structure and character play a particular part in the modification process of the structure and properties of a textile fabric. The modification of textile fabric surface by the LbL method results in a multi-component material with complex structure and very precisely selected properties. The LbL modification technique has no limitation on substrates, thus even textile substrates with nonplanar surfaces are suitable for this technique. Initially, this method was used for other types of materials than textiles but now its implementation in the textile industry is in progress. In textile LbL application it is necessary to take into account a specific structure of the modified material and other such important factors as: type of flat material, its thickness, type of weaves, compaction etc. Because of this, the application process is more complicated, and each measurement of properties is more difficult and requires special treatment and real attention. The first step of textile modification with the LbL method is activation, thus forming functional groups on the outer surface, whose purpose is to attach the first layer. The activation process may be carried out by a chemical reaction using appropriate reagents or surface grafting. These processes are usually carried out in a liquid environment, most often in an aqueous solution [21]. When surface activation is complete, a polymer layer containing basic func-

tional groups can be applied, leading to the formation of a stable polymer complex onto which oppositely charged layers can be deposited.

The very initial stage of the application of LbL deposition technique for textile supports was the modification on the surface of a single straight fibre [14], [18], [22] – [25]. The next natural step of the LbL application in the area of textiles was modification of fibres in real textile material (not only separate fibre in laboratory conditions). The easiest flat textile object for such modification is nonwoven polypropylene. The application of methods used for the modification of really flat surfaces (e.g. mica, glass, gold) for the treatment of textiles creates many difficulties related to the structure of textile products. The LbL method assumes the accessibility of the surface to be modified. This accessibility is provided only for few textile products. One can assume that in nonwoven fabrics composed of monofilaments with smooth surfaces, not too dense and not stuck together or heat sealed, the accessibility of the surface is similar to that in conventional applications of the layer-by-layer method. Polypropylene is a commonly used, inexpensive synthetic polymer. PP fibres belong to the textile raw materials being frequently used. The surface of such monofilaments is really smooth, and this makes the modification procedure and the process control easier. In a series of publications we described the modification of polypropylene and polyester nonwovens [26] – [34]. It has been shown that this method can also be used for textile fabrics. This type of flat textile fabric is very good as a first model of real textiles modification, because there is no influence of weaves and the structure is the most regular and easy. Consequently the following step of modification of flat textile materials should be taking into consideration knitted and woven fabrics. Currently it was described the use of LbL method for woven fabrics made from cotton [35]. In one of our previous papers [31] we mentioned the possibility to apply the LbL technique for knitted fabrics without any deeper analysis, and no other article informed about such investigations. In this paper we want to replace the modification procedure, which we previously applied for nonwovens, for more structurally complicated knitted fabric. The results obtained between a nonwoven model and knitted fabric will be compared and structural differences will be taken into account.

EXPERIMENTAL PART

Materials used

Poly(acrylic acid) (PAA) was prepared by polymerization of acrylic acid (AA) in toluene initiated with azobis-(isobutyronitrile) (AIBN). The polymer was rinsed several times with toluene and dried under vacuum. Its weight-average molecular weight ($M_w = 145\ 000$ g/mol) was determined by gel chromatography. Poly(allylamine hydrochloride) (PAH) from Fluka ($M_w = 70\ 000$ g/mol) was used without purification.

Polypropylene knitted fabric (PR 73/06) (sharmeze, a multi-guide stitch) was produced in Textile Institute, Łódź, Poland with following parameters:

- surface weight 80 g/m²;
- average filament diameter 14.9 μm;
- number of courses 180 dm⁻¹;
- number of wales 140 dm⁻¹;
- yarn Prolen 56 dtex;
- number of filaments in yarn 16.

Nonwoven, polypropylene substrate was prepared by the melt-blown method (Cenaro – Lodz, Poland) with a surface weight of 27.9 g/m² and an average filament diameter of 9.65 μm. Nonwoven substrates were produced using low viscosity polypropylene (lvPP) granulates, completely free from additives (HL604FB) produced by Borealis AG, Austria. More details to the polypropylene nonwoven are provided in our previous publications [28], [31] – [34].

All other reagents were provided by POCH Spółka Akcyjna, Poland and used without purification.

Methods used

Modification procedures

Chemical activation of the fabrics and polyelectrolyte deposition:

- The knitted fabric was activated according to [26], [31] – [34] by heating in a solution of ammonium persulfate (20 g/L, $t = 30$ minutes, $T = 80^\circ\text{C}$, saturated with nitrogen), thoroughly rinsing with water, and grafting with concentrated acrylic acid (AA) (52 g/L, $t = 60$ minutes, $T = 80^\circ\text{C}$, saturated with nitrogen). After grafting the samples were immersed in an aqueous solution of appropriate polyelectrolyte (10^{-2} mol/L);
- Prior to every such operation samples were rinsed with distilled water;
- Polyelectrolyte layers were deposited as described previously [26].

Analytical methods

Microscopic images were taken using standard optical microscope.

SEM microscopy

Scanning electron microscope combined with energy-dispersive X-ray spectroscopy analysis. The chemical and morphological analysis of surface modified knitted fabrics was carried out by means of scanning electron microscope (SEM) Nova Nano-SEM 230 from FEI, Hillsboro, OR, USA (SE Detector, voltage 15 kV, low vacuum 0.3 torr).

Dyeing tests

Samples with different numbers of layers were immersed into 0.001 mol/L methylene blue solution for 10 minutes. After immersion in the dye solution, the knitted materials with multilayer films were soaked in water for 1 minute and then dried with a mild flow of air. All the dyed samples were subjected to measurements of light reemission. Dyed samples were placed in a Spectraflash 300 apparatus

(Datacolor International, Lawrenceville, NJ, USA) to measure their light reemission in the 400 to 700 nm range.

FTIR spectroscopy

The FTIR spectra were collected by a PerkinElmer 2000 FTIR instrument (Perkin Elmer Inc., Waltham, MA, USA). With a Perkin-Elmer specular reflectance variable angle spectrophotometer (VASR) has been used to gather the reflectance FTIR spectra at 60° (50 scans). The unmodified material was used as a background for creating spectra of modified surface. The areas under carbonyl peak were calculated in the 1 650 – 1 800 cm^{-1} range.

XPS analysis

XPS analysis was performed using an Axis Ultra spectrometer (Kratos Analytical, Manchester, U.K.) equipped with a monochromatic Al K α X-ray source of 300 W at 20 mA. Wide-scan and high resolution spectra were obtained at pass energy values of 160 eV and 20 eV, respectively. During all measurements, electrostatic charging of the sample was compensated by means of a low-energy electron source working in combination with a magnetic immersion lens. All recorded peaks were shifted to set the C 1s peak to 285.00 eV. The quantitative elemental compositions were determined from peak areas using experimentally determined sensitivity factors and the spectrometer transmission function. High-resolution spectra were deconvoluted by means of a routine computer programme (Kratos Analytical, Manchester, U.K.) and the free parameters of component peaks were: their binding energy (BE), height, full width at half-maximum and the Gaussian-Lorentzian ratio.

Electrostatic measurements

The electrostatic measurements were made using the Static Meter I (HAUG GmbH & Co. KG, Leinfelden-Echterdingen, Germany) apparatus (distance to the sample = 2 cm). The samples were pre-conditioned for at least one week at a temperature of 22°C and 33% humidity. Each measurement was repeated at least three times and the results averaged.

Hydrophilicity

Capillarity was examined by applying a coloured drop (0.1 cm^3) of 0.1% potassium dichromate solution on a flat surface of previously conditioned fabric ($T = 26^\circ\text{C}$, air humidity 29%, $t = 48$ hours). The sample was left for 24 hours and then the coloured fabric fragments were weighed.

Thermogravimetric measurements

The thermal analysis of all samples was carried out with a Perkin Elmer TGA 7 thermal analyzer in a platinum measuring cell, with the use of Pyris program for data handling (Perkin Elmer Inc., Waltham, MA, USA). The measurements were performed in air atmosphere with the heating rate 15°C min^{-1} . The samples were heated up to 650°C, starting from

room temperature. All measurements were repeated at least three times. For each course, the temperature of 50% degradation ($T_{50\%}$) was determined and then average value calculated.

RESULTS AND DISCUSSIONS

Object of modification

Nonwoven materials

The fabrication of textile flat materials using nonwoven technology can avoid difficult processes of yarn production, weaving, knitting and finishing. It allows to shorten production time and to obtain a product without any preparations on the surface, which makes the technological process easier and additional surface modifications possible.

The spun-bond and melt-blown process is very fast and probably the most economical way to produce nonwovens. It is the technique whereby molten polymers are directly converted into endless filaments lay on a conveyor belt and eventually formed into nonwoven roll goods. The production of nonwovens using melt-blown technology is a younger relative of the spun-bond technology. The process allows the production of ultrafine filament nonwovens under very economical conditions. In such a technology, a thermoplastic fibre-forming polymer is extruded through a linear die containing several hundred small orifices. Streams of hot air rapidly attenuate the extruded polymer streams to form extremely fine filaments. Those filaments are then blown by high-velocity air onto a collector screen, thus forming a fine-filtered, self-bonded nonwoven web. After that, they are bonded and wound to form roll goods. Thanks to its characteristic properties, melt-blown are often used as high-degree filter media for air, liquid and particles. The view taken using optical microscope of the nonwoven modified in papers [31] – [34] can be seen in figure 1.

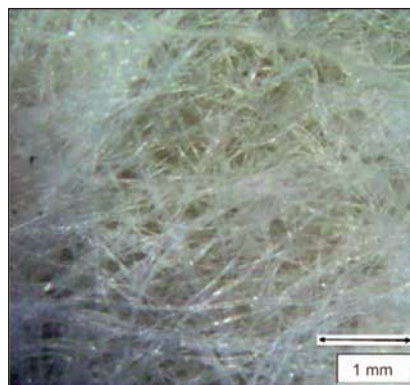


Fig. 1. Microscopic image of the nonwoven modified using LbL technique in papers [27], [30] – [33]

Knitted fabric

Warp-knitted fabrics are a product of a technological process carried out on warp-knitting machines. Their characteristic feature is that the subsequent loops formed from the same warp thread are situated in the

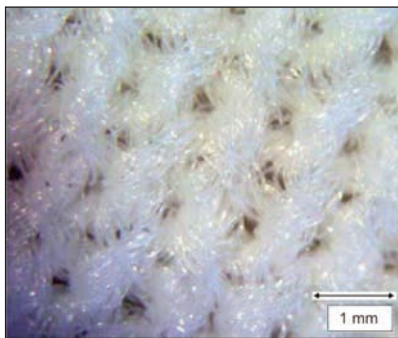


Fig. 2. Microscopic image of the knitted fabric

subsequent courses. This characteristic is the result of the knitting process, which is based on drawing the warp threads simultaneously through the loops of the recently formed course. Warp-knitted fabrics can be characterized by various structures and thanks to that they possess different properties. The range of possible applications is wide. Sharmeze is an example of a multi-guide stitch, consisting of two component stitches – tricot and cord. Both stitches are composed of closed-loops. The optical view of the knitted fabric which results from modification is presented in this paper in figure 2.

As can be seen in figure 2, compared to the nonwoven in figure 1, both materials have completely different structures. The diameter of fibres is quite similar in both materials, but the amount of inactive (not accessible) surface is in knitted fabric larger (because of stitches) than in nonwoven. In experiments discussed in this paper we applied exactly the same modification procedure previously used for nonwovens.

Modification of the surface of fibres in knitted fabrics

The polypropylene knitted fabric was modified using exactly the same procedures as previously for nonwoven. The first step of the modification process with the LbL method is activation, thus forming functional groups on the outer surface, the purpose being to attach the first layer. The activation process may be carried out by a chemical reaction using appropriate reagents or surface grafting. In this paper as a first layer we introduced poly(acrylic acid) using the method of grafting (described above). In next steps oppositely charged layers of poly(allylamine hydrochloride) and poly(acrylic acid) were applied employing the LbL technique. Finally, knitted fabric samples with different architectures on their surfaces were received (table 1).

Table 1

COMPOSITION OF DEPOSITED LAYERS			
Grafting	Type of layer (sample number)		
1	2	3	4
PAA	PAA-PAH	PAA-PAH-PAA	PAA-PAH-PAA-PAH

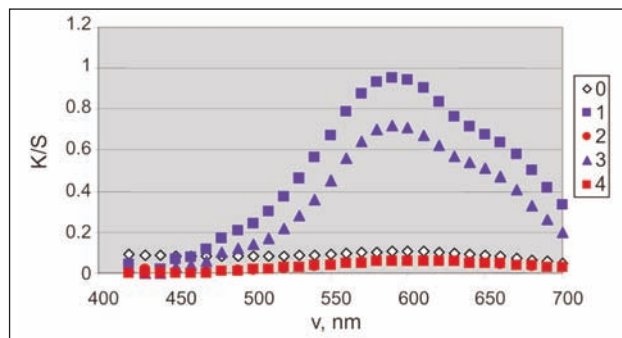


Fig. 3. Methylene blue dyeing tests results

Confirmation of the modification process

To study the surface chemistry and the properties of modified materials a series of analysis and tests were carried out. The types of selected analysis and tests were exactly the same as used previously for nonwovens [31] – [34]. Those tests were performed in order to confirm the modification of the PP knitted fabric, as well as to characterize these novel materials.

Dyeing tests

A dyeing test is a very comfortable way to confirm the structure of knitted fabrics with deposited layers. It allows to obtain very fast and easy results. Methylene blue is a phenothiazine dye used to reveal acidic surfaces. One should expect considerable differences in the intensity of colour of the test dyed fabrics before modification and those containing the last layer of polyacid or the external layer of polyamine. Similar analyses of textiles modified by the LbL method are reported in the literature for nonwovens [31] – [35]. The dyed samples have visual differences in the intensity of colour: sample 1 and sample 3 (table 1) are clearly deeper blue than sample 0, sample 2 and sample 4. To corroborate naked-eye visual evaluation of colour, spectrophotometric measurements of scattered light (S) were also performed and are presented in figure 3. The intensity of reflected colour was measured by means of a spectrophotometer in the range of maximum light reemission for methylene blue (400 – 700 nm).

The relationship between the coefficient of absorption (K) and scattering (S) (K/S) and the coefficient of light reflection (R) has been derived by Kubelka and Munk:

$$\frac{K}{S} = \frac{(1 - R)^2}{2R} \quad (1)$$

The dependence of K/S on wavelength is shown in figure 3.

As can be seen in figure 3, the number of acidic groups on the surface with the external PAA layer is considerably higher than that on the sample with the external PAH layer and on the sample with an unmodified surface. The use of colour tests in the work on the modification of textiles is very useful as it allows a quick and simple evaluation of the deposition process, giving results that can be easily and quickly visually interpreted.

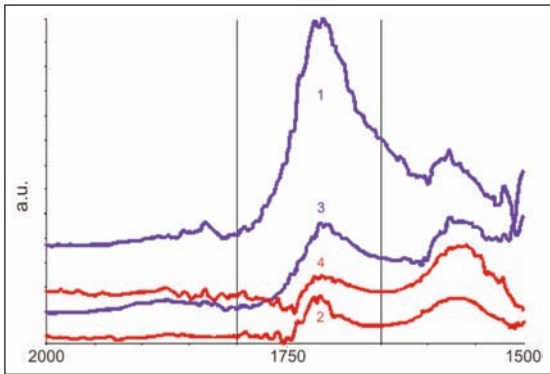


Fig. 4. FTIR spectra of PP knitted fabrics with polyelectrolyte layers:
1 – PAA; 2 – PAA-PAH; 3 – PAA-PAH-PAA;
4 – PAA-PAH-PAA-PAH

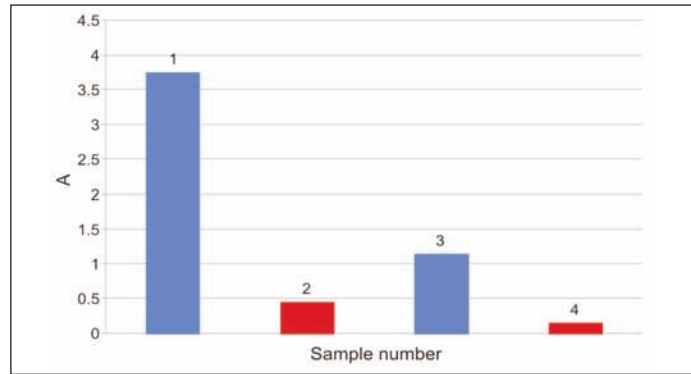


Fig. 5. Average areas under carbonyl peak ($1650 - 1800 \text{ cm}^{-1}$) in FTIR spectra of PP knitted fabrics with polyelectrolyte layers:
1 – PAA; 2 – PAA-PAH; 3 – PAA-PAH-PAA;
4 – PAA-PAH-PAA-PAH

FTIR analysis

Reflectance FTIR spectroscopy is a very efficient tool to monitor the formation of poly(acrylic acid) and poly(allylamine hydrochloride) polyion complex (PAA-PAH) on PP fibres. PAA has a very intensive signal at a maximum of 1710 cm^{-1} , which results from carbonyl groups. The area of this signal should be larger for samples with external PAA layer in comparison to the samples with external PAH layer.

Reflectance spectra of knitted fabrics after each modification step were obtained according to the scheme presented in table 1. Cut-outs of spectra of the samples obtained after different modification steps are shown in figure 4. In the spectrum of the sample grafted with PAA 1, there is a wide signal resulting from the carbonyl groups. In the spectrum of the sample with a PAA-PAH double layer 2 the signal corresponding to the $>C=O$ is much smaller. In spectrum 3 recorded from a sample coated with a triple PAA-PAH-PAA layer with an outer PAA layer the signal intensity was significantly higher, and after applying an additional PAH layer (sample 4) the signal of the carbonyl groups has almost completely disappeared. Calculated areas of the carbonyl group peaks are shown in figure 5.

Microscopic analysis (SEM)

Scanning electron microscopy makes it possible to have a direct visual assessment the surface of modified samples. One can obtain important information about surface topography, structure, and the presence of impurities or uniformity of deposited materials. SEM views of samples after various stages of modification are shown in figure 6.

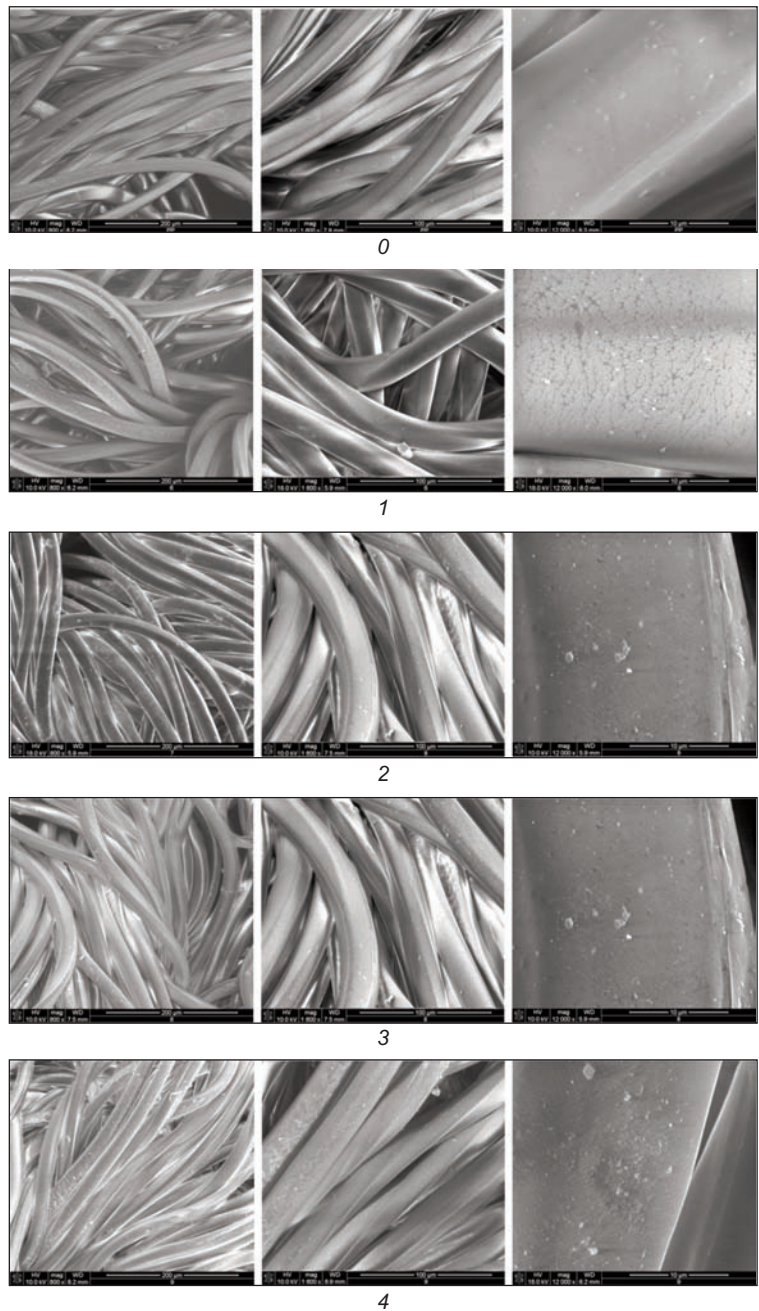


Fig. 6. SEM images of PP knitted fabrics without modification (0) and with polyelectrolyte layers:
1 – PAA; 2 – PAA-PAH; 3 – PAA-PAH-PAA; 4 – PAA-PAH-PAA-PAH

As can be seen, the fibred sample without modification 0 had a very smooth surface. After applying polyelectrolyte layers using grafting procedure 1 or LbL technique 2 – 4 the roughness was increased. Irregularly formed spots showed that not all homopolymer molecules were directly bonded to the surface or involved in the polyelectrolyte film covering the PP substrate homogeneously. Similar findings were observed for nonwoven fabric [33].

XPS analysis

XPS is a highly surface-sensitive technique, where the information depth is not higher than 10 nm at maximum. Beside the qualitative and quantitative element analysis the XPS method can also be used to analyse the binding states of the elements in the surface region of a sample. That means XPS can be considered as a method giving complementary information to the more molecularly oriented method of infrared spectroscopy, which gives the fingerprints of molecular ensembles.

The XPS wide-scan spectra in figure 7 show the PP knitted fabric samples after each step of surface modification. The untreated PP knitted fabric surface contains only traces of oxygen, $[O]:[C] = 0.019$ and no nitrogen. Traces of oxygen are usually found in common PP materials because in spite of the presence of additives preventing oxidation and UV degradation the majority of polyolefins is slightly oxidized on the surface. In the $C 1s$ spectrum, the small amount of oxygen incorporated in the untreated PP knitted surface did not allow to separate component peaks showing the kind of oxygen-containing functional groups. The main component peak in the $C 1s$ spectrum arose from carbon atoms of saturated hydrocarbons (component peak A at 285.00 eV).

The success of the radical grafting of AA on the PP knitted fabric surface in presence of ammonium persulfate can be seen from the strongly increased amount of oxygen in the sample surface, $[O]:[C] = 0.094$ (fig. 7 b). Oxygen radicals produced during the decomposition of ammonium persulfate do not only initiate the polymerization of AA, but they are

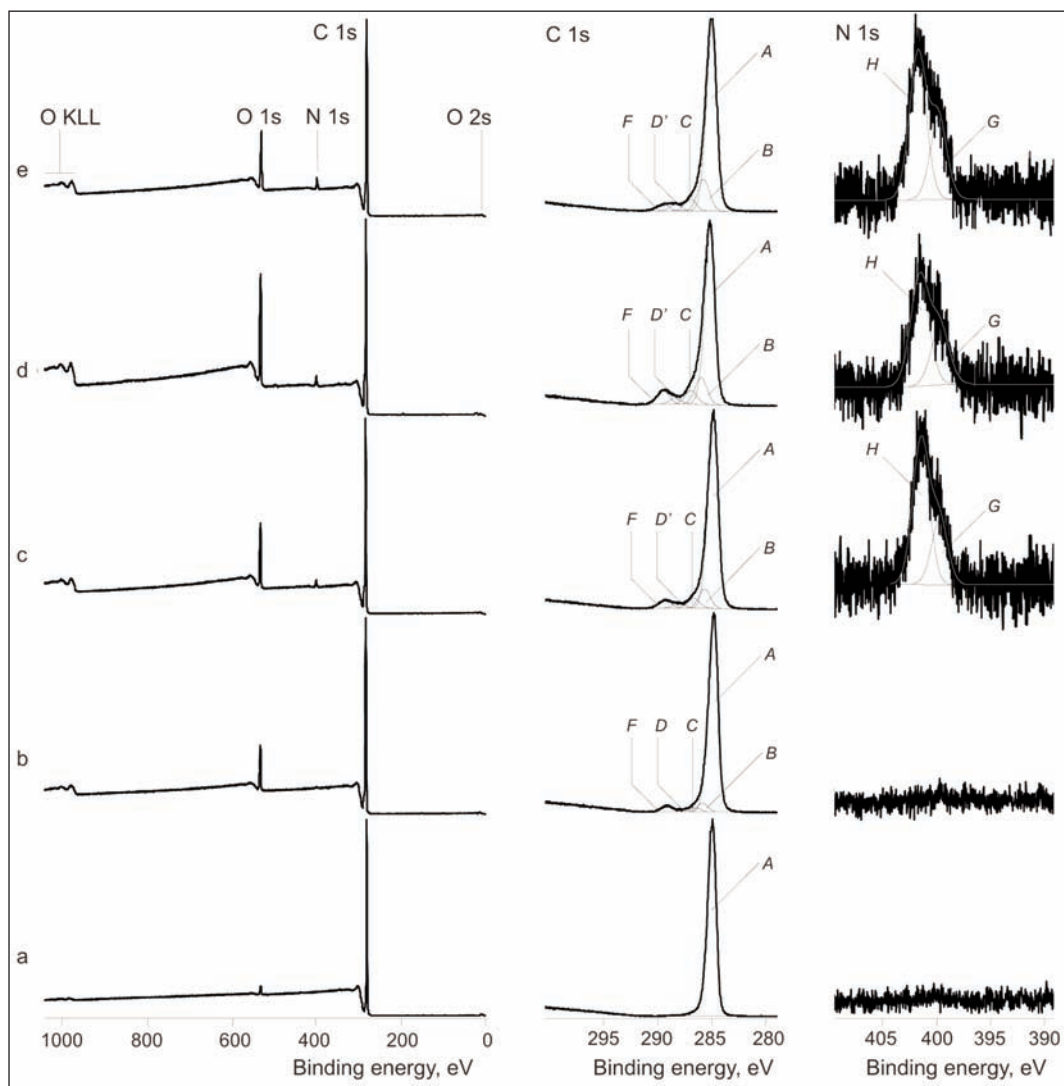
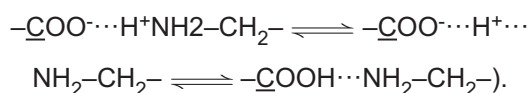


Fig. 7. Wide-scan XPS spectra (left column), $C 1s$ and $N 1s$ high-resolution XPS spectra of: a – an unmodified PP knitted fabric sample; b – the PP knitted fabric sample grafted with PAA; c – the PAA-grafted sample coated with PAH; d - the PAA-PAH coated PP knitted fabric sample with a second PAA layer; e – the PAA-PAH-PAA coated PP knitted fabric sample with a second PAH layer

also reactive towards saturated hydrocarbons and oxidize the PP polymer in different ways. The introduction of oxygen-containing functional groups into the PP surface can be clearly seen in the *C 1s* spectrum of the PAA-grafted sample (fig. 7 *b*). In addition to the main component peak *A* (285.00 eV) appeared from saturated hydrocarbons, the *C 1s* spectrum shows four other component peaks. Component peak *F* (289.4 eV) shows the presence of carbonic acid groups (O=C–OH) and their corresponding carboxylates, which is the result of the oxidation of the PP knitted as well as grafted AA units. Furthermore, carbonyl carbon atoms of keto groups (C=O, component peak *D* at 287.74 eV) and OH groups (component peak *C* at 286.66 eV) were detected. The presence of ether groups, which would also contribute to component peak *C*, is unlikely from the radically initiated reaction mechanism. Component peak *B* (285.9 eV) having the same intensity as component peak *F*, this shows carbon atoms in α -position to the carbonyl carbon atoms of the carbonic acid groups and their carboxylates (C–COO).

As can be seen from the appearing of the *N 1s* peak in the wide-scan spectrum, the application of PAH on the PAA-grafted PP knitted fabric surface introduced nitrogen in the samples surface region, [N]:[C] = 0.034 (fig. 7 *c*). The corresponding *C 1s* spectrum (fig. 7 *c*) is characterized by a more intensive component peak *B*, which shows C–N of the PAH polymer in addition to the α -positioned carbon atoms mentioned above. Compared to the *C 1s* spectrum recorded from the PAA-grafted sample, a small chemical shift of $\Delta = 0.43$ eV was also observed for component peak *D* (288.17 eV).

This component peak was designated with *D'* because it shows carboxylate groups, which are strongly interacting with protonated amino groups of the PAH polymer (formation of salt pairs



The binding energy value found for component peak *D'* is also very typical for the carbonyl carbon of carbonic amide groups (O=C–NH–C). That means it could also be possible that some of the carbonic acid groups reacted with amino groups [35]. Surprisingly, the relative oxygen content of the PAH-layered sample was slightly increased, [O]:[C] = 0.134. We assume that water molecules stabilized by the ionic and highly polar functional groups of the applied polyelectrolytes contribute to the intensity of the *O 1s* peak. As can be seen in the *C 1s* spectrum, the number of oxygen-bonded carbon atoms is not significantly different from the carbon-oxygen bonds detected in the *C 1s* spectrum of the PAA-grafted sample. The *N 1s* spectrum reflects the protonation equilibrium of the surface-bonded PAH polymer. Nitrogen atoms of the protonated amino groups (C–N⁺H₃) contribute to component peak *H* as 401.89 eV (fig. 7 *c*). The co-presence of a high amount of uncharged amino groups analysed by component peak *G* (400.19 eV) supports

the assumption of strong interactions between the carboxylate groups and the protonated amino groups. Involved in the salt pair formation with carboxylate groups (discussed above) the positive net charge of the protonated amino species is formally neutralized by the negative charge of the carboxylate group. Hence, nitrogen atoms of such species appear at lower binding energy values and contribute to component peak *G*. If carbonic amide groups are formed the nitrogen atoms of the amide group (O=C–NH–C) would also contribute to component peak *G*. The excess of protonated amine species (component peak *H*) ensures that the surface potential of the bi-layered PP knitted fabric is positive. Hence, beside the adsorption entropy the adsorption of a second PAA layer should be also driven by specific Coulomb interactions.

Carbonic acid groups of the second PAA layer attached to the PAH-modified PP knitted fabric increased the relative content of oxygen, [O]:[C] = 0.220 (fig. 7 *d*). The increased oxygen content is connected with an increased component peak *F* in the *C 1s* spectrum, which appeared from carbonyl atoms of carbonic acids and their carboxylates. The shape of the *N 1s* spectrum was not significantly affected by the second PAA layer attached. As found for the PAH-modified sample, the *N 1s* spectrum is characterized by an excess of positively charged C–N⁺H₃ groups (component peak *H*) and a considerable amount of formally non-charged primary amino groups (component peak *G*). Correspondingly, the second PAA layer decreased the relative amount of nitrogen only in a small amount, [N]:[C] = 0.025. From these findings it can be concluded that the second PAA-layer did not cover the PAH-layer like a shell. Rather a mixed PAA-PAH polyelectrolyte layer or complexes of these polyelectrolytes seemed to be formed by the electrostatic interactions between the oppositely charged carboxylate and protonated amino groups. These findings are in excellent agreement with the SEM studies, which showed irregularly formed spots on the sample surface. A further PAH layer applied to the PAA/PAH/PAA-modified PP knitted fabrics slightly lowered the relative oxygen content on the sample surface by covering the mixed PAA/PAH layer, [O]:[C] = 0.124 (fig. 7 *e*), and increased the relative nitrogen content, [N]:[C] = 0.038. The additionally introduced protonated amino groups increased also the intensity of component peak *B* in the corresponding *C 1s* spectrum (fig. 7 *e*). The shape of the *N 1s* spectrum was not affected showing that the additionally applied PAH layer was also electrostatically bonded to the mixed PAA/PAH layer.

Analysis of the surface properties of modified materials

Hydrophilic properties

Due to the nearly complete absence of functional polar groups, PP is a typical member of the group of polymers with strong hydrophobic properties. For many applications it is desirable to hydrophilize the PP surface and make it wettable for water, aqueous

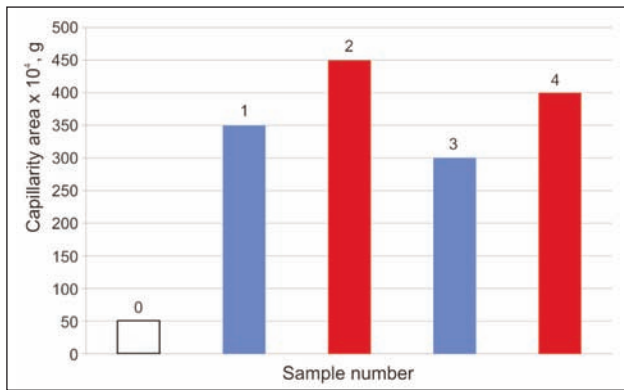


Fig. 8. The weight of capillary area for all samples

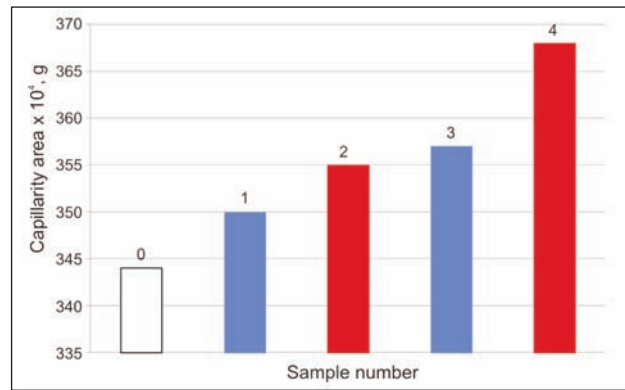


Fig. 9. Calculated temperatures of 50% decomposition

solutions and dispersions. The application of polyelectrolytes on fibres, fabrics and nonwovens opened an easy way to turn the common wetting behaviour of PP materials. For such textile materials the hydrophilicity can be evaluated by capillarity. Textiles do not have isolated capillaries but they are characterized by a complex pore system containing irregularly formed capillaries with various diameters. Hence, in hydrophilic fabrics water passes from greater to smaller capillaries. Thus capillarity plays a very important role in the process of water absorption as it facilitates water transport into areas being beyond the wetting spot. Results of the wettability of the differently polyelectrolyte-coated PP knitted fabrics are shown in figure 8.

As it can be seen in figure 8 the character of PP knitted fabrics was changed by the polyelectrolyte application, becoming more hydrophilic. A strong effect can be seen after the radical grafting of AA on the PP surface. As the XPS results showed, during the grafting reaction the PP surface was endowed with numerous different polar groups. These groups increased the surface free energy and surface polarity and turned in this manner the wetting behaviour from a water uptake of 50 g for untreated PP to 400 g (corresponds to the eightfold) for the sample with two bi-layers of polyelectrolytes [36].

An important effect is easy to see even after the first step of modification – grafting procedure. The final decrease (from 50 g to 400 ~ 8 times) is again similar in comparison to nonwoven (20 g to 170 ~ 8.5 times) [34].

Surprisingly the changes in surface properties in both types of flat textile materials are very similar in spite of important structural differences.

Thermogravimetric measurements (TG)

Surface modifications made by the LbL technique, as described above, affect mainly the surface properties of the material under modification. However, it has been also observed that the modification of PP nonwoven influences also the thermal resistance of the substrate material [33] in oxygen access. Similar investigations we prepared for PP knitted fabric. Figure 9 shows the result of TG analysis for samples after each stage of modification. There are average

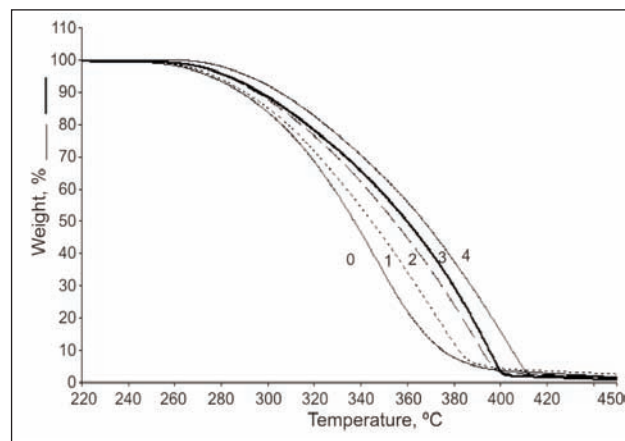


Fig. 10. Parts of representative thermogravimetric curves in air atmosphere (without modification 0) and with polyelectrolyte layers:
1 – PAA; 2 – PAA-PAH; 3 – PAA-PAH-PAA;
4 – PAA-PAH-PAA-PAH

values from many measurements. Figure 10 shows only one curve for each sample. Final change in half decomposition temperature is clearly visible (about 23°C), but little smaller in comparison with nonwoven (~37°C) [33]. This effect is probably due to the formation of a barrier by the deposited layers that insulates the main polymeric matter from oxygen access [33]. In case of knitted fabric there is an additional effect connected with stitches. Based on the above results, it seems that the differences in the thermal curves of polypropylene are created by an insulating barrier to protect the main polymeric matter against the access of oxygen and, consequently, they retard the polymer degradation, which is similar in nonwoven modification [33]. Additionally a minor role is played by the smaller size of active surface in knitted fabric, which may be a reason for some smaller penetration of the modification agents, and as an effect proportionally little volumetric deposition.

Electrostatics charging

In order to evaluate the electrostatic charging, the charge dissipation half-life was selected as a quantitative factor. PP is a material which is particularly easily charged; in previous papers it was shown that it is possible to significantly reduce static electricity

Table 2

THE ELECTROSTATIC PROPERTIES FOR KNITTED FABRICS BEFORE AND AFTER MODIFICATION	
Sample number	The time of the charge half-disappearing, minutes
0	46.0
1	9.1
2	17.4
3	0.9
4	5.7

on the nonwovens using LbL technique [32]. The phenomenon of static charging is one of the major disadvantages of man-made fibres and flat textile materials made from them. Table 2 shows results for knitted fabrics after different stages of modifications. After modification PP knitted fabrics showed, similarly to nonwovens, strong decrease in static electricity. Final change is quite similar for knitted fabric, from 45 minutes to 5.7 – which is about 88%, decrease in comparison with nonwovens, from 229 minutes to 11 – which is about 95% of decrease. The large avoidance of electrostatic charging by the application of

polyelectrolyte layers can be easily explained by the formation of ionic salt pairs between the differently charged polyelectrolytes. Furthermore, the high polarity and hydrophilicity of the polyelectrolyte layers enable the mounting of water in the polyelectrolyte layer, which can provide hydrated hydronium and hydroxyl ions. The flux of these ions compensates charging effects and avoids strongly charged domains on the sample surface.

CONCLUSIONS

Deposition of polyelectrolytes on knitted fabrics is possible and might provide a new approach to create different functions to textiles. It is possible to use exactly the same procedure as for nonwovens to obtain multifunctional product. Effects obtained for knitted fabric are very similar to those previously observed for nonwovens. The deposition of polyelectrolyte layers by the layer-by-layer method considerably modifies dyeability, hydrophilicity and electrostatic properties. The quantity effects obtained are quite similar for surface properties, however thermal decomposition (volumetric property) is slightly different, which can be explained by structural differences in initial material.

BIBLIOGRAPHY

- [1] Adamczyk, Z., Zembala, M., Michna, A. *Polyelectrolyte adsorption layers studied by streaming potential and particle deposition*. In: Journal of Colloid and Interface Science, 2006, vol. 303, issue 2, p. 353
- [2] Adamczyk, Z., Zembala, M., Kolańska, M., Warszyński, P. *Characterization of polyelectrolyte multilayers on mica and oxidized titanium by streaming potential and wetting angle measurements*. In: Colloids and Surfaces A: Physicochemical and Engineering Aspects, 2007, vol. 302, issue 1-3, p. 455
- [3] Lehr, B., Seufert, M., Wenz, G., Decher, G. *Fabrication of poly(p-phenylene vinylene) (PPV) nanoheterocomposite films via layer-by-layer adsorption*. In: Journal of Supramolecular Science, 1995, vol. 2, issue 3-4, p. 199
- [4] Sangrisub, S., Tangboriboonrat, P., Pith, T., Decher, G. *Adsorption of polystyrene-poly(4-vinylpyridine) diblock copolymer on the assembled latex film*. In: European Polymer Journal, 2005, vol. 41, issue 7, p. 1 531
- [5] Kovacević, D., Van der Burgh, S., de Keizer, A., Stuart, M. *Kinetics of formation and dissolution of weak polyelectrolyte multilayers: Role of salt and free polyions*. In: Langmuir, 2002, vol. 18, issue 14, p. 5 607
- [6] Zucolotto, V., He, J., Constantino, C., Barbosa Neto, N., Rodrigues Jr., J., Mendonça, C., Zilio, S., Li, L., Aroca, R., Oliveira Jr., O., Kumar, J. *Mechanisms of surface-relief gratings formation in layer-by-layer films from azo dyes*. In: Polymer, 2003, vol. 44, p. 6 129
- [7] Shinbo, K., Baba, A., Kaneko, F., Kato, T., Kato, K., Advincula, R., Knoll, W. *In situ investigations on the preparations of layer-by-layer films containing azobenzene and applications for LC display devices*. In: Materials Science and Engineering C, 2002, vol. 22, issue 2, p. 319
- [8] Lehr, B., Seufert, M., Wenz, G., Decher, G. *Fabrication of poly(p-phenylene vinylene) (PPV) nanoheterocomposite films via layer-by-layer adsorption*. In: Journal of Supramolecular Science, 1995, vol. 2, issue 3-4, p. 199
- [9] Yoon, H., Kim, H. *Functionalization of a poly(amidoamine) dendrimer with ferrocenyls and its application to the construction of a reagentless enzyme electrode*. In: Analytical Chemistry, 2000, vol. 72, issue 18, p. 922
- [10] Sasaki, T., Ebina, Y., Watanabe, M., Decher, G. *Multilayer ultrathin films of molecular titania nanosheets showing highly efficient UV-light absorption*. In: Chemical Communications, 2000, vol. 21, p. 2 163
- [11] Ladam, G., Schaaf, P., Cuisinier, F., Decher, G., Voegel, J. *Protein adsorption onto auto-assembled polyelectrolyte films*. In: Langmuir, 2001, vol. 17, issue 3, p. 878
- [12] Kovacević, D., Van der Burgh, S., de Keizer, A., Stuart, M. *Kinetics of formation and dissolution of weak polyelectrolyte multilayers: Role of salt and free polyions*. In: Langmuir, 2002, vol. 18, issue 14, p. 5 607
- [13] Ngankam, P., Lavalle, P., Voegel, J., Szyk, L., Decher, G., Schaaf, P., Cuisinier, F. *Influence of polyelectrolyte multilayer films on calcium phosphate nucleation*. In: Journal of American Chemical Society, 2000, vol. 122, issue 37, p. 8 998
- [14] Lu, H., Zheng, A., Xiao, H. *Properties of a novel thermal sensitive polymer based on poly(vinyl alcohol) and its layer-by-layer assembly*. In: Polymers for Advanced Technologies, 2007, vol. 18, issue 5, p. 335
- [15] Seo, J., Lutkenhaus, J., Kim, J., Hammond, P., Char, K. *Development of surface morphology in multilayered films prepared by layer-by-layer deposition using poly(acrylic acid) and hydrophobically modified poly(ethylene oxide)*, In: Macromolecules, 2007, vol. 40, issue 11, p. 4 028

- [16] Yuan, J., Xing, W., Gu, G., Wu, L. M. *The properties of organic pigment encapsulated with nano-silica via layer-by-layer assembly technique*. In: Dyes and Pigments, 2008, vol. 76, issue 2, p. 463
- [17] Yılmaztürk, S., Deligöz, H., Yılmazoğlu, M., Damyam, H., Öksüzömer, F., Naci Koç, S., Durmuş, A., Gürkaynak, A. *A novel approach for highly proton conductive electrolyte membranes with improved methanol barrier properties: Layer-by-layer assembly of salt containing polyelectrolytes*. In: Journal of Membrane Science, 2009, vol. 343, issue 1-2, p. 137
- [18] Wang, Y., Wang, X., Guo, Y., Cui, Z., Lin, Q., Yu, W., Liu, L., Xu, L., Zhang, D., Yang, B. *Electric-field-induced layer-by-layer fabrication of second-order nonlinear optical films with high thermal stability*. In: Langmuir, 2004, vol. 20, issue 21, p. 8 952
- [19] Caruso, F., Lichtenfeld, H., Donath, E., Möhwald, H. *Investigation of electrostatic interactions in polyelectrolyte multilayer films: Binding of anionic fluorescent probes to layers assembled onto colloids*. In: Macromolecules, 1999, vol. 32, issue 7, p. 2 317
- [20] Haji, A., Qavannia, S., Barani, H. *In situ synthesis and loading of silver nanoparticles on cotton fabric*. In: Industria Textilă, 2013, vol. 64, issue 1, p. 8
- [21] Stawski, D. *Application of the Layer-by-layer method for textiles*. Textiles, Uses and Production Methods, Chapter 16, pp. 507-518, Ed. Ahmed El Nembr Nova, New York, 2012
- [22] Hyde, K., Russa, M., Hinstroza, J. *Layer-by-layer deposition of polyelectrolyte nanolayers on natural fibres: cotton*. In: Nanotechnology, 2005, vol. 16, issue 7, p. 422
- [23] Hyde, G., Hinstroza, G. *Nanofibers and nanotechnology in textiles*. Edited by Brown, P. and Stevens, K., Woodhead Publishing Limited, Cambridge, England
- [24] Beknen, R., Buschmann, H. J., Schollmeyer, E. *Coating textile materials with polyelectrolytes*. In: Melland Textilberichte, 2010, vol. 91, issue 1-2, p. 43
- [25] Wang, Q., Hauser, P. *New characterization of layer-by-layer self-assembly deposition of polyelectrolytes on cotton fabric*. In: Cellulose, 2009, vol. 16, issue 6, p. 1 123
- [26] Połowiński, S. *Deposition of polymer complex layers onto nonwoven textiles*. In: Journal of Applied Polymer Science, 2007, vol. 103, issue 3, p. 1 700
- [27] Brzeziński, S., Kowalczyk, D., Połowiński, S. *Deposition of polymer complex nano-layers onto polyester fabrics activated with corona discharges*. In: Fibres & Textiles in Eastern Europe, 2009, vol. 17, issue 1, p. 87
- [28] Stawski, D., Połowiński, S. *Thermogravimetric measurements of poly(propylene) nonwovens containing deposited layers of polyelectrolytes and colloidal particles of noble metals*. In: Fibres & Textiles in Eastern Europe, 2007, vol. 15, issue 4, p. 82
- [29] Połowiński, S. *Polyelectrolyte layer-by-layer processed coated textiles*. In: Fibres & Textiles in Eastern Europe, 2005, vol. 13, issue 6, p. 50
- [30] Połowiński, S., Jantas, R. *Antibacterial and catalytic properties of textiles with modified surfaces*. In: Fibres & Textiles in Eastern Europe, 2008, vol. 16, issue 4, p. 104
- [31] Stawski, D., Bellmann, C. *Electrokinetic properties of polypropylene textile fabrics containing deposited layers of polyelectrolytes*. In: Colloids and Surfaces A: Physicochemical and Engineering Aspects, 2009, vol. 345, issue 1-3, p. 191
- [32] Stawski, D., Halacheva, S., Bellmann, C., Simon, F., Połowiński, S., Price, G. *Deposition of poly(ethylene imine)/poly(2-ethyl-2-oxazoline) based comb-branched polymers onto polypropylene nonwoven using the layer-by-layer technique. Selected properties of the modified materials*. In: Journal of Adhesion Science and Technology, 2011, vol. 25, issue 13, p. 1 481
- [33] Stawski, D., Połowiński, S., Herczyńska, L., Sarna, E., Rabiej, S. *Application of the layer-by-layer deposition method to improve the thermal stability of polypropylene non-woven fabric*. In: Journal of Applied Polymer Science, 2012, vol. 123, issue 3, p. 1 340
- [34] Stawski, D., Połowiński, S. *Hydrophilic properties of polypropylene nonwovens after polyelectrolyte layers deposition*. In: Vlákna a Textil, 2011, vol. 18, issue 1, p. 16
- [35] Gomez, Ana P., Mano, João F., Queiroz, João A., Gouveia, Isabel C. *Layer-by-layer deposition of antibacterial polyelectrolytes on cotton fibres*. In: Journal of Polymers and the Environment, 2012, vol. 20, issue 4, p. 1 084
- [36] Simon, F., Drăgan, E. S., Bucătariu, F. *Reactive polyelectrolyte multilayers onto silica particles*. In: Reactive Functional Polymers, 2008, vol. 68, issue 7, p. 1 178

Authors:

DAWID STAWSKI
STEFAN POŁOWIŃSKI
MICHAŁ PUCHALSKI

Łódź University of Technology
Department of Material, Commodity Sciences
and Textile Metrology
116 Żeromskiego street, 90-924 Łódź, Poland
e-mail: dawid.stawski@p.lodz.pl

FRANK SIMON

Leibniz-Institut für Polymerforschung Dresden e.V.
6 Hohe street, D-01069 Dresden, Germany

DOROTA ZIELIŃSKA

The Institute of Security Technologies "MORATEX",
3 M. Skłodowskiej-Curie street, 90-965 Łódź, Poland
Łódź University of Technology
116 Żeromskiego street, 90-924 Łódź, Poland

Investigation on compression properties of polyurethane-based warp-knitted spacer fabric composites for cushioning applications

Part I. Experiment*

SI CHEN

HAI-RU LONG

REZUMAT – ABSTRACT

Studiul proprietăților de comprimare ale compozitelor poliuretaneice, din tricoturi din urzeală distanțate, utilizate ca materiale de amortizare Partea I. Experiment

În cadrul acestui studiu, a fost dezvoltat un nou tip de material de amortizare, din compozite obținute din tricoturi din urzeală distanțate, pe bază de poliuretan. Pentru producerea acestor compozite, s-au utilizat cinci tipuri de materiale tricotate din urzeală stratificate, cu diferiți parametri structurali. Compozitele au fost fabricate din spumă poliuretanică flexibilă. S-a efectuat un studiu experimental cu privire la proprietățile de comprimare ale noilor materiale de amortizare realizate. Pe baza rezultatelor experimentale, curbele de deformare la comprimare și diagramele eficienței absorbției de energie au fost utilizate pentru evaluarea comportamentului la comprimare al compozitelor pe bază de poliuretan și al efectului fiecărui parametru structural. S-a observat că răspunsul la comprimare a fost influențat, în mod evident, de parametrii structurali, prin urmare există posibilitatea ca, prin modificarea acestor parametri, materialul să fie adaptat pentru a satisface cerințele utilizărilor finale.

Cuvinte-cheie: proprietăți de comprimare, compozite pe bază de poliuretan, parametri structurali, materiale tricotate din urzeală distanțate

Investigation on compression properties of polyurethane-based warp-knitted spacer fabric composites for cushioning applications Part I. Experiment

In the present work, a new type of cushioning material made from polyurethane-based warp-knitted spacer fabric composites has been developed. Five different types of warp-knitted spacer fabrics with different structure parameters were involved to produce the composites. The polyurethane-based composites were fabricated based on a flexible PU foam. An experimental study on the compression properties of these novel cushioning materials was exhibited. Based on the experimental results, both compression stress-strain curves and energy-absorption efficiency diagrams were used to analyze the compression behaviors of polyurethane-based composites and the effect of each structure parameter. It is revealed that the compression responses were obviously influenced by fabric structure parameters and it can be tailored by varying the structure parameters to meet the requirements of end-use.

Key-words: compression properties, polyurethane-based composites, structure parameters, warp-knitted spacer fabrics

Cushioning materials are used to absorb kinetic energy of the impacting mass while keeping subject avoiding high-energy impact. They absorb kinetic mechanical energy under compression actions at a relatively constant stress over a larger range of displacement. To compress these kinds of materials can be seen as the kinetic energy of a mass which might impact on them [1].

There are a larger number of materials with energy absorption characteristics for cushioning applications. Polyurethane (PU) foams are one of the most widely used cushioning materials. They are well known for their excellent elasticity and toughness. However, cushioning applications require PU foams not only have excellent elasticity and toughness, but also outstanding compressive strength [2] – [4]. Thus, in order

to obtain better compression properties, PU foams are often reinforced by other materials in end-use.

Nowadays, textile structures are commonly used as reinforced materials. The growing requirements of complex performance need more and more novel textile structures to be developed [5] – [9]. Warp-knitted spacer fabrics are one of the novel materials. Warp-knitted spacer fabrics have two separate layers connected by spacer yarns. The spacer yarns have different arrangements depending on different functions. And the distance between top and bottom layers can be designed. In addition, the structures of surface layers could be the same or different. All of these advantages offer warp-knitted spacer fabrics a great potential to be used in composite materials [10] – [15].

Therefore, according to the abovementioned feature, the polyurethane-based warp-knitted spacer fabric composites can be seen as a new type of material for

* Part I/ First part

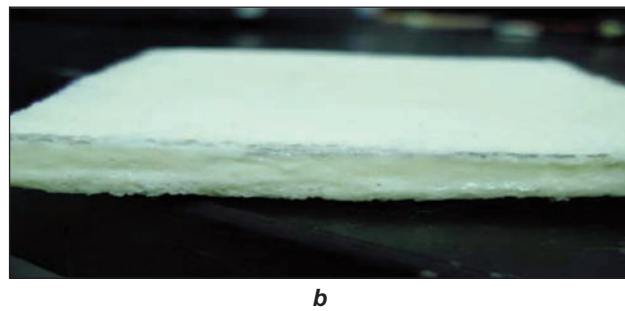
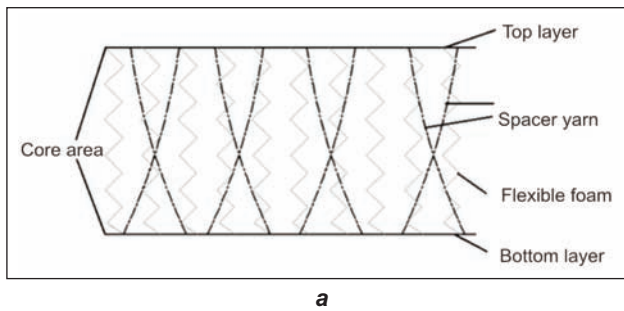


Fig. 1. Schematic illustration and real appearance of polyurethane-based warp-knitted spacer fabric composites

cushioning applications. The schematic and appearance of the composites can be seen in figure 1 a, b. In an attempt to discuss the effect of fabric structural parameters on the compression properties of polyurethane-based composites, a series of warp-knitted spacer fabrics with different parameters (i.e. inclination angle, thickness, fineness of spacer yarn) were fabricated on a double-needle-bar warp knitting machine of gauge 18. It is expected that a regular pattern of compression properties could be found from this study.

EXPERIMENTAL PART

Warp-knitted spacer fabrics preparation

Warp-knitted spacer fabrics were produced on a double-needle-bar Raschel warp knitting machine of gauge 18 (Wuyang Co. Ltd. – Jiangsu, China). Figure 2 shows the basic structure of this machine. The front guide bars (GB 5 and GB 6) knit a surface layer fabric on the front needle bar only, while the back bars (GB 1 and GB 2) knit the other separate surface layer fabric on the back needle bar. The middle bars (GB 3 and GB 4) carry the spacer yarns and knit on both needle bars in succession to connect two outer layers. Figure 3 represents the schematic of warp-knitted spacer fabrics (the real appearances can be seen in figure 8). Five types of warp-knitted spacer fabrics

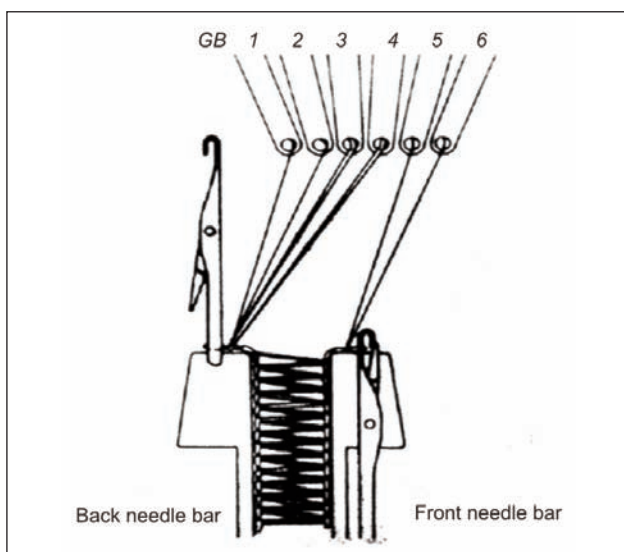


Fig. 2. Model of double-needle-bar warp knitting machine

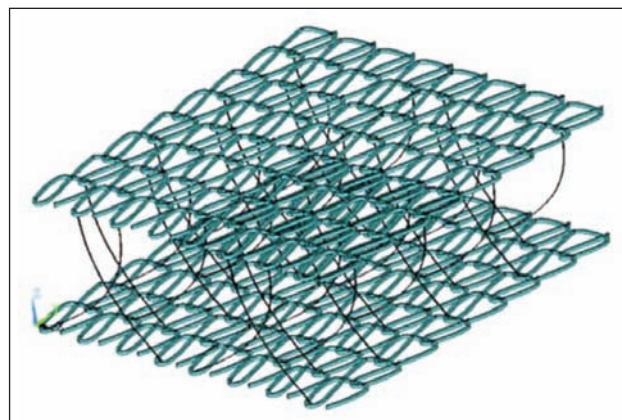


Fig. 3. The schematic display of warp-knitted spacer fabrics

Table 1

STRUCTURE PARAMETERS OF SPACER YARNS			
Symbol	Diameter, mm	Chain notation	Threading
I	0.2	1-0 3-2/3-2 1-0//	1 full 1 empty
II	0.2	1-0 4-3/4-3 1-0//	1 full 1 empty
III	0.16	1-0 4-3/4-3 1-0//	1 full 1 empty

with different structure parameters were prepared in this paper.

The materials of spacer fabrics were polyethylene terephthalate monofilament, 0.2 mm (0.16 mm) in diameter, for spacer yarns and polyethylene terephthalate multifilament, 300 D/96 F, for the surface layer yarns.

And the surface layer structures are chain + inlay. Two chain notations were involved for spacer yarns to connect outer layers. The structure parameters of spacer yarns are presented in table 1. The resultant thickness and density of spacer fabrics after setting at 180°C for 3 minutes are listed in table 2.

Polyurethane-based composites preparation

The flexible polyurethane foam was formed by having a polymer compound and water reacting, in a 10/0.8 mixing ratio – by weight (Dubang Materials Co. Ltd. – Shanghai, China). The polymer compound whose density is 0.876 g/cm³ is obtained by the reac-

STRUCTURE PARAMETERS OF WARP-KNITTED SPACER FABRICS					
Specimen	Thickness, mm	Course-wise density, w/5 cm	Wale-wise density, c/5 cm	Spacer yarn	Spacer yarn/cm ² *
A ₁	7.68	34.95	28.25	I	69.98
A ₂	7.72	35.35	27.86	II	53.48
A ₃	7.71	35.15	28.96	III	52.31
A ₄	6.12	33.35	28.24	I	68.79
A ₅	10.62	35.12	29.15	I	70.32

* Spacer yarn/cm² means the number of spacer yarns per square centimeter

Table 3

FINISHED PROPERTIES OF POLYURETHANE FOAM AND SANDWICH COMPOSITES			
Sample	Fabric area density, g/m ²	Density of foam filling, g/cm ³	Weight ratio of fabric/foam, %
A ₁	889.1	0.795	10.3/89.7
A ₂	881.7	0.795	10.2/89.8
A ₃	760.38	0.795	8.9/91.1
A ₄	820.3	0.795	9.9/90.4
A ₅	1097.6	0.795	12.4/87.6

tion of polyisocyanate with polyhydroxy polyether polyol. The foaming work can be done at room temperature. The foaming and filling process was fulfilled in mould. The reactants were filled into warp-knitted spacer fabrics in wale direction. After foaming, the specimens were placed for 72 hours until the foam is cured. The weight ratio of spacer fabrics/polyurethane foam and finished properties of polyurethane foam are listed in table 3.

Compression test

The compression tests were conducted by using Shanghai HL WDW series material test instrument, and the test was done at 23°C and 65% relative humidity based on the Chinese standard GB/T8168-2008. The compression plate is a circle whose diameter is 60 mm. The specimens were pressed to a deformation with 60% of the initial thickness at a load speed of 12 mm/minutes and five repeats were carried out for each specimen. Each compression stress-strain curve showed in figure 4 is an average of the five experimental results.

RESULTS AND DISCUSSIONS

Compression curves of stress-strain and energy absorption

Based on stress-strain diagrams, the absorbed energy which is defined as the area below stress curve can be investigated. However, it is more directly to use the energy-absorption diagrams to understanding

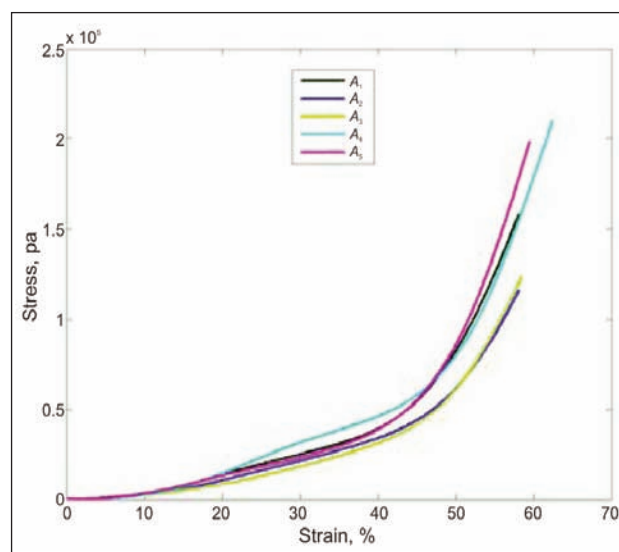


Fig. 4. The stress-strain curves of polyurethane-based composites

the energy absorption properties [5]. An energy absorption diagram is obtained by plotting the absorbed energy per unit volume W as a function of the strain ε . It can be calculated by equation (1):

$$W = \int_0^{\varepsilon} \sigma(\varepsilon) d\varepsilon \quad (1)$$

where:

W is the absorbed energy per unit volume;

σ – the stress at the strain ε ;

ε – the strain.

In order to better investigate the energy absorption capacities, the energy absorption efficiency E is involved to analyze its energy absorption process. The energy absorption efficiency E is defined as the ratio of the energy absorbed by a real material at a given strain and energy absorbed by an ideal one that transmits the same but constant force at the same strain condition [14]. The absorption efficiency E can be expressed by equation (2):

$$E = \frac{\int_0^{\varepsilon} \sigma(\varepsilon) d\varepsilon}{\sigma} \quad (2)$$

Based on stress-strain and efficiency curves, it's easy to find out the relationships between stress and

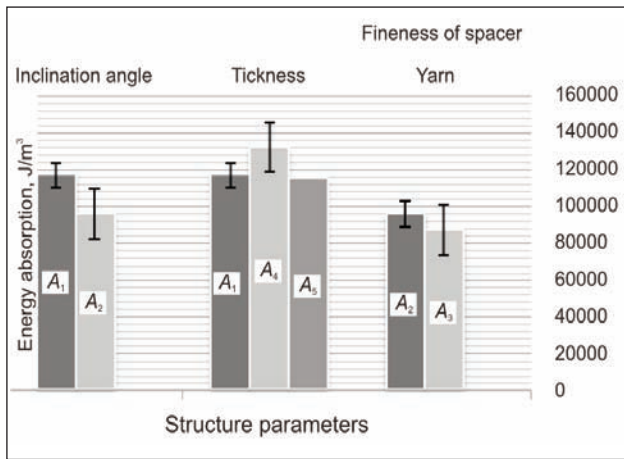


Fig. 5. The amount of absorbed energy at 60% strain

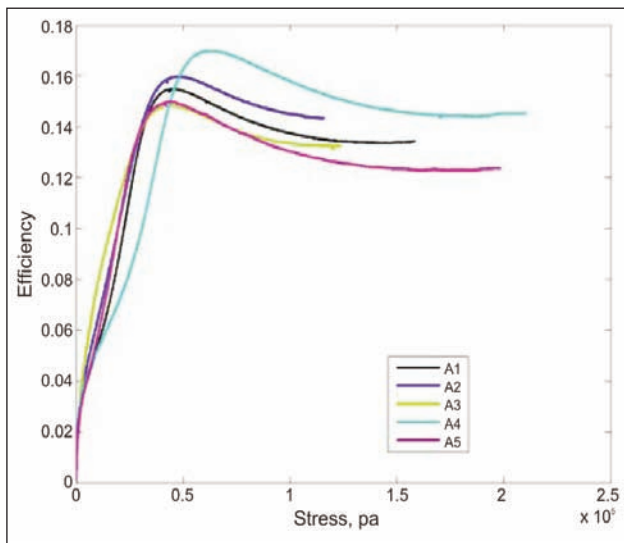
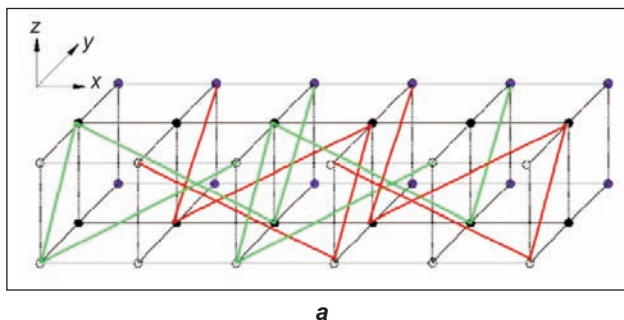


Fig. 6. The energy-absorption efficiency curves of polyurethane-based composites

energy absorption behaviors. It is convenient to choose the appropriate materials for special applications for which the amount of energy to be absorbed is determined according the investigations. In light of the abovementioned equations, the amount of absorbed energy at 60% strain is shown in figure 5 while the energy-absorption efficiency diagrams are presented in figure 6.



Effect of the spacer yarn inclination angle

Spacer yarns are used to connect two surface layers, the angle between spacer yarns and surface layers along weft direction is defined as inclination angle. Inclination angle depends on the chain notations of *GB 3* and *GB 4* (table 1 and table 2). Figure 7 shows the global arrangements of spacer yarns of type I and type II. In figure 7, the *X*, *Y* and *Z* axes indicate the direction of weft, wale, and thickness of spacer fabrics, respectively. Three adjacent courses are put in three planes: the white dots representing the first course are placed in the first plane, while the black and blue dots representing the second and third courses are placed in the subsequent two planes.

The red lines and green lines represent the chain notations of *GB 3* and *GB 4*, respectively. It can be found that the chain notations of *GB 3* and *GB 4* are exactly symmetrical and the inclination angle decreases as the chain notations increase. The sequence of inclination angle for specimens A_1 and A_2 is $A_1 > A_2$. The real arrangements of spacer yarns are shown in figure 8.

The compression stress-strain curves of A_1 and A_2 are shown in figure 4, it can be revealed that the compression resistance abilities increase as the inclination angle increases. Based on the energy-absorption curves shown in figure 5, it can be found that the specimen with larger inclination angle has ~17.8% higher amount of absorbed energy per unit volume when compared to the corresponding sample. And in figure 6, it can be observed that the maximum efficiency decreases as the inclination angle increases. And the stress value at maximum efficiency point increases with the inclination angle decreasing. It is shown that at a higher stress level, the specimen with smaller inclination angle has higher efficiency of energy absorption.

However, if the stress level is lower, the efficiency of specimen with smaller inclination angle will become lower whereas the efficiency of specimen with larger inclination angle will be higher.

In summary, the specimen with smaller inclination angle has better performance on the energy absorption capacities at higher stress level as the specimen with larger inclination angle is more appropriate for absorbing energy at lower stress level.

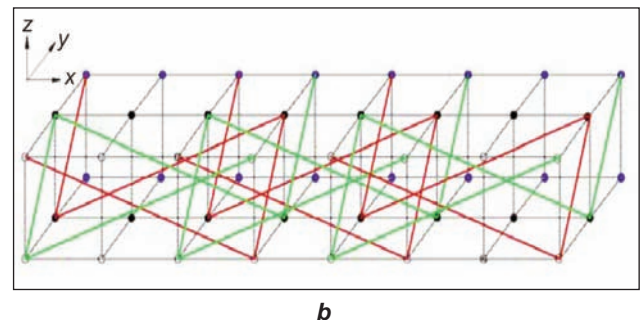
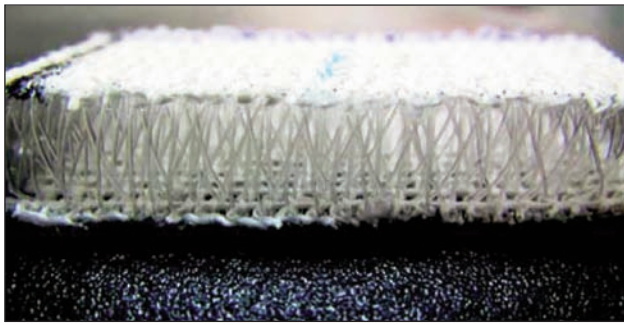
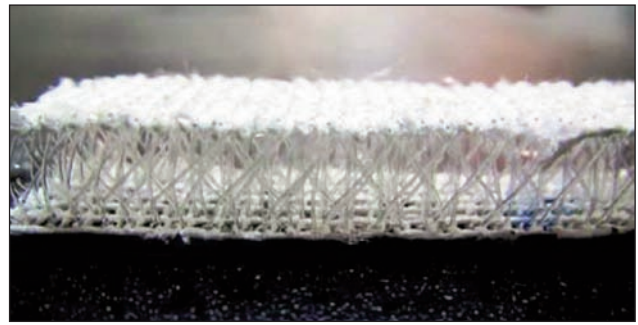


Fig. 7. The global arrangements of spacer yarns: a – type I; b – type II



a



b

Fig. 8. The real appearances of spacer yarn arrangements:
a – type I; b – type II

Effect of the thickness

Three specimens, A_1 , A_4 and A_5 , with the same spacer yarn type and surface layer structure were involved in this section. However, the thickness of these specimens is different.

It can be revealed from stress-strain curves that the anti-compression abilities decrease as the thickness increases at the small strain stage. After the strain reaches about 50%, the phenomenon is reversed. It is indicated that the compression resistance capacities and thickness are closely related. However, the amount of absorbed energy for specimen with lowest thickness is higher than the others. It can be seen from figure 6 that the maximum efficiency points decrease as the thickness increases. However, the thinner specimen achieves its maximum efficiency point at a higher stress level while the thicker one reaches its maximum efficiency value at a lower stress level. In that case, the specimens made by different thickness have their own ranges of applications. It is inappropriate to simply compare the energy absorption capacities of different thickness specimens. It is needed to take the amount of energy to be absorbed and allowed stress level into consideration when choosing the thickness of materials. Moreover, the efficiency diagram can be a good tool for determining the thickness of composites.

Effect of the fineness of spacer yarn

Specimens A_2 and A_3 have the same spacer yarn type but different diameters (0.2 mm and 0.16 mm). These two specimens also have the similar thickness and outer layer density.

The stress-strain curves of these two specimens show that the effect of fineness of the spacer yarns on anti-compression capacities is not significant. The specimen with coarser spacer yarn has better performance on the compression resistance abilities when the deformation is lower than $\sim 50\%$. However, after the strain reaches $\sim 50\%$, the situation is reversed. According to the energy absorption diagrams, it is found that A_2 absorbs $\sim 8.9\%$ higher amount of absorbed energy per unit volume than that of A_3 at the same deformation condition. It can be revealed from the energy -absorption efficiency diagrams that the maximum efficiency value increases with diameter

increasing. And the stress level at maximum efficiency point is a little higher for specimen made with coarser spacer yarn when compared to the finer one. However, it is observed that the specimen made with finer spacer yarn has a higher efficiency in the condition that the stress level is below 0.3 Mpa. If the stress value is higher than 0.3 Mpa, the specimen made with coarser spacer yarn will have higher efficiency. In a word, the specimen made with coarser space yarn is suitable for absorbing energy at a higher stress level and specimen made with finer space yarn is suitable for lower stress level energy absorption.

CONCLUSIONS

In this paper, a new type of cushioning material made from polyurethane-based composites reinforced by warp-knitted spacer fabrics was successfully manufactured. Compression tests were carried out to investigate the compression properties of polyurethane-based composites. The following conclusions were based on this work:

- The structure parameters of warp-knitted spacer fabrics obviously influence the energy absorption capacities. Thus, the energy absorption characteristics of polyurethane-based composites can be tailored by easily varying the fabric structure parameters to meet end-use requirements.
- The energy-absorption efficiency diagrams can be used as a useful tool for investigating the energy absorption behaviors. With the help of efficiency diagrams, it is easy to choose the specimens with suitable structure parameters for absorbing a given amount of energy at its allowed stress level.
- The composites with larger inclination angle, finer spacer yarn, higher fabric thickness are suitable for absorbing energy at lower stress level with higher efficiency. In contrast, the composites with smaller inclination angle, coarser spacer yarn, lower fabric thickness can be used to absorb energy at higher stress level. Therefore, it is important to select the appropriate fabric structure parameters when the composites are used as an energy absorber.

ACKNOWLEDGEMENT

The authors would like to thank the Chinese Universities Scientific Fund for the financial support given to this work [grant number 13D310104].

BIBLIOGRAPHY

- [1] Avalle, M., Belingardi, G., Montanini, R. *Characterization of polymeric structure foams under compressive impact loading by means of energy-absorption diagram*. In: International Journal of Impact Engineering, 2011, vol. 25, issue 2, p. 11
- [2] Lu, Q. S., Sun, L. H., Yang, Z. G. *Optimization on the thermal and tensile influencing factors of polyurethane-based polyester fabric composites*. In: Composites. Part A, 2010, vol. 41, issue 4, p. 997
- [3] John, J., Bhattaeharya, M. *Characterization of polyurethane foams from soybean oil*. In: Journal of Apply Polymer Science, 2002, vol. 86, p. 3 097
- [4] Suhreta, H., Ivan, J., Zoran, S. P. *Thermal and mechanical properties of glass reinforced soy - based polyurethane composites*. In: Composites Science Technolygy, 2005, vol. 65, p. 19
- [5] Liu, Y. P., Hu, H. *Compression behavior of warp-knitted spacer fabrics for cushioning applications*. In: Textile Research Journal, 2011, vol. 82, issue 1, p. 11
- [6] Pamuk, G., Ceken, F. *Comparison of the mechanical behavior spacer knit cotton and flax fabric reinforced composites*. In: Industria Textilă, 2013, vol. 64, issue 1, p. 3
- [7] Verpoest, I., Wevers, M., de Meester, P., Declercq, P. *2.5D- and 3D-fabrics for delamination resistant composite laminates and sandwich structures*. In: SAMPE Journal, 1989, vol. 25, issue 3, p. 51
- [8] Mehment, K., Hakan, G., Ivens, J., Nevin, K. *Low velocity impact characteristics of 3D integrated core sandwich composite*. In: Textile Research Journal, 2012, vol. 82, issue 9, p. 945
- [9] Bruer, S. M., Smith, G. *Three-dimensionally knit spacer fabrics: a review of production techniques and applications*. In: Journal of Textile Apparel Technology Manage, 2005, vol. 4, issue 6, p. 23
- [10] Miao, X. H., Ge, M. Q. *Indentation force deflection property of cushioning warp-knitted spacer fabrics*. In: Journal of Textile Research, 2009, vol. 30, issue 4, p. 43
- [11] Hu, H., Sun, B. Z. *A comparative study of the impact response of 3D textile composites and aluminum plates*. In: Journal of Composite Materials, 2010, vol. 44, issue 8, p. 593
- [12] Luo, D., Daniel, I. M., Luo, J. J., Schubel, P. M. *Three-dimensional characterization of textile composites*. In: Composites - Part B, 2008, vol. 39, issue 1, p. 13
- [13] Mouritz, A. P., Bannister, M. K., Falzon, P. J. *Review of applications for advanced three-dimensional fiber textile composites*. In: Composite - Part A, 1999, vol. 30, issue 12, p. 1 445
- [14] Liu, W. J., Sun, B. Z., Hu, Hong, Gu, B. H. *Compressive behavior of biaxial spacer weft knitted fabric reinforced composite at various strain rates*. In: Polymer Composite, 2007, vol. 28, issue 2, p. 224
- [15] Miltz, J., Gruenbaum, G. *Evaluation of cushioning properties of plastic foams from compressive measurements*. In: Polymer Engineering Science 1981, vol. 21, issue 2, p. 1 010

Authors:

SI CHEN
HAI-RU LONG
School Of Textile
Donghua University
2999 North Renmin Road, Shanghai 201620
P. R. China

Corresponding author:

HAI-RU LONG
e-mail: ansn9119@126.com; 40989087@qq.com



ESD properties assessment of fabrics with bilayer structure

ANDREI SEBASTIAN ARDELEANU
EFTALEA CĂRPUȘ
RĂZVAN SCARLAT

EMILIA VISILEANU
CARMEN MIHAI
ALEXANDRA ENE

REZUMAT – ABSTRACT

Estimarea proprietăților ESD ale materialelor textile cu structură bistrat

În articol sunt studiate proprietățile ESD ale materialelor textile cu structură bistrat, prin intermediul a două metode: analiza curentului de descărcare electrostatică și analiza timpilor de repartizare a sarcinilor. Pentru a efectua analiza curentului de descărcare s-a recurs la o metodă numerică, aceasta putând fi utilizată pentru studierea diferitelor configurații ale structurii bistrat. Scopul analizei l-a constituit stabilirea modului în care curentul de descărcare este influențat de conductivitatea electrică a stratului aflat în contact cu arc electric. Cea de-a doua metodă a fost utilizată pentru a investiga modul în care se comportă o structură bistrat cu două fețe active, în comparație cu o structură bistrat cu o singură față activă.

Cuvinte-cheie: materiale textile ESD, curent de descărcare, timp de descărcare, structură bistrat

ESD properties assessment of fabrics with bilayer structure

This paper aims to investigate the ESD properties of fabrics with bilayer structure, using two methods: electrostatic discharge current analysis and the charge decay time analysis. For the discharge current analysis a numerical method was used as it can be used to evaluate different configurations of the bilayer structure. The purpose of this analysis was to determine how the discharge current is influenced by the electrical conductivity of the layer in contact with the electrical arc. The second method was used to investigate how a bilayer structure with two active faces behaves in comparison with a bilayer structure with only one active face.

Key-words: ESD fabrics, discharge current, charge decay time, bilayer structure

The electrostatic discharge (ESD) can be defined as a sudden transfer of electrostatic charge between two objects of different potentials. The charge can be accumulated on an object through different mechanism (friction, corona or induction charging) [1] – [3], modifying its potential. When this charged object comes in the vicinity of an uncharged object, an electrostatic discharge appears. This is accompanied by a high energy transfer and may cause malfunctions and even irreparable damages of sensitive devices. To overcome these issues, ESD protective solutions are developed, which reduce the risk of an electrostatic discharge. These solutions must be continuously improved as the electrical components become increasingly more sensitive to electrostatic events, due to their miniaturization.

Development of new improved solutions can be achieved by assessing, through proper testing methods, their abilities to prevent an ESD. Over the years the researchers have developed a series of testing methods with the role to investigate different parameters which could relate to the ability of a solution to protect against ESD events. These methods investigated parameters such as: surface and volume resistivity, charge decay time or discharge current.

Surface and volume resistivity measurement is driven by the fact that charge accumulation and dissipation is strongly related with the material's resistivity. However, this type of measurement raises contradic-

tory requirements that must be achieved by an ideal ESD protective material:

- it must have a high conductivity, in order to quickly dissipate the potential accumulated charge;
- it must have a high resistivity in order to minimize the energy transfer during an ESD event [4].

The solution to these requirements is to use dissipative materials which, according to Standard EN 1149-5: 2008, must have a half decay time of the electric field under 4 seconds or a surface resistance under $2.5 \times 10^9 \Omega$ [5]. The method of measuring the surface resistivity consists in using two electrodes placed at a certain distance on the tested material and measuring the resistivity between them [6] – [9]. Similar, the volume resistivity is measured by placing the electrodes on each of two sides of the material and measuring the resistivity between them.

A material that can quickly dissipate the electrostatic charge rarely will accumulate sufficient charge to cause an ESD. Thus, measuring its charge decay time will provide a measure about the material's ESD performances. The methods consist in charging the material through different mechanisms and measuring the time needed for the charge to decay up to a certain level. Considering the charging mechanisms, methods that use contact charging [10] – [13], corona charging [14], induction charging [15] and triboelectric charging [15] – [17] can be distinguished. The parameters measured within these methods are:

- $t_{50\%}$ – time needed for the charge to decay to 50% of the maximum value;
- $t_{1/e}$ – time needed for the charge to decay to 1/e of the maximum value;
- $t_{10\%}$ – time needed for the charge to decay to 10% of the maximum value or t_{30} – the charge measured after 30 seconds.

The peak discharge current is another important parameter to be investigated when testing ESD protective materials, as its value is closely related with ESD damages. If the peak value exceeds a certain threshold supported by an electrical component, then ESD damage will appear. The methods used to analyze the discharge current consist in charging the material up to a certain level and after that measuring the discharge current from the material to an ESD probe [4], [17] – [21].

All the previously presented methods are analytical methods based on experiments made on real ESD protective materials. A different approach to test the materials is by using numerical simulations [22], [23]. These simulations present a series of advantages as they can easily vary different parameters which in real experiments would be hard to achieve. For example, the concentration of the active element that helps dissipate the charge, the configuration of an ESD structure or dimensional parameters of the constituent elements can be given.

In this paper, different configurations of a bilayer ESD fabric are analyzed through numerical simulations. The tested fabric consists in two overlapping layers, one made from electrical conductive yarns and the other one from non-conductive yarns. The parameter which will be analyzed is the discharge current generated by an ESD simulator, also known as ESD Gun, for different configurations of the ESD fabric. The role of these simulations is to find which configuration is best: the one with the outer layer made from conductive yarns or from non-conductive yarns. According to the obtained results, different samples will be manufactured and tested for their ESD performances. For these samples an analytical method will be used, namely measuring the charge decay time.

EXPERIMENTAL PART

Discharge current analysis method

Assessing the ability of a material to provide protection against electrostatic discharges can be achieved by analyzing the discharge current generated by an electrostatic discharge simulator, also known as electrostatic discharge gun (ESD gun). These simulators reproduce typical human-metal discharges and can provide information about a system's immunity to electrostatic discharges. For an easier analysis of ESD properties, software modelling of these simulators can be used. In figure 1, the equivalent structure of an ESD gun made in CST Studio Suite, MWS module, is presented. It consists of metal and dielectric elements, lumped circuits and ports. The metallic elements are made from perfect electrical conductor (PEC), while the dielectric elements are made from a

material with the following properties: electric permittivity $\epsilon = 1$ F/m, magnetic permeability $\mu = 1$ H/m and electrical conductivity $\sigma = 1$ S/m. The lumped circuits are used to obtain a better match between the measured and simulated discharge current. These circuits actually are RLC series or parallel circuits (fig. 2). Port P_1 is used to generate the excitation signal, modelled as a step function with a 1 ns rising time and a 4 kV maximum value, while port P_2 is used to measure the discharge current.

The fabric subject to ESD simulations consists of two layers with a knitted structure. The materials used for the two layers were rubber and polyamide as non-conductive materials and copper and graphite as conductive materials. The investigation was performed considering the layer in contact with the electrical arc as the inner layer, while the other one as the outer layer (fig. 3). The materials of the two layers were changed to investigate which configuration gives the best results: conductive or non-conductive layer in contact with the electrical arc.

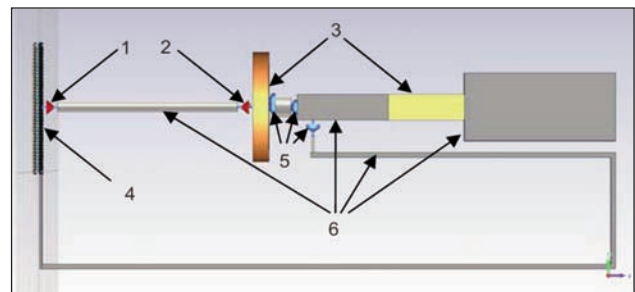


Fig. 1. ESD gun equivalent structure: 1 – P_1 is discharge current analysis port; 2 – P_2 is signal generator port; 3 – dielectric elements; 4 – ESD tested sample; 5 – lumped circuits; 6 – metallic elements

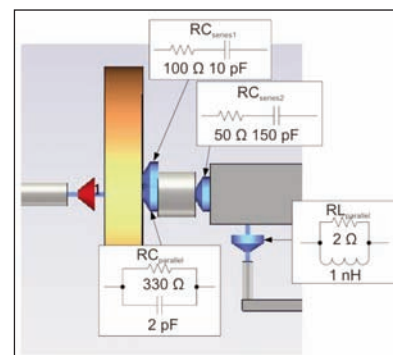


Fig. 2. ESD Gun's lumped circuits

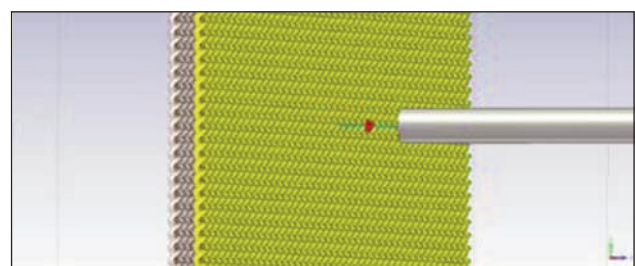


Fig. 3. Detail of tested fabric

Charge decay analysis method

Charge decay analysis provides information about the ability of an ESD fabric to dissipate the accumulated charge. As the time needed for the charge to reach a certain level is smaller, the tested fabric presents better ESD properties. The method consists in charging the fabric up to a certain level, connecting it to the ground and monitoring the charge dissipation. The experimental setup consists in a Charge Plate Monitor (CPM), an oscilloscope, a discharge electrode, a switch normally open and a set of insulators made from polycarbonate. The fabric is placed on the CPM's plate while one of its ends is connected to ground through the discharge electrode and the switch normally open. To prevent the charge leaking to ground through the discharge electrode, the electrode was placed on the polycarbonate insulators. The CPM has a 5 kV internal power source used to charge the fabric placed on the CPM's plate. After the charging is performed, the power source is disconnected and the switch is closed so as the charge is dissipated to the ground. The discharge signal is recorded with the oscilloscope and the data will be used to determine the charge decay times.

For charge decay time analysis, a series of bilayer knitted samples with two active faces (table 1) were tested, based on the conclusions of a previous research [12] when a type of yarn was recommended to be used for one face of the fabric F_1 and other three yarns were recommended to be used for the other face of the fabric F_2 . Within the present paper F_1 was made with the recommended yarn (f_2) while for F_2 two of the three yarns were used (f_3 and f_5) and an additional yarn (f_4) was added for testing. To evaluate the improvement obtained by using a bilayer structure with two active faces, 4 bilayer structures with one active face made with each of the four yarns ($f_2 - f_5$) were tested for their charge decay times. The samples' sizes were dimensionally conceived based on CPM plate's dimensions. Thus, the samples had a width of 15 cm, equal with the plate's side, and a length of 30 cm, so as the clamping area of the discharge electrode is at a distance equal with the plate's side. Two measurements were made for each sample: one when F_1 is connected to the discharge path and the other when F_2 is connected to the discharge path. This way charge dissipation can be analyzed separately for each two faces.

Table 1

STRUCTURE AND COMPOSITION OF THE TESTED SAMPLES				
Sample	Structure	Face 1, F_1	Face 2, F_2	Conductive yarn percentage
M_1	Plated jersey	1 × cotton + 1 × f_2	1 × cotton + 3 × f_4	6%
M_2	Plaited rib	1 × cotton + 1 × f_2	1 × cotton + 2 × f_3	5%
M_3	Plaited jersey	1 × cotton + 1 × f_2	1 × cotton + 2 × f_3	5%
M_4	Plaited rib	1 × cotton + 1 × f_2	1 × cotton + 3 × f_3	6%
M_5	Plaited jersey	1 × cotton + 1 × f_2	1 × cotton + 1 × f_3	4%
M_6	Plaited jersey	1 × cotton + 1 × f_2	1 × cotton + 2 × f_4	6%
M_7	Plaited jersey	1 × cotton + 1 × f_2	1 × cotton + 1 × f_4	5%
M_8	Plaited rib	1 × cotton + 1 × f_2	1 × cotton + 1 × f_4	4.5%
M_9	Plaited rib	1 × cotton + 1 × f_2	1 × cotton + 2 × f_4	6%
M_{10}	Plaited jersey	1 × cotton + 1 × f_2	1 × cotton + 1 × f_5	4.5%
M_{11}	Plaited jersey	1 × cotton + 1 × f_2	1 × cotton + 2 × f_5	6%
M_{12}	Plaited jersey	1 × cotton + 1 × f_2	1 × cotton + 3 × f_5	7.5%
M_{13}	Plaited rib	1 × cotton + 1 × f_2	1 × cotton + 3 × f_5	7.5%
M_{14}	Plaited rib	1 × cotton + 1 × f_2	1 × cotton + 2 × f_5	6%
M_{15}	Plaited rib	1 × cotton + 1 × f_2	1 × cotton + 1 × f_5	4.5%
M_{16}	Plaited rib	1 × wool + 1 × f_2	1 × wool + 1 × f_5	4.5%
M_{17}	Plaited rib	1 × wool + 1 × f_2	1 × wool + 2 × f_5	6%
M_{18}	Plaited rib	1 × wool + 1 × f_2	1 × wool + 2 × f_5	7.5%
M_{19}	Plaited jersey	1 × wool + 1 × f_2	1 × wool + 3 × f_5	7.5%
M_{20}	Plaited jersey	1 × wool + 1 × f_2	1 × wool + 2 × f_5	6%
M_{21}	Plaited jersey	1 × wool + 1 × f_2	1 × wool + 1 × f_5	4.5%

Note: f_2 is cotton yarn (75%) + epitropic yarn (25% – carbon coated polyester);

f_3 – Nega-Stat P210, polyester filament with outer trilobal carbon core;

f_4 – Nega-Stat P190, polyester filament with inner trilobal carbon core;

f_5 – nylon filaments surface saturated with carbon particles

RESULTS AND DISCUSSIONS

Discharge current

In figure 4 the signals of the discharge currents obtained for the configurations where the inner layer (Int) was made from materials with good electrical conductivity (copper – Cu and graphite – Gr) while the outer layer (Ext) was made from materials with low electrical conductivity (polyamide – Pa and rubber – Cc) are presented. From figure 4 a and figure 4 b it can be observed that by changing the low conductive material of the outer layer, the shape and values of the discharge current remains the same. In figure 4 c the discharge currents for the configurations when the outer layer remains the same (polyamide) and the inner layer is changed (copper versus graphite) are presented. It can be observed that the shapes of the discharge currents remain the same but the values for the configuration based on copper are greater than the values for the configuration based on graphite. As expected, the graphite determines lower values of the discharge current, as its conductivity is smaller than that of copper. In figure 5 different configurations where the outer layer is made from good conductive materials (Cu or Gr) while the inner layer is made from low conductive materials (Pa or Cc) are presented. Yarns' diameter of the inner layer was varied between 0.02 mm and 0.5 mm. From the simulated results it can be observed that by changing the thickness of the inner yarn, the shape of the discharge current present significant changes, but when the outer material is changed the shape of the discharge current doesn't show significant changes (figures 5 a–d). In figures 5 e–f it can be observed that the discharge current's values vary

when the inner material is the same while the outer material is changed. Again the values for the graphite version are smaller than that of copper. Analyzing these simulations it can be observed that the peak values of the discharge current are much smaller when the layer in contact with the electrical arc is made from materials with low electrical conductivity than when it's made from materials with high electrical conductivity (1.5 – 2.5 A versus 40 – 45 A). Therefore, a bilayer structure can provide a good protection to accidental electrostatic discharges on low conductive layer and a good drainage of the accumulated charge on its high conductive layer. This will be further investigated, by analyzing the charge decay times of different samples with a bilayer structure and two active faces.

Charge decay time

Four bilayer samples, where one face was made from textile yarns (passive face) while the other one was made with each of the four yarns $f_2 - f_5$ (active face) were tested for their charge decay times. Since f_2 is set to be used on F_1 , it will be compared with the other three yarns $f_3 - f_5$ (fig. 6). $U/2$ and U/e are the half value respectively $1/e$ value of the maximum potential reached by the samples at their charged state. Next, the 21 bilayer samples with two active faces, described in table 1, are tested for their charge decay times and the results for 6 representative samples are presented in figure 7. On the first column the samples with a plating patent structure are presented while in the second column the samples with a plating stitch structure are presented. The first row is designated to the samples containing the f_3 fibre, the second row for the f_4 fibre and the third row for the f_5

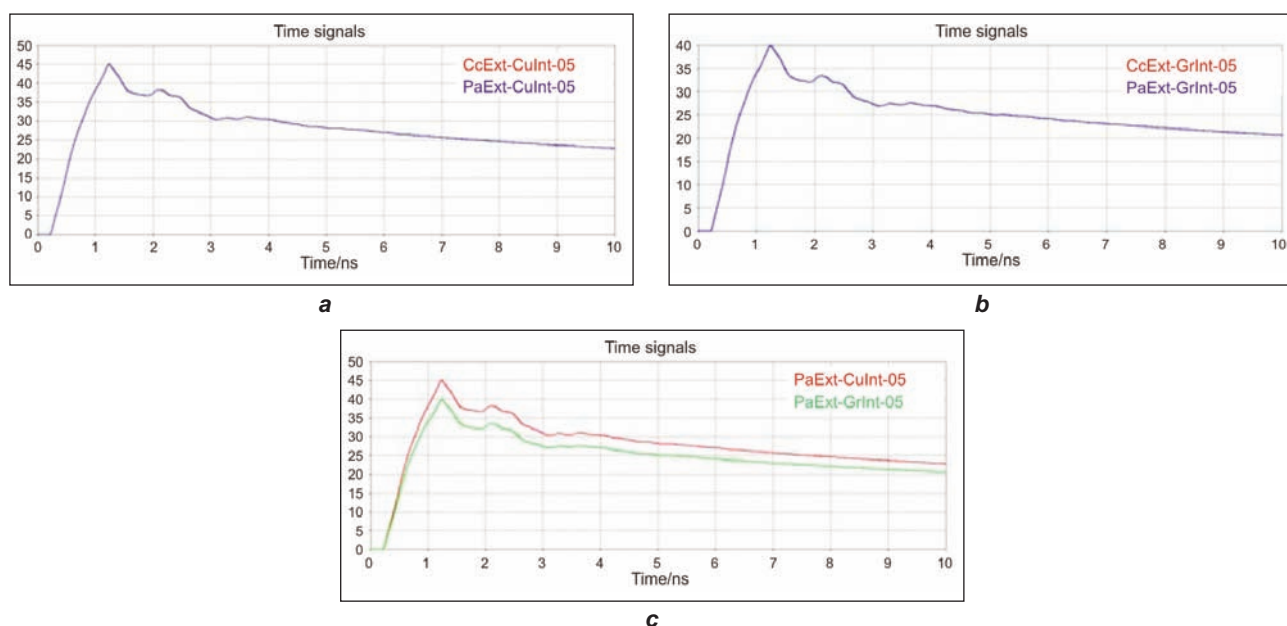


Fig. 4. Discharge current for the following configurations:
a – inner layer copper (CuInt) + outer layer rubber (CcExt) or polyamide (PaExt);
b – inner layer graphite (GrInt) + outer layer rubber (CcExt) or polyamide (PaExt);
c – inner layer copper + outer layer polyamide versus inner layer graphite + outer layer polyamide

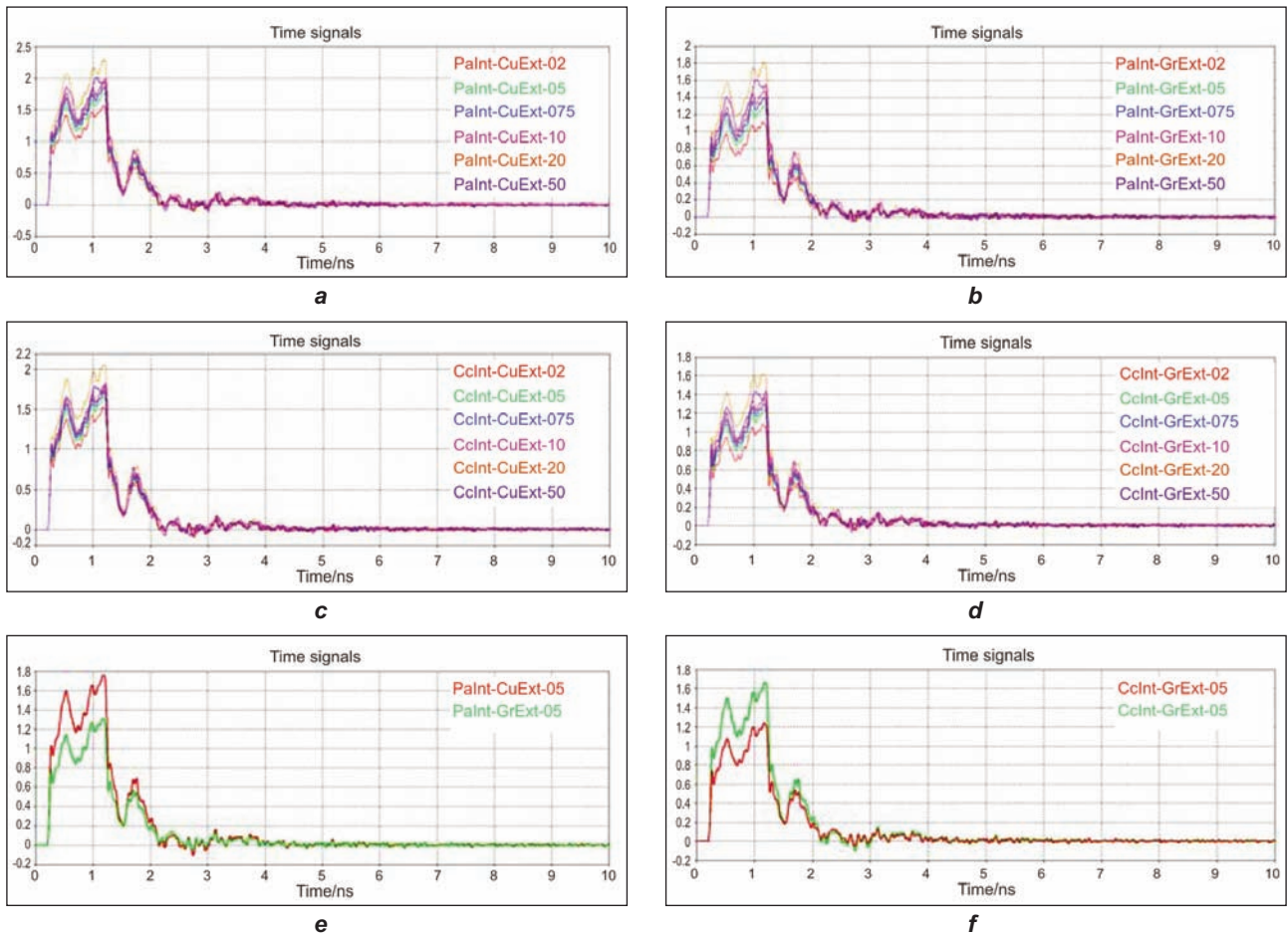


Fig. 5. Discharge current for the following configurations:
 a – inner layer polyamide (PaInt) + outer layer copper (CuExt); b – inner layer polyamide (PaInt) + outer layer graphite (GrExt); c – inner layer rubber (Cclnt) + outer layer copper (CuExt); d – inner layer rubber (Cclnt) + outer layer graphite (GrExt); e – inner layer polyamide + outer layer copper versus inner layer polyamide + outer layer graphite; f – inner layer rubber + outer layer copper versus inner layer rubber + outer layer graphite

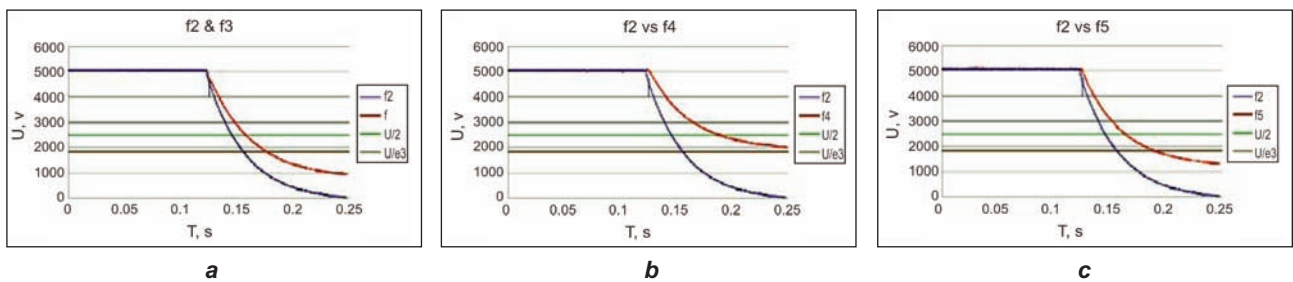


Fig. 6. Comparison of charge decay times for bilayer structures with one active face:
 a – f_2 versus f_3 ; b – f_2 versus f_4 ; c – f_2 versus f_5

fibre. Within this bilayer setup, with two active faces, an improvement can be observed in the charge decay times of the F_2 face. If in figure 6 the charge decay times were weaker for F_2 than those for F_1 , in figure 7 an improvement can be observed as the times for F_2 became similar with those of F_1 . It can be said that the presence of the f_2 yarn in F_1 improves the performances, in terms of charge decay time, of the F_2 face where the weak yarns $f_3 - f_5$ are used. If the results are analyzed based on the knitting technique, it can be said that no significant changes are observed.

CONCLUSIONS

Within this paper, the properties of knitted fabrics with bilayer structure were investigated using two methods. The parameters which were investigated are the discharge current and the charge decay time. For the discharge current, a numerical method was used which consisted in modelling the bilayer structure and the ESD gun in a software environment. Using software simulations provide a series of advantages, as the parameters of the tested fabric can be easily modified. This way, the discharge current was analysed for different yarns with various sizes and different

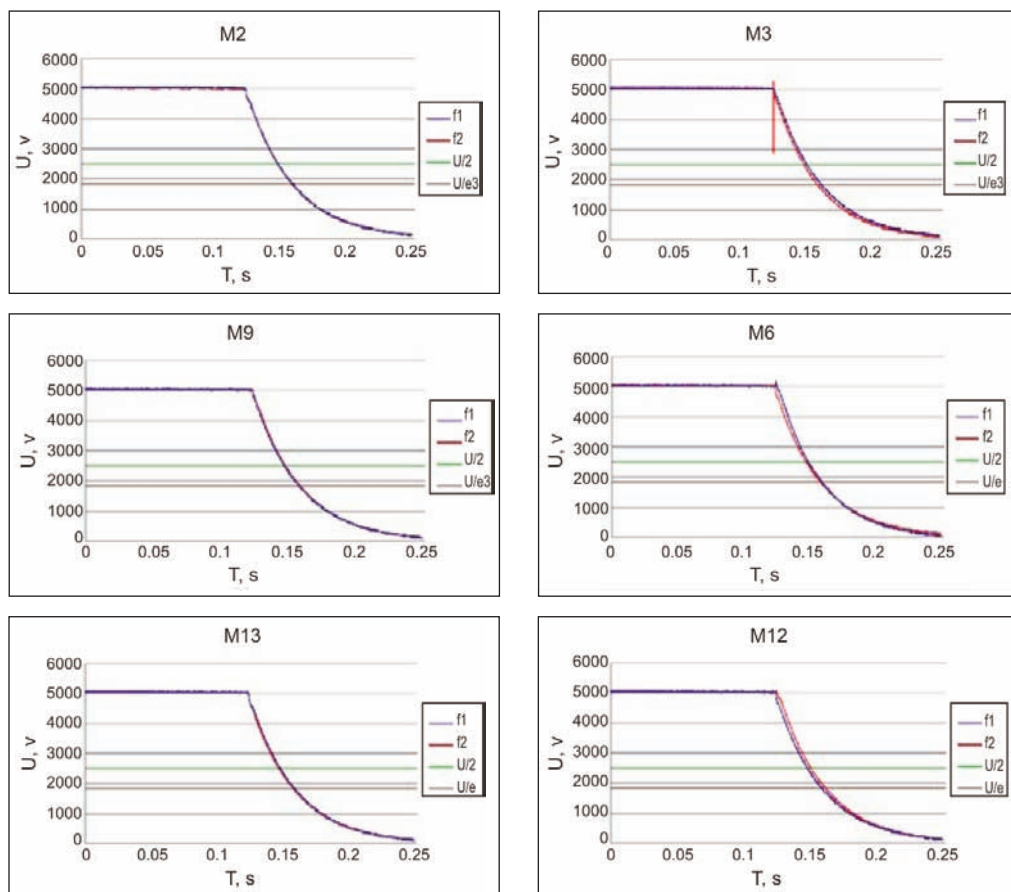


Fig. 7. Charge decay times for bilayer samples

configurations of the bilayer structure. It was observed that for the layer with low electrical conductivity the discharge current takes smaller values than for the layer with high electrical conductivity. Thus it can be said that a bilayer structure can provide protection against accidental electrostatic discharges through its low conductive layer (small discharge current) and good charge drainage through its high conductive layer.

The charge decay analysis was intended to investigate how the ESD performances of a bilayer structure with two active faces are improved compared with a bilayer structure with only one active face. Four types of yarns were tested, one of which presented better charge decay times than the others.

This was observed when the samples with only one active face were tested for their charge decay time. When the samples with two active layers, one made with the yarn with the best performances and the other made with each of the other yarns, were tested for their charge decay times, it an improvement was observed for the other three yarns. Combined with the more efficient yarn, the other three yarns presented better charge decay times, similar with the ones obtained for the first yarn.

ACKNOWLEDGEMENT

This work was supported by a grant of the Romanian National Authority for Scientific Research, CNDS-UEFISCDI, project PCCA 179 - 2012 "Haine ESD realizate din fibre cu miez conductor tricotate bistrat".

BIBLIOGRAPHY

- [1] Schmeer - Lioe, G. *Anwendungsorientierte Prufung des elektrostatischen Verhaltens von Textilien*. In: Technische Textilien, 2000, vol. 43, p. 182
- [2] Chubb, J. N. *Comments on methods for charge decay measurement*. In: Journal of Electrostatics, 2004, vol. 62, p. 73
- [3] Cieslak, M., Wrobel, S. *Assessment of textiles based on three test methods of charge decay time*. 7th International Symposium EL-TEX, 2006, pp. 16-17
- [4] Paasi, J., Nurmi, S., Kalliohaka, T., Coletti, G., Gustavino, F. et al. *Electrostatic testing of ESD protective clothing for electronics industry*. In: Electrostatics Conference, 2003, p. 239
- [5] Standard EN 1149-5:2008: *Protective clothing – Electrostatic properties*. Part 5: Material performance and design requirements, 2008

- [6] Standard IEC 61340-5-1: *Protection of electronic devices from electrostatic phenomena*. General requirements, 1998
- [7] Standard EN 1149-1: *Protective clothing – Electrostatic properties*. Part 1: Test methods for measurement of surface resistivity, 1996
- [8] Standard EN 100015-1: *Protection of electrostatic sensitive devices*. Part 1: General requirements, 1992
- [9] Cieslak, M., Wrobel, S., Kaminska, I., Lao, M. *Functional upholstery materials for protection against electrostatic risk*. In: *Fibres & Textile in Eastern Europe*, 2009, issue 17, p. 52
- [10] Donciu, C. *Core conductive yarn based integral knitted ESD garments*. Part I. Metallic core conductive yarns investigation. In: *Advanced Materials Research*, 2013, vol. 772, p. 467
- [11] Donciu, C. *Core conductive yarn based integral knitted ESD garments*. Part II. Carbon composite yarns investigation. In: *Advanced Materials Research*, 2013, vol. 772, p. 474
- [12] Donciu, C. *ESD Garments with bilayer structure*. In: *Advanced Materials Research*, 2014, vol. 837, p. 682
- [13] Donciu, C. *Estimating ESD properties of fabrics based on correlation between dielectric losses and charge decay time*. In: *Advanced materials Research*, 2014, vol. 837, p. 688
- [14] Standard IEC 61340-2-1: *Electrostatics*. Part 2.1: Measurement methods - Ability of materials and products to dissipate static electric charge, 2002
- [15] Standard EN 1149-3: *Protective clothing - Electrostatic properties*. Part 3: Test method for measurement of charge decay, 2004
- [16] Gustavino, F., Coletti, G., Dardano, A., Torello, E. *Some experiments about the triboelectric performances of composite textiles*. Annual Report Conference on Electrical Insulation and Dielectric Phenomena, 2004, p. 85
- [17] Chubb, J. N. *Tribocharging studies on inhabited cleanroom garments*. In: *Journal of Electrostatics*, 2008, vol. 66, p. 531
- [18] Fast, L., Paasi, J., Kalliohaka, T., Borjesson, A., Smallwood, J. *Direct discharges from ESD fabrics*. The 1st Nordic ESD Conference, 2003
- [19] Paasi, J., Smallwood, J., Salmela, H. *New methods for the assessment of ESD threats to electronic components*. Proceedings EOS/ESD Symposium, EOS-25, 2003, p. 151
- [20] Paasi, J., Salmela, H., Tamminen, P., Smallwood, J. *ESD sensitivity of devices on a charged printed wiring board*. Proceedings EOS/ESD Symposium, EOS-25, 2003, p. 143
- [21] Paasi, J., Salmela, H., Kalliohaka, T., Fast, L., Smallwood, J. *Experimental comparison of probes for air discharge measurements*. International Conference Applied Electrostatics, 2004
- [22] Tappura, K., Nurmi, S. *Computational modelling of charge dissipation of fabrics containing conductive fibers*. In: *Journal of Electrostatics*, 2003, vol. 58, p. 117
- [23] Fast, L., Börjesson, A., Paasi, J. *Can ESD-protective garments screen static electric fields?* In: *Journal of Electrostatics*, 2005, vol. 63, issues 6–10, p. 621

Authors:

Asist. univ. drd. ANDREI SEBASTIAN ARDELEANU
 Electrical Engineering Faculty
 Ghe. Asachi Technical University
 21-23 Dimitrie Mangeron Bvd., 700050 Iași
 e-mail: a.ardeleanu@ee.tuiasi.ro

Prof. dr. eng. EFTALEA CĂRPUȘ
Eng. RĂZVAN SCARLAT
Dr. eng. EMILIA VISILEANU
Dr. eng. ALEXANDRA ENE
Dr. eng. CARMEN MIHAI

National Research and Development Institute for Textiles and Leather
 16 Lucrețiu Pătrășcanu street, 030508 Bucharest
 e-mail: eftalea.carpus@ns.certex.ro



Textile materials treated with antimicrobial skin care emulsion optimized by mathematical modelling

ANGELA CEREMPEI
ABRAMIUC DANKO
CRIȘAN POPESCU

RODICA MUREȘAN
AUGUSTIN MUREȘAN

REZUMAT – ABSTRACT

Materiale textile tratate cu emulsie antimicrobiană de îngrijire a pielii, optimizată prin modelare matematică

Produsele aromaterapeutice au un rol important în industria medicală, în special în domeniul cosmetic. Utilizarea produselor naturale în acest domeniu asigură o îmbunătățire a efectelor terapeutice, păstrând biocompatibilitatea și nontoxicitatea, fapt dovedit de medicina tradițională. Proprietățile antibacteriene au fost obținute prin utilizarea propolisului, iar aromaterapia a fost asigurată de uleiul esențial de salvie. Acest amestec poate fi folosit cu succes atât ca tonifiant pentru piele, reducând efectele îmbătrânirii, cât și pentru tratarea acneei sau a rănilor apărute pe piele. Pentru a asigura o eliberare controlată a produselor, acestea au fost înglobate într-o matrice de chitosan. Compoziția emulsiei a fost optimizată cu ajutorul modelului matematic central compozițional rotabil 2k, cu trei variabile independente.

Cuvinte-cheie: ulei esențial de salvie, propolis, chitosan, optimizare matematică

Textile materials treated with antimicrobial skin care emulsion optimized by mathematical modelling

Aromatherapy products have an important role in medical industry, especially in modern cosmetic field. The use of natural products in this field grants enhanced therapeutically effects proven also by traditional medicine maintaining biocompatibility and toxic free. Antimicrobial properties have been obtained using propolis and aromatherapy is provided by the sage essential oil. The mixture can be successfully used as skin toner, improving anti-aging and as treatment of acne or other skin wounds. The products are embedded in chitosan matrix in order to ensure controlled release. The emulsion composition has been optimised using mathematical modelling 2k composed central rotatable program with 3 independent variables.

Key-words: sage essential oil, propolis, chitosan, mathematical optimisation

Multifunctional textiles applications in the medical field are generated from the needs of practice as well as from continuous evolution of medical science. A personal skin care product should grant skin healthiness comfort, refreshing feeling and protection. The performance of a skin care product is judged by numerous factors where most important should be compatibility, biodegradability, environmental friendly, lack of toxicity and efficiency. Embedding the biologically active component into the macromolecular biopolymer is a procedure studied over the last decades worldwide [1] – [3]. The polymer is used as protective carrier for the bioactive compound during the transfer until it is released. Natural products are used in modern cosmetic industry because of the benefits people found using them. Essential oils extracted from plants can be used for toning, acne treatment and scar healing regaining the natural and healthy state of the skin. Sage is used in traditional medicine for more than 2 500 years, known to have therapeutic characteristics [4]. Propolis is used today as supplements, or preventing inflammatory infections, diabetes, heart and hepatic diseases, known because its antibacterial, antiseptic, antifungal properties [5] – [6].

This paper deals with development of skincare textiles with optimised biologically active emulsion containing propolis and sage essential oil embedded in chitosan film. The optimisation process was based on mathematical modelling 2k composed central rotatable program with three independent variables [7]. Controlled release, enhanced treatment efficiency without side effects of the natural products contributed to the development of new biodegradable polymer/biologically active compound system that can provide an ideal solution to obtain skincare products with targeted delivery of active compounds.

EXPERIMENTAL PART

Materials and methods

Sage essential oil (extract of *Salvia Officinalis*) purchased from Fares S.A., Romania. Propolis ethanol extract (EEP) solution 30% (w/v) was prepared from raw propolis with ethanol pro analysi. The extraction took place at 25°C, in a dark environment for 48 hours. Raw propolis was procured from a private apiary in the North-East region of Romania. Chitosan (molecular weight 100 000–300 000 and degree of deacetylation 85%) was obtained from Fluka Chemie GmbH,

Switzerland. The polysorbate 80 "Tween 80" was supplied by Merck, Germany. Vegetable glycerol (purity 99.5%) was purchased from S.C. Elemental SRL, Romania. Scoured and bleached 100% cotton knitted fabrics were used in the experiment.

Antibacterial study was conducted against *Staphylococcus aureus* ATCC– 6538 and *Escherichia coli* ATCC – 10536. The microbial dilution was 11.8 UOI. The incubation took place at 37°C for 24 hours. Kirby-Bauer disc diffusion method was used and as result the inhibition diameter was determined.

Camspec M501 Single Beam Scanning UV/Visible Spectrophotometer was used in order to evaluate the controlled release of bioactive compounds.

The textile substrate used in this study was produced on a circular knitting machine Mesdan Lab Knitter, gauge 10E. The yarn count was Nm 60/1. The structural parameters of the finished fabrics are:

- horizontal density, $D_h = 50$ wales/5 cm;
- vertical density, $D_v = 58$ rows/5 cm;
- stitch length = 4.25 mm;
- fabric mass = 105 M/m².

An important advantage in using knitted fabrics is that such materials present significantly less transfer of fibres on the human skin, compared to traditional woven materials. The transfer is practically eliminated when the fabrics are impregnated with the emulsion considered for the current study.

Emulsion development

The chitosan solution was obtained by solving chitosan in acetic acid 1% solution (in order to ensure the complete solving of chitosan). The solution was stirred for 24 hours at room temperature and filtered in order to remove impurities, and sterilised at 120°C for 15 minutes 1% (w/v) chitosan solution was used for experiments. To develop the mathematical model, experimental planning has been made considering (X_i) as independent variables:

- X_1 is chitosan concentration, ml/l;
- X_2 – ethanol extracted propolis concentration, ml/l;
- X_3 – sage essential oil concentration, ml/l;

According to experimental planning generated by the mathematical model the emulsion was obtained as follows: in the chitosan solution, at room temperature (25°C), a mixture of essential oil and propolis was added under magnetic stirring for 15 minutes. For every experimental sample, 25 ml/l glycerine and 200 ml/l Tween 80 were added over the pre-obtained

mixture and the emulsion obtained is maintained under stirring 10 minutes at room temperature.

RESULTS AND DISCUSSIONS

Variation step and limits for the real and coded independent variables were selected based on previous experiments (table 1). The experimental plan and the results obtained for antimicrobial activity of each sample (on *Staphylococcus aureus* bacteria) are shown in table 2. Also predicted values for the antibacterial activity (Y_{calc}) were obtained from the mathematical model for the regression equation and presented in table 2.

The regression equation of the mathematical model with three independent variables is:

$$Y = b_0 + b_1X_1 + b_2X_2 + b_3X_3 + b_{12}X_1X_2 + b_{13}X_1X_3 + b_{23}X_2X_3 + b_{11}X_1^2 + b_{22}X_2^2 + b_{33}X_3^2 \quad (1)$$

The coefficients of the regression equation have been determined by the method of least squares using the matrix relation:

$$b = (XT \cdot X)^{-1} \cdot XT \cdot Y \quad (2)$$

where:

b is column matrix of regression coefficients, b_i ;

X – coded variables matrix, X_i ;

Y – experimental values column matrix of regression equation, Y_i .

The significance of the regression equation coefficients has been tested by means of the "t" test (Student), the non-significant values being removed. Applying the "t" test following has been considered:

- for a b_i coefficient, $t_{b_i} calc. = b_i/s$, where s is the standard deviation of b_i ;
- for a b_{ij} coefficient, $t_{b_{ij}} calc. = b_{ij}/s$, where s is the standard deviation of b_{ij} .

If $|b_{calc} > t \cdot b_{crit}|$ (critical value, dependent on the freedom degree ($f_1 = 10$; $f_2 = 1$) and the significance level ($\alpha = 0,05$)), it is admitted that at the chosen significance level the coefficient is significant and it is kept in the regression equation. Otherwise the value of that coefficient can be omitted. The coefficients and the trust limit are shown in table 3. After the "t" test the b_1 , b_{12} and b_{13} coefficients were insignificant and therefore the value considered for them in the regression equation is 0. From this test it has been concluded that the chitosan concentration doesn't have

Table 1

VARIATION STEP AND LIMITS FOR INDEPENDENT REAL AND CODED VARIABLES						
Component	Variation step	Coded values				
		-1.682	-1	0	1	1.682
		Real values				
Chitosan – X_1 , ml/l	89.18	0	60.8	150	239.2	300
Propolis – X_2 , ml/l	29.73	0	20.3	50	79.7	100
Sage es. oil – X_3 , ml/l	11.89	0	8.1	20	31.9	40

Table 2

EXPERIMENTAL PLANNING AND THE RESULTS FOR THE ANTIBACTERIAL ACTIVITY								
Experiment variant	Chitosan, X_1		Propolis, X_2		Sage es. oil, X_3		Antibacterial Activity, Y , mm	Antibacterial activity, Y_{calc} , mm
	coded	real	coded	real	coded	real		
1	-1	60.8	-1	20.3	-1	8.1	9	5.51
2	+1	239.2	-1	20.3	-1	8.1	6	5.51
3	-1	60.8	+1	79.7	-1	8.1	10	10.39
4	+1	239.2	+1	79.7	-1	8.1	8	10.39
5	-1	60.8	-1	20.3	+1	31.9	10	7.44
6	+1	239.2	-1	20.3	+1	31.9	8	7.44
7	-1	60.8	+1	79.7	+1	31.9	10	10.82
8	+1	239.2	+1	79.7	+1	31.9	8	10.82
9	-1.682	0	0	50	0	20	5	7.12
10	+1.682	300	0	50	0	20	9	7.12
11	0	150	-1.682	0	0	20	0	4.14
12	0	150	+1.682	100	0	20	15	11.09
13	0	150	0	50	-1.682	0	10	10.63
14	0	150	0	50	+1.682	40	13	12.61
15	0	150	0	50	0	20	12	12.83
16	0	150	0	50	0	20	12	12.83
17	0	150	0	50	0	20	14	12.83
18	0	150	0	50	0	20	12	12.83
19	0	150	0	50	0	20	14	12.83
20	0	150	0	50	0	20	13	12.83

Table 3

COEFFICIENTS FOR REGRESSION EQUATION AND THE SIGNIFICANCE LIMITS		
Coefficient	Value	Significance limit
b_0	12.8277	-
b_1	-	0.235966
b_2	2.0660	
b_3	0.5899	
b_{12}	-	0.245798
b_{13}	-	
b_{23}	-0.3750	
b_{11}	-2.0185	0.181891
b_{22}	-1.8418	
b_{33}	-0.4278	

a significant importance for the antibacterial activity. This response was predicted from previous experiments were chitosan was tested and found that at concentrations of 1% the antibacterial activity is insignificant.

The mathematical equation (3) describes the dependences between the proposed independent values for obtaining cosmetic disks (X_1 is chitosan concen-

tration, X_2 – EEP concentration and X_3 – essential oil concentration) and dependent value as optimisation criteria – antibacterial activity:

$$Y = 12.827 + 2.066X_2 + 0.589X_3 - 0.375X_2X_3 - 2.018X_1^2 - 1.841X_2^2 - 0.427X_3^2 \quad (3)$$

The adequacy of mathematical model was verified using Fisher test, F :

$$F_{calc} = \frac{(n-1) \sum_{i=1}^n (Y_{ei} - \bar{Y}_e)^2}{(k-1) \sum_{j=1}^k (Y_{ekj} - \bar{Y}_{ek})^2} \quad (4)$$

where:

Y_{ei} is experimental values of dependent variable;

\bar{Y}_e – average value of dependent variable;

Y_{ekj} – experimental values of dependent variable from the centre matrix;

\bar{Y}_{ek} – average value of dependent variable from the centre matrix;

$k = 6$ – total number of experiments from the centre matrix;

$n = 20$ – total number of experiments from the experimental matrix.

The obtained value F is compared with the tabled value F_{tab} ($\alpha = 0.05$; $f_1 = 10$, $f_2 = 1$) = 242. The values obtained for the model adequacy are

VALUES OBTAINED FOR THE MODEL ADEQUACY					
Function	$\sum_{i=1}^n (Y_{ei} - Y_e)^2$	$\sum_{i=1}^n (Y_{eki} - Y_{ek})^2$	F_{calc}	F_{tab}	$F_{calc} < F_{tab}$
Y	4594.2	24.16667	190.1048	242	Adequate

presented in table 4. If $F_{calc} < F_{tab}$, the mathematical model is adequate (95% probability), and the concordance of the model and the experimental data is statistically acceptable for a level of significance of $\alpha = 0.05$. The mathematical model adequacy for $n = 20$ and $k = 6$ is shown.

Matlab software was used to generate a series of 3D and 2D graphics. Highlighting the interaction effects of significant factors on the regression equation (Y) was performed by drawing the response surfaces and constant level curves which represents the values of dependent variables.

First the values are computed and the graphic is drawn varying only one independent variable, $Y_i = Y_i(X_i)$ and the other two are kept in the centre of experimental space ($X_j = 0$), aiming at the variation of the dependent value. Second, it is computed and plotted the regression equation values obtained by holding

one independent value in the centre of experimental space and the other two having values from the entire experimental space.

Analysing the graphical representation of the variation of one independent value and the other two maintained in the centre of experimental space (fig. 1) the following conclusions can be drawn:

- maximal values for antibacterial activity are obtained for medium values of all three independent variables located in the centre of the experimental space;
- the antibacterial activity is rising with the increase of concentrations for propolis and essential oil, the maximum value is between 0 and 1. Over this level the antibacterial activity is no longer improved and therefore the product will be inefficient.

Varying the parameters X_1 and X_2 , while $X_3 = 0$ – constant in the centre of the experimental space (fig. 2) it

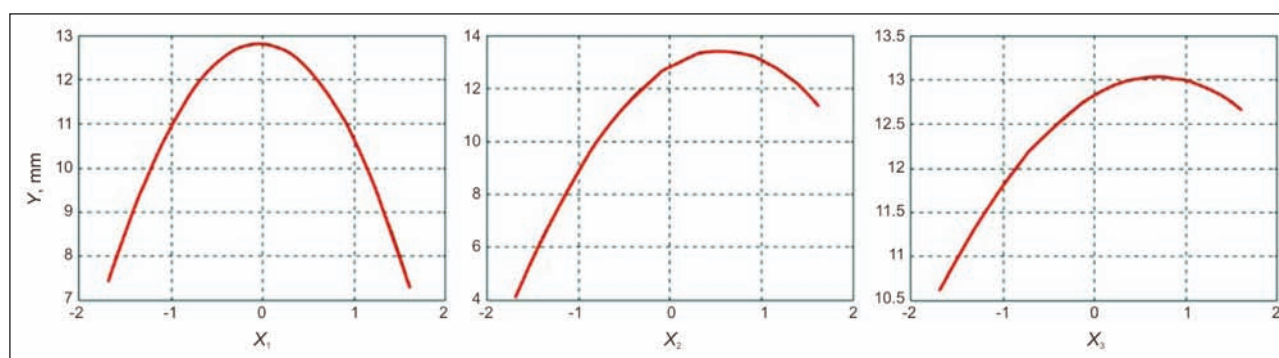


Fig. 1. Independent variables influence on the antibacterial activity, Y

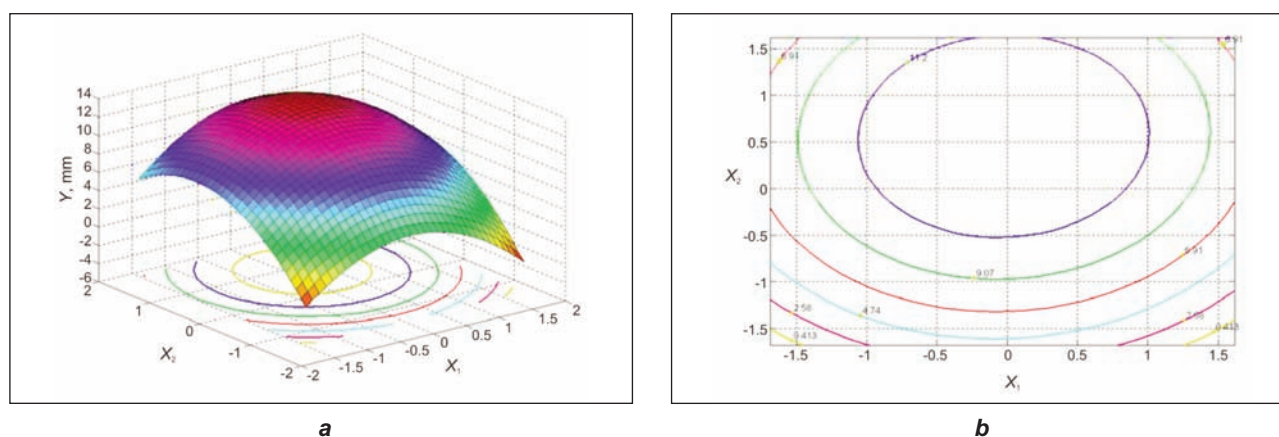
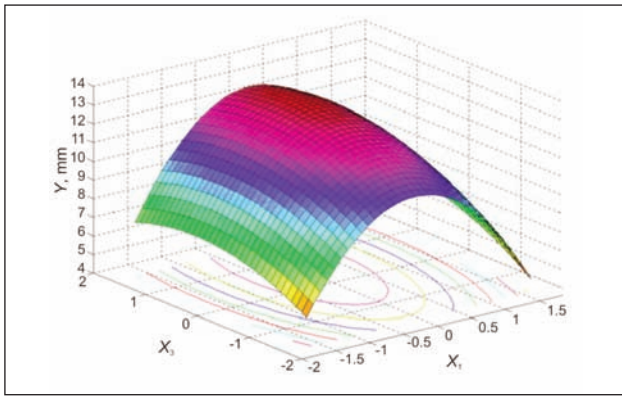
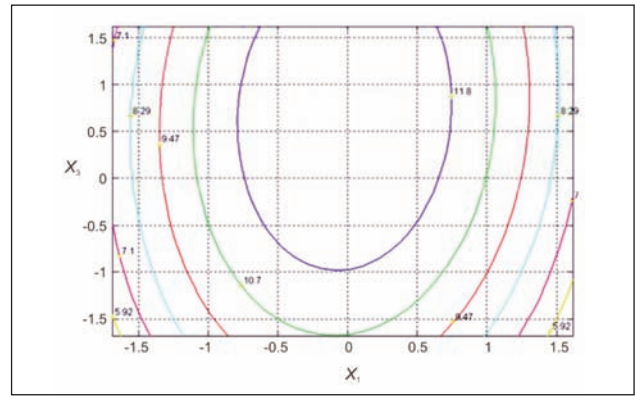


Fig. 2. Influence of the independent variables X_1 and X_2 on antibacterial activity, Y:
a – response surface; b – constant level curves

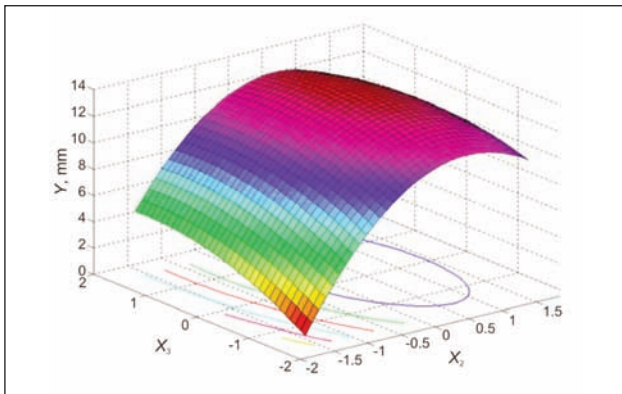


a

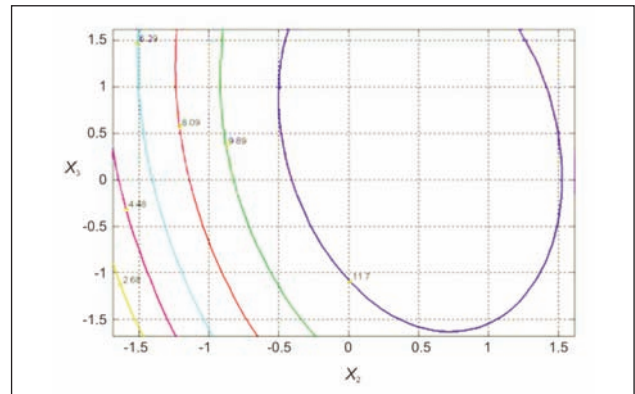


b

Fig. 3. Influence of the independent variables X_1 and X_3 on antibacterial activity, Y :
a – response surface; b – constant level curves



a



b

Fig. 4. Influence of the independent variables X_1 and X_3 on antibacterial activity, Y :
a – response surface; b – constant level curves

can be seen that maximum values for antibacterial activity are obtained for concentration of $X_1 = -0.5 \div 0.5$ and $X_2 = -0.5 \div 1.682$. Through derivation the exact values are $X_1 = 0$; $X_2 = 0.561$, $X_3 = 0$, and after encoding the values: $X_1 = 150$ ml/l; $X_2 = 66.7$ ml/l; $X_3 = 20$ ml/l.

The antibacterial activity influenced by variation of X_1 , X_3 , meanwhile $X_2 = 0$ (fig. 3) is maximum for: $X_1 = -0.5 \div -1.5$ and $X_3 = -1 \div 1.682$. Through derivation the exact values are $X_1 = 0$; $X_2 = 0$; $X_3 = 0.69$, meaning: $X_1 = 150$ ml/l; $X_2 = 50$ ml/l; $X_3 = 28.2$ ml/l.

Varying the concentrations for X_2 , X_3 and maintaining $X_1 = 0$ (fig. 4), the antibacterial activity is good for values between: $X_2 = 0 \div 1$; $X_3 = -1.6 \div 1.682$. Through derivation, the optimal values are: $X_1 = 0$; $X_2 = 0.514$; $X_3 = 0.464$, and after encoding the values: $X_1 = 150$ ml/l; $X_2 = 65.3$ ml/l; $X_3 = 25.5$ ml/l.

To obtain the optimal value from the regression equation Y , the classic method of finding the stationary minimum or maximum points (X_1 , X_2 and X_3) was used. Finding those points consists in solving a

3 equation system with 3 unknowns, obtained from equalling with 0 the partial derivatives of the regression equation in relation with each independent variable. After solving the system the following results are presented:

- $X_1 = 0.0000$ and the encoded value for chitosan concentration is 150 ml/l;
- $X_2 = 0.5136$ and the encoded value for propolis extract concentration is 65.3 ml/l;
- $X_3 = 0.4644$ and the encoded value for sage essential oil concentration is 25.5 ml/l.

A new emulsion with those concentrations was created and applied on textile substrate, to determine the antibacterial activity of the emulsion obtained. The antibacterial results are presented in figure 5 where the diameter of inhibition of *Escherichia coli* is 13 mm and for *Staphylococcus aureus* is 15 mm.

The study of controlled release of the active compounds from the textile substrate, the sample was immersed in 0.3% Tween 80 solution, and analysed by spectrophotometer the concentration of the released chemicals over a preset time intervals. The maximum absorbance wave length for sage essential



Fig. 5. Antibacterial activity

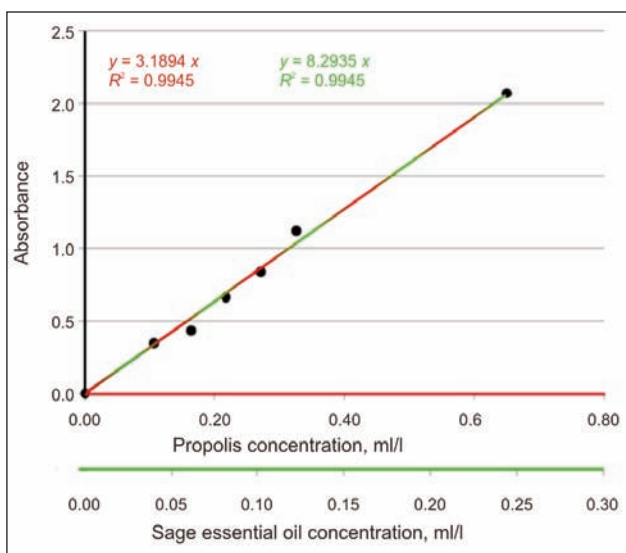


Fig. 6. Standard fitting curves

oil as well as for propolis extract was determined for $\lambda = 290$ nm.

From the emulsion composition the concentrations for sage essential oil and propolis extract were calculated according to standard curves presented in figure 6.

The regression equation for propolis concentration is: $y = 3.1894 \cdot X$; $R^2 = 0.9945$ and for sage essential oil concentration is: $y = 8.2935 \cdot X$; $R^2 = 0.9945$.

The control released curves presented in figure 7 show that a significant amount of active compounds

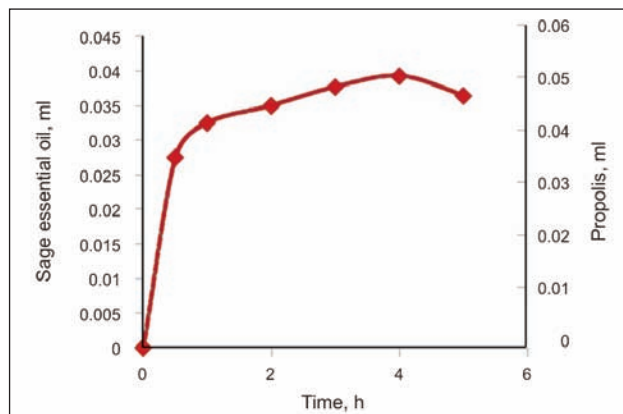


Fig. 7. Controlled released of biological active compounds

are released in the first hour. The products continue to disperse in the Tween 80 solution for 4 hours. This proves that those products are appropriate to be used in cosmetic treatments because of the short time needed for the active substances to transfer from the textile onto the skin.

CONCLUSIONS

Using mathematical modelling 2k composed central rotatable program with 3 independent variables the optimal emulsion was obtained.

The optimised emulsion applied on the 100% cotton knitted fabric presented good antibacterial activity against gram-negative bacteria *Escherichia coli* as well as gram-positive bacteria *Staphylococcus aureus*. The controlled release study reveals that the bioactive product is released fast in the first hour and slow until 4 hours.

Antibacterial activity and biocompatibility combined with a environment friendly obtaining process of the emulsions using natural compounds recommend this product to be used as skin care product.

ACKNOWLEDGEMENT

This paper was realised with the support of POSDRU CUANTUMDOC "Doctoral studies for European performances in research and innovation" ID79407 project funded by the European Social Fund and Romanian Government.

BIBLIOGRAPHY

- [1] Majeti, N. V. R. K. *A review of chitin and chitosan applications*. In: Reactive & Functional Polymers, 2000, vol. 46, p. 1
- [2] Bansal, V. et al. *Application of chitosan and chitosan derivatives in drug delivery*. In: Advances in Biological Research, 2011, vol. 5, issue 1, p. 28
- [3] Fu, X. et al. *Chitosan derivatives with dual-antibacterial functional groups for antimicrobial finishing of cotton fabrics*. In: Carbohydrate Polymers, 2011, vol. 85, p. 221
- [4] Miladinovic, D., Miladinovic, L. *Antimicrobial activity of essential oil of sage from Serbia*. In: Physics, Chemistry and Technology, 2000, vol. 2, issue 2, p. 97
- [5] Vassya, B. et al. *Chemical composition of European propolis: expected and unexpected results*. In: Zeitschrift für Naturforsch, 2002, vol. 57c, p. 530
- [6] Sforcin, J. M. *Propolis and the immune system: a review*. In: Journal of Ethnopharmacology, 2007, vol. 113, p. 1
- [7] Fras, L., Šauperl, O. *Chitosan and its derivatives as an adsorbate for cellulose fibres antimicrobial functionalization*. In: Industria Textilă, 2012, vol. 63, issue 6, p. 296

Authors:

Asist. univ. dr. ing. ANGELA CEREMPEI
Drd. ing. ABRAMIUC DANKO
Conf. dr. chim. RODICA MUREȘAN
Prof. dr. ing. AUGUSTIN MUREȘAN
Universitatea Tehnică Gheorghe Asachi
Facultatea de Textile-Pielărie și Management Industrial
Bd. D. Mangeron nr. 53, 700050 Iași
e-mail: angela.cerempei@yahoo.com;
dabramiuc@tex.tuiasi.ro; amuresan@tex.tuiasi.ro

Prof. dr. ing. CRIȘAN POPESCU
DWI at RWTH Aachen University, Germany
e-mail: popescu@dw.rwth-aachen.de

DOCUMENTARE



MEMBRANE BIODEGRADABILE PENTRU REGENERAREA CORNEANĂ

Electrospinning Company, cu sediul în Didcot, Marea Britanie, a furnizat membrane sintetice biodegradabile, electrofilate, pentru *Universitatea din Sheffield*, care dezvoltă tehnici de regenerare a corneei, în colaborare cu experți din India. Tehnologia a fost elaborată de către cercetătorii de la Universitatea Sheffield pentru a trata una dintre cauzele majore ale orbirii, în întreaga lume, și anume leziunile corneei. Cercetătorii au dezvoltat un nou implant biodegradabil, acoperit cu celule stem, care au avantajul de a continua să se multiplice și să vindece ochiul în mod natural. Celulele corneene au fost cultivate cu succes pe o membrană biodegradabilă sintetică sterilizată, pornind de la celule izolate în laborator sau cultivate din bucăți foarte mici de țesut.

Celulele stem din partea frontală a ochiului au rolul de a menține corneea curată și rezistentă. Dacă o persoană pierde o parte din celulele care reînnoiesc epiteliul cornean, atunci pe ochi poate apărea un țesut tip cicatrice, care provoacă durere și chiar pierderea vederii.

În ultimii 15 ani, doar în câteva centre specializate din întreaga lume a fost posibilă recoltarea unei bucăți mici de țesut de la nivelul ochiului neafectat, pentru a multiplica aceste celule într-un laborator de specialitate, și apoi a le retransplanta pe bucăți de membrană amniotică în corneea deteriorată a donatorului. Acest lucru necesită accesul la o bancă de țesuturi, camere curate pentru recoltarea celulelor, precum și o dexteritate foarte mare din partea chirurgilor.

Colaborarea dintre Universitatea din Sheffield și India, finanțată de Wellcome Trust, are ca scop simplificarea acestei tehnici, pentru a o face disponibilă medicilor

chirurgi oftalmologi din întreaga lume. Există două etape ale acestui proces: regenerarea unui nou epiteliu cornean dintr-o porțiune mică de țesut neafectat al ochiului și producerea unei membrane sintetice ca alternativă la membrana amniotică umană, care să poate fi depozitată și disponibilă pentru chirurgii din întreaga lume.

Echipa a testat deja primul concept prin care epiteliul cornean poate fi regenerat din porțiuni foarte mici de țesut (cultivate pe o membrană amniotică umană) și a finalizat dezvoltarea unei membrane biodegradabile sintetice sterilizate, care poate fi depozitată la -20°C , cel puțin un an. Echipa speră ca, în următoarele 12 luni, să se efectueze primul studiu pilot pe om.

Compania Electrospinning dezvoltă și produce matrici polimerice realizate prin electrofilare, care oferă un mediu ideal pentru susținerea creșterii celulelor 3D. Aceasta comercializează o gamă largă de medii pentru culturi celulare și țesuturi sterile care conțin matricea Mimetix, pentru cercetări în domeniul ingineriei tisulare, medicinei regenerative și descoperirii medicamentelor.

În anul 2013, compania a lansat o placă de cultură cu 96 de godeuri, care conține matricea Mimetix, sudate cu laser printr-un proces brevetat, ce pot fi utilizate în descoperirea medicamentelor. Multe teste predictive in vitro ale celulelor 3D pot reduce rata eșecurilor clinice costisitoare și înlocuirea unor studii pe animale. Aceasta oferă, de asemenea, un serviciu de dezvoltare a matricilor personalizate.

Electrospinning Company a fost înființată în anul 2010, cu scopul de a dezvolta produse care utilizează platforma de electrofilare din cadrul Laboratorului Rutherford Appleton, din Oxfordshire, Marea Britanie.

Smarttextiles and nanotechnology, februarie 2014, p. 5

REZUMAT – ABSTRACT

Fenomene de interfață și capacitatea de vopsire cu coloranți reactivi a bumbacului cationizat

Fenomenele de interfață au un rol important în procesele de finisare în stare umedă a bumbacului. În lucrare au fost studiate fenomenele de interfață în cazul țesăturilor din bumbac cationizat cu compuși cationici existenți pe piață. În urma procesului de cationizare, s-a realizat o caracterizare a suprafeței, folosind metodele de analiză FTIR-ATR și SEM. Modificările survenite la nivelul suprafeței au fost studiate cu ajutorul fenomenelor electrocinetice, a energiei libere de suprafață și a absorbției. Potențialul zeta, punctul izoelectric și punctul de sarcină electrică nulă au fost analizate folosind metoda curentului/potențialului de scurgere, cantitatea specifică a sarcinii de suprafață și absorbția agentului tensioactiv ionic prin metoda de titrare potențiometrică, iar energia liberă de suprafață prin metoda penetrării capilare a straturilor subțiri. Gradul de afinitate a bumbacului modificat pentru diverși coloranți reactivi, cu grupări funcționale diferite, a fost determinat cu ajutorul valorilor coeficientului K/S . S-a studiat, de asemenea, efectul adăugării unor electroliți asupra băii de vopsire.

Cuvinte-cheie: bumbac, cationizare, fenomene de interfață, energie liberă de suprafață, absorbție de agenți tensioactivi, vopsire cu coloranți reactivi

Interface phenomena and dyeability with reactive dyes of cationized cotton

Interface phenomena have a significant role in wet finishing processes of cotton. Therefore, interface phenomena of cotton fabric, cationized with commercial cationic compound, were studied in this paper. The characterization of surface after cationization, was performed by FTIR-ATR and SEM. Interface phenomena were studied through electrokinetic phenomena, surface free energy and adsorption. Zeta potential, isoelectric point and point of zero charge were determined according to streaming current/streaming potential method; specific amount of surface charge and adsorption of a ionic surfactant by potentiometric titration method, surface free energy by thin layer wicking method. The affinity of such modified cotton for reactive dyes having different functional groups was investigated through the K/S values. The effect of electrolyte addition on dye bath was investigated as well.

Key-words: cotton, cationization, interface phenomena, surface free energy, surfactant adsorption, reactive dyeing

In textile wet finishing processes the interface phenomena, such as zeta potential, electrokinetic surface charge of textile material, adsorbency of chemical compounds and substances on the surface of textile materials, wettability, as well as the strength of fiber bonds play the important role. Interface phenomena occur between liquid and solid phase, like between aqueous solution and textile material, resulting in change of textile material surface state. Electrokinetic phenomena, such as zeta potential and specific amount of surface charge, characterize electric charge of textile material [1] – [4]. Although these systems are extremely complex, systematic study of interface phenomena on cotton fabric lead to knowledge of the mechanisms of textile wetting, finishing and dyeing processes setting the base that can be used to predict fabric behavior in the wet finishing, and to some extent to assess the value and utilization characteristics, and environmental acceptability of the product for a particular application. The electrokinetic potential/zeta potential (ζ) is part of the total potential drop occurring in the intermediate surface layer at the boundary of the solid/liquid phases as a consequence of the ions distribution from the

solid surface to the bulk fluid [1]. At the interface of an electrically charged textile fibers and an aqueous solution of electrolyte, surfactants or dyes, an electric double layer is formed. Moving one of these two charged surfaces results by electrokinetic (zeta) potential. There are several principles for measuring zeta potential, like electrophoresis, sedimentation potential, electro-osmosis, streaming potential/current, potential of colloidal vibration, electrokinetic sound amplitude [3], [4]. In the most cases the method of streaming current/streaming potential or electro osmosis is used for fibres, whereas electrophoresis is used for dyestuffs [2], [4], [5]. It is to point out that different measuring methods result in different values of zeta potential under identical conditions. On the other hand, the isoelectric point, IEP , the concentration value of potential determining ions where the zeta potential is zero, is the parameter which gives an insight in character of testing material [2]. Generally, for Brönstead acids and bases, IEP is the pH value at which $\zeta = 0$ (pH_{iep}). Another electrokinetic parameter is the point of zero charge, PZC . It represents the amount of opposite charged ionic surfactant added to

electrolyte adsorbed to surface to reach zeta potential equal to zero.

Electrokinetic phenomena give information about nature and dissociation of functional groups, hydrophilicity or hydrophobicity of fiber surface as well as ions or water sorption. Fiber sorption properties are influenced by molecular (chemical structure, molecular mass, number of functional groups) as well as the supramolecular structure of fiber (molecular orientation, degree of crystallinity, crystallite dimensions, portion of amorphous regions, size and shape of voids etc.), swelling capacity as well as ionogenicity, structure and concentration of adsorbate. Significant influence on the sorption properties of fibers has the amount of accessible groups (hydroxyl, carboxyl, sulfate and amino groups) and the portion of amorphous regions where the adsorption processes take place [5]. The change of number of functional fiber surface groups, e.g. by blocking in dyeing and finishing processes, and their dissociation affect the distribution of surface charge, causing changes in the thickness and distribution of the electric double layer, resulting in different fabric electrokinetic phenomena, surface free energy and wettability.

Textile fibers, immersed in water (pH 6.5 – 7.0), show negative values of the ζ -potential and negative surface charge, because chemical functional groups dissociate in water releasing or absorbing anions. The ζ -potential values for fibers vary from -10 mV to -60 mV. By increasing pH the ζ -potential becomes more negative [3], [5]. Therefore, the adsorption processes of anionic substances on cotton cellulose occur with difficulties due to repulsive forces between particles of the same electrical sign [5], [6]. During mercerization process cotton unit cell changes from cellulose I to cellulose II resulting in more energetically favorable material, but the repulsive forces are still present.

Reactive dyestuffs, used in cotton dyeing, consists of more than 50% of all dyes [7] by virtue of their variety of brilliant shades, excellent color fastness and environmental safety, in alkaline medium, they are able to make covalent bond between carbon atoms in dyestuff molecule and oxygen atoms in hydroxyl groups of cellulose [8]. The most common commercial systems involve vinyl sulphon (VS) and monochlorotriazine (MCT) reactive groups. The main problem in dyeing with reactive dyes is low affinity caused by existing repulsion forces between electronegative charges both of cellulose in cotton fiber as well as of reactive dye. To overcome these forces in dyeing processes, a large amount of electrolyte is needed, making them economically and ecologically unfavorable. On the other hand, during the dyeing process with reactive dyes, the dyestuff reacts both with fiber, and with water producing a hydrolyzed dye which remains in dyeing bath or adheres on fiber similarly as direct dyes, where it may reduce color fastness. Increasing the degree of exhaustion and fixation of reactive dye and saving electrolyte is the purpose of physical and chemical modifications of cellulose

fibers. Therefore alternative methods of cotton dyeing have been researched in recent years. One of them is based on cotton modification using amines and/or quaternary ammonium compounds which bonds to fiber blocking $-OH$ groups of cotton, resulting in charge reversal. In that case cationized cotton becomes less negative or even gets positive electric charged on the fiber surface, increasing its affinity for anionic compounds [9] – [14]. The results of chemical, structural and morphological changes of cotton cellulose after treatment with triazine derivatives which contain anionic and cationic groups [12] and the effects of such treatment in reactive dyeing were recently published [6], [13]. On modified cotton cellulose were identified several phenomena: formation of new molecular structures that contain cationic and anionic groups decreasing the level of crystallinity and modifying surface morphology. Modified cotton cellulose showed greater degree of exhaustion and fixation of reactive dye than unmodified cellulose, as a result of newly formed groups.

Therefore, it was of great interest to research interface phenomena on cotton fabric treated with commercial cationic agents in order to improve dyeing ability of cotton using reactive dyestuff with different functional groups.

EXPERIMENTAL PART

Material and methods

The plain weave bleached fabric of 100% cotton fiber was used. The mass per surface area is 204.5 g/m². It was cationized with commercial cationic agent Sintegal V7 conc. (Chemapol – Czech Republic) in three concentrations (0.5 g/l, 1 g/l and 2 g/l). Sintegal V7 conc. is a quaternized polyglykol ether of fatty amine with cationic character. The exact chemical structure of this commercial compound is not available, but it is well known that amine polyglycol ethers are nonionic surfactants which can exhibit a cationic character (fig. 1).

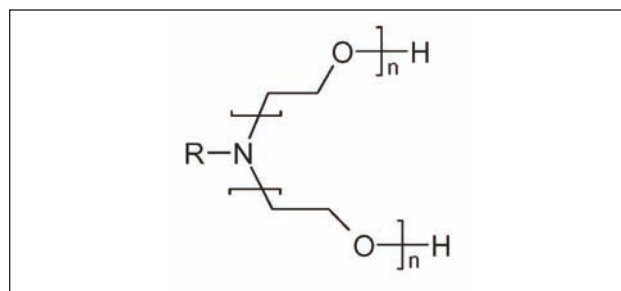


Fig. 1. Amine polyglycol ethers:
R is alkyl chain, aryl etc.

Sintegal V7 was applied by exhaustion method at $50^{\circ}C$ for 30 minutes. Then the 10 g/l Na_2CO_3 was added and the treatment continued for another 30 minutes. Cationized cotton fabric were neutralized in 5% CH_3COOH , rinsed with distilled water and dried at room temperature. Table 1 shows the labels and treatments of cotton fabric.

Table 1

SAMPLE LABELS AND TREATMENT PARAMETERS	
Sample label	Treatment
P_0	Untreated cotton fabric
$P_{0.5}$	Cotton fabric treated with Sintegal V7 conc. solution 0,5 g/l
P_1	Cotton fabric treated with Sintegal V7 conc. solution 1 g/l
P_2	Cotton fabric treated with Sintegal V7 conc. solution 2 g/l

For the surface characterization of cationized cotton fabrics Fourier Transform Infrared – Attenuated Total Reflectance (FTIR-ATR) spectroscopy and Scanning Electron Microscopy (SEM) analysis were performed. FTIR-ATR was performed on Spectrum GX FT-IR (Perkin-Elmer). SEM analysis was performed for the characterization of surface morphological changes, applying scanning electron microscope JEOL JCM 5300 (Jeol – Japan). The samples were prepared for scanning using the standard preparation procedure applying gold vapor to fiber surface for five minutes to make it conductive for cathode deposition of gold vapor. The presented images are representative and were selected among 10 images taken at 7 different spots on the fabric.

Components of surface free energy, *SFE*, were determined according to thin-layer wicking method proposed by Chibowski et al. [15]. According to this technique the rate of liquid penetration (wicking) into the porous solid can be described using general form of Washburn equation for the horizontal capillary:

$$\frac{x^2}{t} = \frac{R}{2\eta} \Delta G \quad (1)$$

where:

x is the penetrated distance;

R – the effective radius of porous solid;

t – the penetration time of the distance x ;

η – the liquid viscosity;

ΔG – the free energy change, accompanying the liquid penetration process.

If the wicking experiments are carried out in four wicking systems, four different values of ΔG appear in equation (1).

In the first system the penetration rate of a low-energy liquid, which is assumed as a completely spreading liquid, is measured through the textile fabric pre-contacted with the liquid saturated vapor. In this case equation (1) may be written as:

$$\frac{x^2}{t} = \frac{R}{2\eta} \gamma_L \quad (2)$$

The parameter R can be determined from it. γ_L is the liquid surface tension. In the second system the same completely spreading liquid is used and the penetration rate is measured through the bare fabric. In this case ΔG in equation (2) is equal to:

$$\Delta G = W_A - W_C \quad (3)$$

According to the theoretical consideration the following relationship exists:

$$\gamma_L (\cos \theta_a - \cos \theta_r) = W_A - W_C \quad (4)$$

It appears from this that W_A can be determined from the results of the liquid penetration rates. Using the van Oss approach [13] W_A can be expressed by the following equation (5):

$$W_A = 2\sqrt{\gamma_S^{LW}\gamma_L^{LW}} + 2\sqrt{\gamma_S^+\gamma_L^-} + 2\sqrt{\gamma_S^-\gamma_L^+} \quad (5)$$

from which apolar Lifshitz-van der Waals (γ_S^{LW}) and polar electron donor (γ_S^-) and electron acceptor (γ_S^+) components of the solid surface free energy, can be calculated, if the components γ_L^{LW} , γ_L^- and γ_L^+ of the liquids are known. For determination of the solid surface free energy components from the equation (5) at least three liquids, one non-polar and two polar liquids are necessary. In this paper for thin-layer wicking experiments n-heptane (p.a. 99.5%, Fluka) as a non-polar completely spreading liquid and water and formamide as polar non-completely wetting liquids were used.

Electrokinetic potential was measured by streaming potential/current method using Brookhaven-Paar Electrokinetic Analyzer (EKA) with a stamp cell and calculated according to Helmholtz-Smoluchowsky equation [4].

Zeta potential was investigated versus pH and versus ionic surfactant addition. Isoelectric point (*IEP*) of textile fabrics was determined as well as point of zero charge (*PZC*) using N-cetylpyridinium chloride (N-CPC).

Specific quantity of surface charge was calculated after back-titration method [5] applying Titrino 736 (Metrohm) using ionic surfactant electrode 6.0507.120 (Metrohm). N-CPC was used as cationic, and Sodium dodecyl sulphate (SDS) as anionic surfactant polyelectrolyte solution. The specific amount of surface charge per 1 g of fabric was calculated from the difference in anionic and cationic surfactant consumption.

Water adsorption of cotton fabrics was determined through water retention value, *WRV*, according to DIN 53814:1961 – Bestimmung der Wasserrückhaltevermögens von Fasern und Fäden.

Adsorption of 0.001 M ionic surfactants was carried out in Linitest, Original (Hannau). Anionic surfactant sodium dodecyl sulfate (SDS) and cationic surfactant, dodecyl trimethyl ammonium bromide (DDTMAB) by Merck were adsorbed at 40°C for duration of 30 minutes at pH 7. Amount of adsorbed surfactants was determined indirectly from solution by potentiometric titration method on Titrino 736 (Metrohm) using ionic surfactant electrode 6.0507.120 (Metrohm) and N-CPC and SDS as titrants.

The adsorption ability of reactive dyestuffs – monochlorotriazine Ostazin Red H-3B (CI Reactive Red 45) by Chemapol, Czech Republic, and vinylsulfone

Remazol Brilliant Blue B (CI Reactive Blue 27) by Dy Star, Germany, was determined after dyeing through K/S values using remission spectrophotometer SF 600 PLUS CT (Datacolor). Dyeing was performed in concentration of 1% owf reactive dyestuff without and with the addition of electrolyte (10 g/l and 50 g/l NaCl), LR 1:45, at 80°C for Ostazin and 60°C for Remazol, for 2 hours, in Ahiba G7B (Datacolor). After rinsing it was dried at room temperature. Color measurements were carried out on both sides of the sample to determine parameters for calculation of the color intensity, K/S , and the increase of color intensity, I , at $\lambda = 550$ nm for Ostazin Red H-3B and $\lambda = 600$ nm for Remazol Brilliant Blue B, using the Kubelka-Munk equation (6):

$$\frac{K}{S} = \frac{(1 - R)^2}{2R} \quad (6)$$

where:

K is absorption coefficient;

S – scattering coefficient;

R – reflection of light $D_{65/10}$.

In this case:

$$I = \frac{(K/S)_c - (K/S)_0}{(K/S)_0} \cdot 100 [\%] \quad (7)$$

where subscript c stands for cationized and 0 for untreated cotton fabrics.

RESULTS AND DISCUSSIONS

The surface characterization of cationized cotton fabrics were researched by FTIR-ATR (fig. 2) and SEM (fig. 3) analysis.

From FTIR-ATR analysis of the cotton fabrics presented in figure 2 it is evident that in the fingerprint area (1450 cm^{-1} to 850 cm^{-1}), characteristic bands appear at 1155 cm^{-1} , 1105 cm^{-1} , 1050 cm^{-1} , 1025 cm^{-1} , 1005 cm^{-1} , 985 cm^{-1} and 895 cm^{-1} for all fabrics. Even after cationization occurred, there were no changes in chemical composition of cotton cellulose. From IR spectrums it is evident that the significant change (detectable by IR) in chemical composition during the modification did not occur because all spectrum peaks are in the same position.

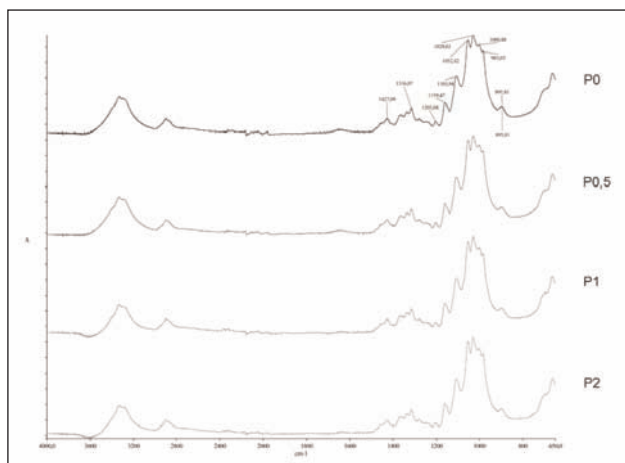


Fig. 2. FTIR-ATR analysis of the cotton fabrics

On the other hand, it is evident that the absorption of IR spectra is changed by cationization. Applying higher concentration of cationic compound produces higher absorption.

The surface morphology of cotton fiber was examined by scanning electron microscopy in order to estimate the effect of cationization on surface morphology. Figure 3 *a* shows a micrograph of untreated cotton fiber surface where a system of shallow parallel grooves can be seen. Figure 3 *b*, *c*, *d* depicts micrographs of cationized fiber surface. It can be noticed, based on these micrographs, that there are no significant changes in surface morphology, though the cationized fiber surfaces are slightly rougher than those of untreated cotton fiber, due to deposition of cationization agent. Apart from increased roughness of modified cotton fibers, it can be concluded that the extent of cationization did not affect the fiber physical structure, so the hand of treated samples remained unchanged. This is an advantage of the treatment compared to polymer material treatment which produces certain stiffness of fabrics.

Surface free energy highly depends on inter- and intra-yarn pores, as well as furrows observed on SEM micrographs. The size of pores as well as surface free energy components was determined by thin-layer wicking and presented in table 2.

From the results presented in table 2 it can be seen that the untreated cotton fabric *B* can be described as monopolar surfaces with a strong electron donor capacity, having the high γ_S^- value, and low γ_S^+ . On the other hand, cationization increases γ_S^+ indicating the change of cotton surface charge while its electron acceptor capacity gets higher. The reason for that is the dissociation of functional groups, or specific ion

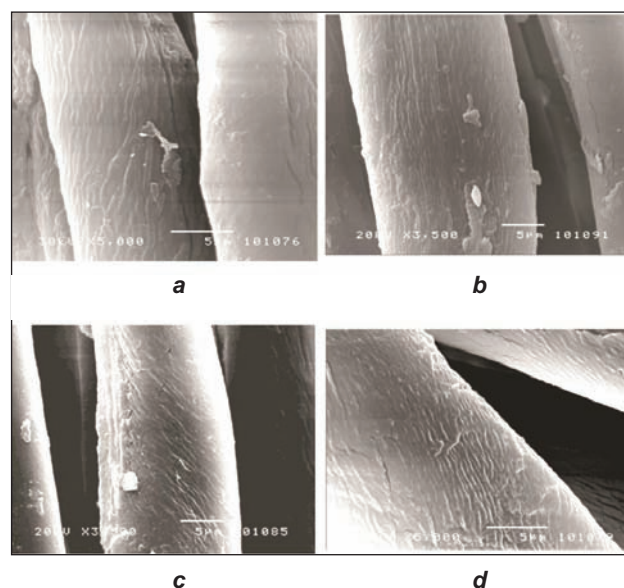


Fig. 3. SEM micrographs of: *a* – untreated cotton; *b* – and cotton treated with 0.5 g/l Sintegal V7 conc solution; *c* – and cotton treated with 1 g/l Sintegal V7 conc solution; *d* – and cotton treated with 2 g/l Sintegal V7 conc solution

SURFACE FREE ENERGY (SFE) COMPONENTS, TOTAL SFE, PORE RADIUS (R) AND WORK OF SPREADING (W_S) OF COTTON FABRICS DETERMINED FROM THE THIN-LAYER WICKING EXPERIMENTS						
Sample	γ_S^{LW} , mJ/m ²	γ_S^+ , mJ/m ²	γ_S^- , mJ/m ²	γ_S^{AB} , mJ/m ²	γ_S^{TOT} , mJ/m ²	R, μ m
P_0	34.21	1.29	51.68	16.33	50.54	11.35
$P_{0.5}$	37.37	2.12	53.06	21.20	58.57	11.48
P_1	41.31	2.16	44.64	19.64	60.95	7.31
P_2	51.43	2.45	34.83	18.50	69.93	8.70

adsorption of solution to the surface in neutral aqueous solutions. The dissociation of surface acidic or basic functional groups which belong to a class of Bronstead acids and bases is probably the main source of surface charge as shown by equations (8) – (11):



where:

FibAH is acidic surface functional group, such as $-\text{COOH}$;

FibB – basic group, such as $-\text{NH}_2$.

In the case of raw (untreated) cotton material hydroxyl and carboxylic groups exists but they are covered by non-cellulose compounds. Scouring and bleaching processes makes it available and causes formation of new surface groups ($-\text{CO}$, $-\text{CHO}$ and $-\text{COOH}$). Cationized cotton besides $-\text{COOH}$ has $-\text{NH}_2$ groups as well, due to bonded cationic compound, and it can be considered as Bronstead base. Further, the surface complexation can take place, similarly to general case shown by equations (10) and (11):



The processes shown by equations (8) and (9) are typical pH dependent processes and with respect to surface charge and potential do not differ, at least in principle, from metal oxide/solution interface. The processes shown by equations (10) and (11) assume the formation of surface complexes without presuming the character of bonds.

The results of surface free energy and electrokinetic phenomena presented in table 2 and table 3, and in figure 4 and figure 5, confirm that.

Untreated cotton fabric, P_0 , shows a negative charge as a result of the dissociation of surface acidic functional groups of cotton cellulose (hydroxyl and carboxylic groups). It has low zeta potential (ζ) = -18.9 mV, and highly negative specific surface charge (q) = -2.28 C/g. The treatment of cellulose fibers with cationic surfactants or quaternary ammonium ions leads to significant modification of fiber surface resulting in the reversal of charge. In this paper the

Table 3

ZETA POTENTIAL (ζ), ISOELECTRIC POINT (IEP), POINT OF ZERO CHARGE (PZC) AND SPECIFIC AMOUNT OF SURFACE CHARGE (Q) OF MODIFIED COTTON FABRICS				
Sample	ζ , at pH 10, mV	IEP	PZC*, μ g/ml	q, C/g
P_0	-18.9	<2.8	67.72	-2.2870
$P_{0.5}$	-15.3	3.82	59.12	-0.1638
P_1	-14.9	3.98	53.05	0.1998
P_2	-13.7	4.34	49.94	0.2989

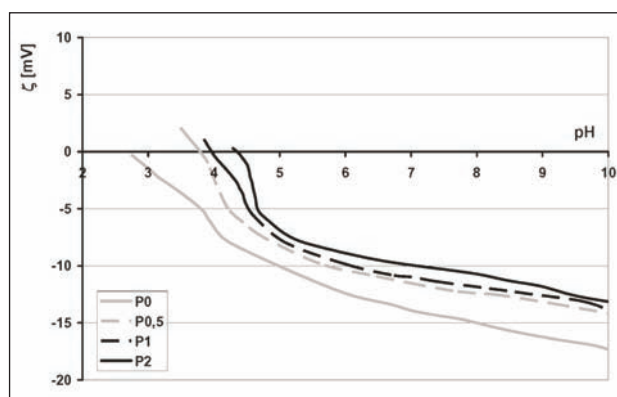


Fig. 4. Zeta potential (ζ) of the cotton fabrics versus pH of 0.001 M KCl

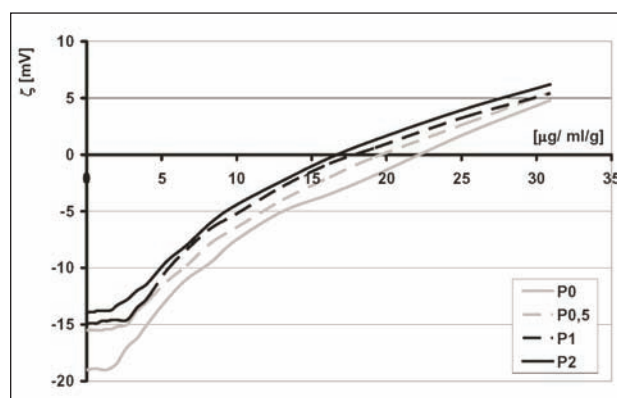


Fig. 5. Zeta potential (ζ) of the cotton fabrics versus ionic surfactant addition (N-CPC) in 0.001 M KCl at pH 10

Table 4

WATER RETENTION VALUE (WRV) AND
ADSORPTION OF IONIC SURFACTANTS (ANIONIC
SDS, CATIONIC DDTMAB) ON COTTON FABRICS

Sample	WRV, %	SDS, %	DDTMAB, %
P_0	54.5	28.30	51.23
$P_{0.5}$	51.3	58.42	37.50
P_1	49.9	76.20	31.96
P_2	49.2	84.42	26.42

commercial product, long-chain cationic compound Sintegal V7, was applied in three different concentrations. Sintegal V7 conc. is a quaternized polyglykol ether of fatty amine which can exhibit a cationic character. This cationic property can be tuned by the length of the hydrophilic polyglykol ether chain (amount of EO) and provide higher adsorption and adhesion. It is to assume that Sintegal V7 conc., as a nonionic surfactant, bonds to the fabric via hydrogen bonding or attractive dispersion forces. It is adsorbed with interactions involving hydrogen bonding between surface hydrogen atoms and proton acceptors in the polar groups and hydrophobic bonding between the surface and the hydrocarbon tails. At higher concentrations tail-tail interactions may begin to cause association of the adsorbed surfactants into aggregates, with the head groups facing the surface. Bonding of this long-chain pseudo-cationic compound in cationization causes a change in surface charge because of quaternization. In figure 1 b the model of cationized surface is proposed together with the potential profile in the electrical interface layer. This adsorption, which is primarily electrostatic, reverses the original negative charge of the solid. This process occurs within the Stern layer at inner Helmholtz plane. Because of long hydrophobic tails the next phase of adsorption results in tail-tail interaction where as the positively charged heads are directed from the solid toward bulk of liquid. Such an excess of positive charge results in positive zeta potential, as well. For that reason zeta potential increases in cationization with Sintegal V7 from $\zeta = -18.9$ mV for P_0 , to $\zeta = -15.3$ mV for $P_{0.5}$; $\zeta = -14.9$ mV for P_1 , and $\zeta = -13.7$ mV for P_2 .

Besides zeta potential at pH 10, it is important to know isoelectric point, *IEP*, and point of zero charge, *PZC*. For the determination of these points it was necessary to measure the change in zeta potential in dependence on the electrolyte pH and ionic surfactants addition. *IEP* is an important parameter in the dyeing and finishing. Obtained results presented in table 3 indicate that bleached cotton fabric has *IEP* in the area of less than pH 2.5. In that pH area number of ionic groups is higher than the number on fabric surface, therefore the correct value could not be determined. By cotton cationization *IEP* moves towards higher values depending on the concentration of cationic compound applied (from 3.82 for $P_{0.5}$ to 4.34 for P_2).

Point of zero-charge, *PZC*, was determined at pH 10 because in that pH area the zeta potential has the highest and constant value. The results presented in table 3 and in figure 6 showed that as the surface is more negative, it adsorbs more cationic surfactants for reaching zero-charge. Therefore, bleached cotton fabric has the highest *PZC* (67.72 $\mu\text{g/ml}$) and the most positive fabric, cationized with 2 g/l Sintegal V7, has the lowest one ($P_2 = 49.94$ $\mu\text{g/ml}$), respectively. The specific amount of surface charge determined by the back-titration method confirms assumptions

about the cotton fabric surface charge placed by the zeta potential and *PZC*. Bleached cotton fabric has highly negative surface charge. Cationization with various concentrations of Sintegal V7 conc. significantly reduces the electrical negative charge to $q \approx 0$. From the results of zeta potential at pH 10 and the specific amount of charge on the surface, it is obvious that all cationized cotton fabrics are significantly positively charged. Therefore, these fabrics are excellent substrate for the adsorption of anionic dyestuffs and surfactants. Additionally, that confirms the results of work of spreading, *Ws*. The change from $W_S P_0 = -6.89$ mJ/m^2 to $W_S P_2 = -3.19$ mJ/m^2 (table 2) indicates lowering the barrier for adsorption of anionic substrates. For that reason, in this paper, the cotton fabric adsorption ability of water, ionic surfactants and anionic reactive dyestuffs with different functional groups was researched. The results of water and ionic surfactants are collected in table 4, and for reactive dyestuffs in table 5.

Wetting, transport and retention of liquids in porous textile materials are complex phenomena depending on fiber surface morphology and geometry of fabric pores. Changes of chemical composition, fiber surface morphology, and structure of fiber pores can modify fabric hydrophilic characteristics. It is well known that adsorption of water, surfactant and dyestuff occurs primarily on the available-OH groups. Since cationization changed electrokinetic phenomena and surface free energy, it was important to research adsorption of water, ionic surfactant and anionic dyestuff.

From table 4 it is evident that water retention values, *WRV*, is minimally reduced for cationized cotton fabrics. The reason for that is in cationization which occurs mainly on primary hydroxyl groups of C-6 atom of cotton cellulose, so certain number of functional groups is blocked for water molecules. As can be seen from SEM micrographs (fig. 2), and from the pore radius presented in table 2, the pore structure is changed as well, resulting in slightly reduced water retention values.

On the other hand, the aminization of cellulose led to better anionic surfactant and dyestuff adsorption. Surfactant adsorption on the textile fibers is very complex mechanism, which can be explained on the

COLOR INTENSITY (<i>K/S</i>) AND ITS INCREMENT (<i>I</i>) OF CATIONIZED COTTON FABRICS DYED WITH ANIONIC REACTIVE DYESTUFFS WITHOUT AND WITH ELECTROLYTE ADDITION							
Dyestuff	Sample	No electrolyte		10 g/l NaCl		50 g/l NaCl	
		<i>K/S</i>	<i>I</i> , %	<i>K/S</i>	<i>I</i> , %	<i>K/S</i>	<i>I</i> , %
Ostazin Red H-3B	P_0	0.51	-	0.80	-	1.96	-
	$P_{0.5}$	0.78	53	0.94	17	2.58	32
	P_1	1.26	147	1.62	102	2.67	36
	P_2	1.50	194	1.65	106	3.03	54
Remazol Brilliant Blue B	P_0	0.39	-	0.44	-	0.64	-
	$P_{0.5}$	0.51	32	0.63	43	0.85	33
	P_1	0.61	56	0.91	107	0.99	55
	P_2	0.67	73	0.98	124	1.06	65

base of hydrophilic-hydrophobic balance, electrical charge, ionisation degree of surfactants and nature of fibers chemical reactive groups. It occurs mainly by electrostatic interactions between surfactant surface groups and specific accessible fiber groups. From the results of the adsorption of ionic surfactants (anionic SDS, cationic DDTMAB) on cotton fabrics presented in table 4 it is evident that untreated cotton fabric, negative in neutral aqueous solutions, adsorbs 51% of cationic surfactant DDTMAB, and only 28% of anionic one as a result of electrostatic repulsion interactions. The reason for that is a necessity to overcome potential barrier of the negatively charged fiber surface. Change of cotton surface charge in cationization influenced higher adsorption of anionic surfactant, while adsorption rate of DDTMAB on cationized cotton is low, due to the repulsive forces between fiber and surfactant in solution.

As can be seen from the table 5 the electrolyte addition to dye bath increases dyestuff adsorption. It was expected because electrolyte neutralizes cotton surface negative charge as well as dyestuff negative charge, making the dyestuff absorption easier. Adsorption of ionic surfactants and dyestuff on cotton fibers, with opposite charge in relation to the fibers, takes place in Stern layer, and then passes into the surface layer of fiber. Therefore, the electrolyte in the dyeing bath has another role as well – it increases dyestuff chemical potential moving the equilibrium distribution toward the fiber. In the dyestuff adsorption mechanism, cationized cotton partially replaces the role of cationic surfactants, what was confirmed by zeta potential and surface free energy results. For that reason the results of dyeing of cationized cotton without electrolyte can be explained as a contribution of cationic compound to the exhaustion efficiency from dye bath.

The comparative data of the increase of color intensity, *I*, of cationized cotton fabrics dyed with anionic reactive monochlorotriazine dyestuff Ostazin Red H-3B without addition of NaCl are significantly higher than the cotton fabrics dyed with NaCl addition. By

the cationising of the cotton fabrics using cationising agents produces a dramatic improvement (from 53% increase for $P_{0.5}$ to 194% increase for P_2) in colour intensity, *K/S*. The improvement in colour intensity, *I*, of the cationised cotton fabrics can be explained taking into account that the hydrolyzed reactive dye has high anionic character which can be bound to the cationic amine of the pseudo-cationic agent on the cotton fabrics.

For the cationized cotton fabrics dyed with anionic reactive vinylsulfone Remazol Brilliant Blue B dyestuff this is not the case. The improvement in color intensity is not the highest for fabric dyed without electrolyte addition (73% increment for P_2), but for cotton dyed with addition with 10 g/l NaCl (124% increment for P_2). The *K/S* values of cationized cotton fabrics dyed without NaCl addition, depending on the concentration of cationic compound, are equal or greater compared to the *K/S* values of untreated bleached cotton fabrics dyed with addition of 10 g/l NaCl, regardless of the type of dyestuff reactive group. However, untreated cotton fabrics dyed with addition of 50 g/l NaCl, have lower *K/S* values than cationized cotton treated with 2 g/l Sintegal V7 conc. (P_2) and dyed without electrolyte addition. The reason for lower or no consumption of electrolyte lies in lowered zeta potential (ζ) and potential barrier (*W*s) for adsorption of anionic substrates. Considering this, it is necessary to point out that cationic treatment can achieve savings in electrolyte consumption in reactive dyeing with vinylsulfone dyestuff, or even exclude with monochlorotriazine dyestuff. The electrolyte in dyeing bath can be considered as a cooperative contribution to cationic treatment.

CONCLUSIONS

Treatment of cotton fabrics with commercial cationic compound does not change chemical composition, but significantly change fiber surface. The change of cotton fiber surface free energy and charge is proportional to the concentration applied – the higher concentration, the higher zeta potential, surface

charge, surface free energy and electro acceptor capacity which led to high adsorption of anionic substrates.

Cationic compound on the fiber surface increases the amount of positive functional groups which can bond anionic reactive dyestuff by ionic interaction, as well as hydrogen and van der Waals interactions. These additional intermolecular bonds are the main reason for increased color intensity of the modified cotton fabrics compared to with untreated one.

The color intensity increased dramatically for cationized cotton fabrics dyed with anionic reactive monochlorotriazine dyestuff even without electrolyte addition, because the hydrolyzed reactive dye has high anionic character which improves the attractive force between the anionic dyestuff and adsorbed

cationic compound come to full effect. Applying standard amount of NaCl it suppresses the ionic dissociation of dyestuff, ionic attraction is weaker and that increase of the color intensity is less. For the cationized cotton fabrics dyed with anionic reactive vinylsulfone Remazol Brilliant Blue B dyestuff the improvement in color intensity without electrolyte is very high, but not the highest. On the other hand, it is still higher than in untreated cotton fabrics dyed with addition of 50 g/l NaCl. Therefore, cationic treatment can achieve savings in the electrolyte consumption in reactive dyeing with vinylsulfone dyestuff, or even exclude with monochlorotriazine dyestuff as a result of lowered zeta potential and potential barrier for adsorption of anionic substances.

BIBLIOGRAPHY

- [1] Dukhin, S. S., Derjaguin, B. V. *Electrokinetic phenomena in surface and colloid science*. Chapter 2. John Wiley & Sons, New York, 1974
- [2] Biscan, J., Grancaric, A. M., Tarbuk, A. *The electrokinetic potential at the textile fibers/solution interface*. In: Book of Proceedings of 4th ITC & DC, 5-8 Oct. 2008, p. 310
- [3] Jacobasch, H. J. *Oberflächenchemie faserbildender polymerer*. Akademie Verlag, Berlin, 1984
- [4] Grancaric, A. M., Pusic, T., Soljacic, I., Biscan, J. *Electrokinetic behaviour of textile fibers*. In: Polimeri, 2002, vol. 23, issue 6, p. 121
- [5] Grancaric, A. M., Tarbuk, A., Pusic, T. *Electrokinetic properties of textile fabrics*. In: Coloration Technology, 2005, vol. 121, issue 4, p. 221
- [6] Grancaric, A. M., Ristić, N., Tarbuk, A., Ristić, I. *Electrokinetic phenomena of cationized cotton and its dyeability with reactive dyes*. In: Fibres & Textiles in Eastern Europe, 2013, vol. 21, issue 6, p. 106
- [7] Petrinic, I., Curlin, M., Racyte, J., Simonic, M. *Textile wastewater treatment with membrane bioreactor and water re-use*. In: Tekstil, 2009, vol. 58, issues 1-2, p. 11
- [8] Tam, K. Y., Smith, E. R., Booth, J., Compton, R. G., Brennan, C. M., Atherton, J. H. *Kinetics and mechanism of dyeing processes: the dyeing of cotton fabrics with a Procion blue Dichlorotriazinyl reactive dye*. In: Journal of Colloid Interface Science, 1997, vol. 186, issue 2, p. 387
- [9] Lewis, D. M., McIlroy, K. A. *The chemical modification of cellulosic fibers to enhance dyeability*. In: Review of Progress in Coloration 1997, vol. 27, issue 1, p. 5
- [10] Hauser, P. J., Tabb, A. H. *Improving the environmental and economic aspects of dyeing cotton*. In: Coloration Technology, 2001, vol. 117, issue 5, p. 282
- [11] Grancaric, A. M., Tarbuk, A., Dekanic, T. *Electropositive cotton*. In: Tekstil, 2004, vol. 53, issue 2, p. 47
- [12] Liu, Z. T., Yang, Y., Zhang, L., Liu, Z. W., Xiong, H. *Study on the cationic modification and dyeing of ramie fiber*. In: Cellulose, 2007, vol. 14, issue 4, p. 337
- [13] Xie, K., Hou, A., Sun, Y. *Chemical and morphological structures of modified novel cellulose with triazine derivatives containing cationic and anionic groups*. In: Carbohydrate Polymer, 2007, vol. 70, issue 3, p. 285
- [14] Ćarkit, G., Bahtiyari, M. I., Üstüntağ, S., Örtlek, H. G. *Applying causticizing process on bamboo/cotton blended knitted fabrics*. In: Industria Textilă, 2014, vol. 65, issue 2, p. 113
- [15] Grancaric, A. M., Tarbuk, A., Chibowski, E. *Surface free energy of textiles*. In: Tekstil, 2008, vol. 57, issues 1-2, p. 28

Authors:

NEBOJŠA RISTIĆ
IVANKA RISTIĆ
MIODRAG ŠMELCEROVIĆ
High Professional School of Textile
V. Pusmana 17, 16000 Leskovac, Serbia
e-mail: bojana1998@ptt.rs

ANITA TARBUK
ANA MARIJA GRANCARIĆ
University of Zagreb
Faculty of Textile Technology
Prilaz Baruna Filipovica 28a
10000 Zagreb, Croatia

REZUMAT – ABSTRACT

Îmbunătățirea capacității de vopsire a fibrelor poliolefinice prin încălzirea cu microunde

Recent, au fost realizate ample cercetări cu privire la utilizarea energiei microundelor în procesele textile desfășurate în mediu umed, datorită numeroaselor avantaje, cum ar fi: reducerea consumului de energie, scurtarea timpului de prelucrare și îmbunătățirea calității produsului. Polipropilena este o fibră poliolefinică importantă, cu un preț relativ scăzut, cu proprietăți hidrofobe și rezistență la pătare și la o serie de produse chimice. Cu toate acestea, fibrele polipropilenice sunt dificil de vopsit prin metodele clasice de vopsire, deoarece grupele receptorilor de culoare lipsesc din structura lor moleculară. În cadrul studiului, pentru realizarea procesului de vopsire a fibrelor polipropilenice prin epuizarea băii, s-a recurs la încălzirea cu microunde, acest lucru sporind capacitatea de vopsire a fibrei cu coloranți de dispersie, special selectați. Rezultatele au fost comparate cu cele obținute prin vopsirea convențională. Tehnicile de vopsire a fibrelor au fost comparate în ceea ce privește randamentul tinctorial, rezistența la vopsire și rezistența la rupere. S-a constatat că, prin încălzirea cu microunde, s-a redus timpul de vopsire, iar randamentul tinctorial a fost îmbunătățit.

Cuvinte-cheie: polipropilenă, vopsire prin încălzire cu microunde, vopsire prin epuizarea băii, fibre sintetice

Improving the dyeability of polyolefin fibres by microwave heating

Recently, extensive research has been carried out using microwave energy in the textile wet processes due to the many potential advantages such as energy saving, reduced processing time and improved product quality. Polypropylene is a significant polyolefin fibre with a relatively low price, hydrophobic properties and resistance to staining and many chemicals. However, this fibre is difficult to dye by means of the conventional dyeing techniques, because its molecular structure lacks dye receptor sites. In this work, microwave heating was utilized in the exhaust dyeing of polypropylene to enhance the dyeability of the fibre by specially selected disperse dyes. The results were compared with the conventional dyeing's results. Dyeing techniques were compared in terms of colour yields, fastness values and tensile strengths of the dyed fibres. Microwave heating shortened the dyeing time and the colour yield was improved.

Key-words: polypropylene, microwave dyeing, exhaust dyeing, synthetic fibres

Since their introduction into the textile industry, the use of polypropylene fibres has gained importance because they offer a price advantage over Nylon and polyester. However, conventional dyeing techniques do not work well on polypropylene fibres. One reason for this shortcoming is that their molecular structure lacks dye receptor sites onto which the dye molecules may become attached. Moreover, because of its high crystallinity level, certain types of dye molecules cannot penetrate into the fibre structure thoroughly. In spite of these drawbacks, extensive research on developing a dyeable polypropylene fibre has been carried out in recent years.

Several methods to overcome this deficiency can be applied. One of the major applications is the use of mass pigmentation [1]. The fibres are dyed with pigments which exhibit high fastness properties. Currently available methods in manufacturing dyeable polypropylene are based on copolymerization [2] and grafting [3] technologies. Plasma treatment [4], nanotechnology and oxidation treatment [5] are other available modification methods which make polypropylene dyeable.

Most industrial dyeing methods apply heat to increase to intensity of dyeing and to enhance dye exhaustion or fixation. However, the conventional heating techniques used for dyeing and drying often cause dye migration problems. Therefore, dye migration must be controlled very carefully. In this sense, new energy sources, such as microwave energy and radio frequency help control dye migration.

Microwaves are high frequency radio waves which are capable of penetrating many materials and causing heat to be generated in the process. In conventional heating, the material's surface heats first and then the heat moves inward.

Microwave (MW) heating generates heat within the material so the entire volume is heated at the same rate. In spite of this advantage, the application of microwave techniques is limited in textile industry. Microwave irradiation heating is used in textile dyeing [6], [7], [15] – [18], finishing, surface modification [8] – [13] and fixation processes [14].

In general, the benefits of MW technology will be in fuel, electricity and time saving [19], increased process yield, environmental compatibility, space savings and unique characteristics of the textile products [20].

In this study, the use of conventional, high temperature techniques and microwave energy in the exhaust dyeing of polypropylene have been studied in order to improve the exhaustion of dye for a given processing time. Selected disperse dyes were used in the dyeing process. Dyeing techniques were compared in terms of colour yields, fastness values and tensile strengths of the dyed yarn.

EXPERIMENTAL PART

Materials used

In this study, for the dyeing of polypropylene yarn (100%, 300 denier/144 filaments) Sumicaron Red E C-D (Sumitomo Chemical Co., Ltd.), Sumicaron Blue E C-D (Sumitomo Chemical Co., Ltd.), and Sumicaron Yellow E C-D (Sumitomo Chemical Co., Ltd.) were used.

A carrier (Sarapol, CHT), a dispersing agent (Levegal DLP, Bayer), a non-ionic surfactant (Perlavin, Dr. Petry) were used as the dyeing auxiliaries. All other chemicals were supplied by Merck.

Dyeing methods

For each dyeing method 5 g material was used throughout this work. Each dyeing was repeated three times. The atmospheric dyeing with a carrier, HT dyeing and MW irradiation dyeings were carried out respectively in beakers, in Roaches HT Dyeing Machine and in a microwave oven. In the atmospheric dyeing procedure, Sarapol (1 g/L, carrier) was added to each dye liquor. The amount of dye used was 1% o.w.f. at a liquor ratio of 40:1.

The atmospheric dyeing process was initiated at 30°C, and the temperature was raised to 98°C at a heating rate of 2°C/minute. The dyeing went on for 45 minutes at 98°C and, eventually, the bath was cooled and the materials were soaped at 75°C for 15 minutes with a liquor ratio of 15:1, including 2 g/L Perlavin as a non-ionic surfactant and 0.5 g/L Na₂CO₃. The total dyeing time was 80 minutes.

In the high temperature (HT) dyeing, 200 mL capacity dye pots were employed. Each dye pot contained 1% o.w.f. dye and 1 g/L Levegal DLP (dispersing agent) at a liquor ratio of 40:1. In the HT dyeing, the dyeing process was started at 30°C, and after 5 minutes the temperature was raised to 130°C (at a heating rate of 1.5°C/minutes). The dyeing went on for 45 minutes at 130°C and, eventually, the bath was cooled and the materials were given a reductive cleaning at 75°C for 15 minutes with a liquor ratio of 20:1, including 2 g/L NaOH and 2 g/L Na₂S₂O₄. Total dyeing time was 116 minutes.

Microwave dyeing procedures

Microwave-assisted dyeings were carried out in a White Westinghouse (USA) microwave oven (model KM06VF2W, with a maximum input power of 1 100 W and output power of 700 W, operating at 2 450 MHz) in accordance with the time – temperature diagram given in figure 1.

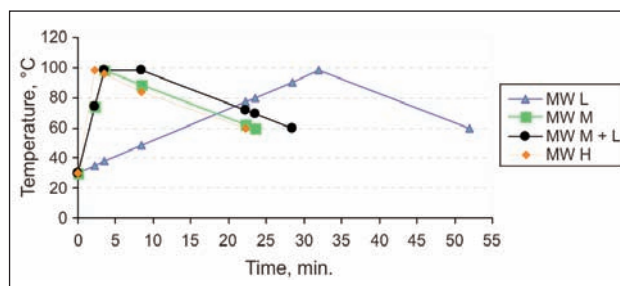


Fig. 1. Dyeing methods assisted by microwave energy

Microwave dyeing processes were carried out in accordance with the following four conditions:

- Low Power Level (MW – L) 120 W;
- Medium + Low Power Level (MW – M + L) 260 W;
- Medium Power Level (MW – M) 460 W;
- High Power Level (MW – H) 700 W.

In each dyeing condition the liquor ratio was 40:1, the colour strength was 1% and the material weight was 5 grams. The dye bath contained 1 g/L Sarapol (carrier).

All dyeings were carried out in 400 mL glass beakers contained dye bath at 30°C. The temperature raised to 98°C in 32 minutes at low level; in 3.5 minutes at medium level and in 2¼ minutes at high level. Both of medium level and low level were used together as the fourth condition for MW dyeing. At first MW oven was adjusted to the medium level and the temperature increased to 98°C in 3.5 minutes; then the energy level was shifted to low level and the dye bath was kept at this temperature for 5 minutes.

Finally, the bath was cooled down to 60°C. Eventually dyeing samples were rinsed out in cold water and were soaped at 75°C for 15 minutes with a liquor ratio of 15:1, including 2 g/L Perlavin as a non-ionic surfactant and 0.5 g/L Na₂CO₃.

Measurements and standards

Colour values of the dyed samples were assessed using Datascolor SF600+ spectrophotometer. The wash fastness of dyed materials was carried out in accordance with the methods described in the method ISO 105-C06 (A1S). Mechanical properties of dyed materials were tested in accordance with the TS 245 (EN ISO 2062) standard.

The results of the energy values were also proved by the calculations from the equation (1):

$$E = P_t \quad (1)$$

where:

E is energy consumption, Wh;

P – power, W;

t – time, h.

RESULTS AND DISCUSSIONS

The CIELab colour values, the colour differences and the fastness results are given in tables 1, 2, 3.

In table 1, the colour differences of the dyed materials were compared according to CMC (2:1) formula.

According to values in table 2, better dyeing results were obtained by the “MW M + L” and “HT” methods. As shown in table 3, the colour change values were found to be “3” to “4” according to Grey scale ratings. The staining test results of adjacent multifibers were generally found to be of grade “4-5” to “5”.

As shown in table 4 there are small differences in the tensile strengths between the undyed materials and MW dyed materials.

Total process time and energy consumption for each dyeing method were summarized in table 5.

Table 1

CIELAB VALUES OF THE SAMPLES DYED WITH SUMICARON DYES BY DIFFERENT METHODS									
Dye	Dyeing method	L^*	a^*	b^*	C^*	h°	X	Y	Z
Sumicaron Red E C-D	ATM	81.41	24.99	-3.26	25.20	352.57	66.78	59.22	67.33
	HT	81.60	23.22	-3.21	23.44	352.14	66.35	59.57	67.65
	MW L	83.33	18.80	-5.53	19.60	343.62	67.72	62.79	74.12
	MW M	80.23	21.18	-4.21	21.59	348.76	62.85	57.10	66.06
	MW M + L	80.14	25.83	-3.91	26.12	351.40	64.71	56.93	65.52
	MW H	83.14	20.23	-3.97	20.61	348.88	67.99	62.42	71.78
Sumicaron Blue E C-D	ATM	87.44	-3.54	-9.34	9.99	249.24	65.64	70.91	88.69
	HT	88.86	-4.14	-8.94	9.85	245.17	68.14	73.88	91.63
	MW L	87.15	-1.73	-8.20	8.38	258.06	65.88	70.30	86.38
	MW M	86.34	-4.11	-9.27	10.14	246.11	63.30	68.66	85.93
	MW M + L	85.83	-4.04	-9.15	10.01	246.19	62.38	67.65	84.56
	MW H	87.31	-1.93	-8.49	8.71	257.18	66.10	70.63	87.17
Sumicaron Yellow E C-D	ATM	95.13	-7.70	25.74	26.86	106.67	79.40	87.92	61.22
	HT	95.13	-7.69	24.61	25.78	107.35	79.41	87.93	62.48
	MW L	94.63	-7.37	23.70	24.82	107.27	78.50	86.75	62.54
	MW M	95.22	-7.97	26.43	27.61	106.78	79.48	88.15	60.63
	MW M + L	94.84	-7.99	27.46	28.60	106.22	78.63	87.24	58.79
	MW H	94.99	-7.37	24.31	25.40	106.86	79.28	87.60	62.55

Table 2

THE COLOUR DIFFERENCE RESULTS OF THE DYED MATERIALS WITH SUMICARON DYES					
Dye	Dyeing method	$\Delta E_{CMC(2:1)}$	ΔL^*	ΔC^*_{ab}	ΔH^*_{ab}
Sumicaron Red E C-D	HT	0.967	0.069	-0.954	-0.140
	MW L	3.733	1.027	-3.331	-1.338
	MW M	2.320	-0.431	-1.953	-1.176
	MW M + L	0.791	-0.466	0.500	-0.399
	MW H	2.791	0.630	-2.482	-1.111
Sumicaron Blue E C-D	HT	0.989	0.506	-0.116	-0.842
	MW L	2.151	-0.104	-1.335	1.683
	MW M	0.776	-0.391	0.129	-0.658
	MW M + L	0.854	-0.571	0.017	-0.635
	MW H	1.878	-0.047	-1.066	1.545
Sumicaron Yellow E C-D	HT	0.619	0.001	-0.568	0.224
	MW L	1.108	-0.170	-1.074	0.213
	MW M	0.395	0.033	0.391	0.043
	MW M + L	0.930	-0.100	0.909	-0.169
	MW H	0.771	-0.046	-0.767	0.071

* The atmospheric dyed fiber was taken as “standard”.

Table 3

FASTNESS PROPERTIES OF SUMICARON DYES ON PP WASH FASTNESS								
Dyes	Methods	Colour change	Staining					
			Wool	Acrylic	Polyester	Polyamide	Cotton	Cellulose acetate
Sumicaron Red E C-D Blue E C-D Yellow E D-C	ATM	3	4-5	4-5	4	3-4	4-5	4
		4	5	5	5	4-5	5	5
		3-4	5	5	5	4-5	5	5
Sumicaron Red E C-D Blue E C-D Yellow E D-C	HT	3	5	5	4-5	4	4-5	4-5
		4	5	5	4-5	5	4-5	4-5
		4	4-5	5	5	4-5	4-5	5
Sumicaron Red E C-D Blue E C-D Yellow E D-C	MW L	3-4	5	5	4-5	4	4-5	4-5
		4	5	5	5	5	5	5
		3-4	5	5	5	5	5	5
Sumicaron Red E C-D Blue E C-D Yellow E D-C	MW M	4	5	5	4-5	4	5	4-5
		3-4	5	5	5	5	4-5	4-5
		4	5	5	5	4-5	4-5	4-5
Sumicaron Red E C-D Blue E C-D Yellow E D-C	MW M + L	3	5	5	4-5	4	4-5	4-5
		3	5	5	5	5	5	5
		4	5	5	5	5	5	5
Sumicaron Red E C-D Blue E C-D Yellow E D-C	MW H	3	5	5	4-5	4	4-5	4-5
		3-4	5	5	5	4-5	5	5
		4	5	5	5	4-5	5	5

Table 4

TENSILE STRENGTH TEST RESULTS OF THE PP YARN SAMPLES, DYED WITH SUMICARON RED E C-D, SUMICARON BLUE E C-D, SUMICARON YELLOW E C-D						
Undyed PP yarn	Strength, kgf			Elongation, %		
	1.081 ± 0.015			28.51 ± 1.80		
Methods	Sumicaron Red E C-D	Sumicaron Blue E C-D	Sumicaron Yellow E C-D	Sumicaron Red E C-D	Sumicaron Blue E C-D	Sumicaron Yellow E C-D
ATM	0.985 ± 0.115	1.039 ± 0.070	0.978 ± 0.025	34.03 ± 0.50	36.78 ± 2.54	31.87 ± 1.98
HT	0.943 ± 0.110	1.166 ± 0.004	0.931 ± 0.065	23.42 ± 0.32	28.17 ± 2.76	28.18 ± 3.71
MW L	1.059 ± 0.090	0.928 ± 0.036	1.063 ± 0.016	29.87 ± 3.30	30.86 ± 1.78	33.68 ± 1.06
MW - M	1.087 ± 0.070	1.159 ± 0.210	1.161 ± 0.040	29.83 ± 4.50	32.94 ± 0.44	34.68 ± 6.43
MW - M + L	1.098 ± 0.036	1.073 ± 0.060	1.030 ± 0.175	30.79 ± 2.98	36.22 ± 3.45	32.06 ± 1.75
MW - H	0.994 ± 0.050	0.983 ± 0.049	1.146 ± 0.110	34.97 ± 1.80	34.29 ± 1.30	35.25 ± 0.14

Table 5

TOTAL PROCESS TIMES AND ENERGY CONSUMPTION IN DIFFERENT DYEING METHODS			
Dyeing method	Output power, W	Dyeing time, min.	Energy consumption, Wh
ATM	3 000	80	4 000
HT	4 000	116	7 730
MW - L	1 100	32	587
MW - M	1 100	3.5	64
MW - M + L	1 100	8.5	156
MW - H	1 100	2¼	41

CONCLUSIONS

In this study reached the following conclusions:

- The selection of the dye is a vital process for the exhaust dyeing of polypropylene.
- The dyeing times were reduced in microwave dyeing as a result of the enhanced hydrophilicity which was gained from the microwave irradiation of the dye bath as described in the literature [8].
- As the results obtained from the conventional dyeing procedure of polypropylene were compared to the microwave irradiated dyeing, the good results were obtained by the "MW - M + L" microwave dyeing condition.

- The yarn strengths were only slightly affected in the all dyeing methods.
- The wash fastness results of the dyed materials were quite good.
- The use of MW irradiation dyeing technique in textile dyeing is promising and as far as the energy conservation, time saving and cost effectiveness are considered.
- The use of ultrasonic energy was previously attempted to improve the dyeing yield of PP [16], however, the microwave technique has appeared to be more promising for the exhaust dyeing of PP.

BIBLIOGRAPHY

- [1] Maier, C., Calafut, T. *Polypropylene. The Definitive User's Guide and Databook*, William Andrew Publishing/Plastics Design Library, 1998
- [2] Mukherjee, A. K., Gupta, B. D. *Radiation-induced graft copolymerization of methacrylic acid onto polypropylene fibers VI. Dyeing behaviour*. In: *Journal of Applied Polymer Science*, 2003, vol. 30, pp. 4 455-4 466
- [3] Zhang, D., Liu, Z., Han, B., Pei, X., Liu, L., Yang, G. *Modification of isotactic polypropylene films by grafting methyl acrylate using supercritical CO₂ as a swelling agent*. In: *The Journal of Supercritical Fluids*, 2004, vol. 31, pp. 67-74
- [4] Kang, J. Y., Sarmadi, M. *Plasma treatment of textiles-synthetic polymer-based textiles*. In: *AATCC Review*, 2004, vol. 4, issue 11, pp. 29-33
- [5] Tehrani, B. A. R., Shoushtari, A. M., Malek, R. M. A., Abdous, M. *Effect of chemical oxidation treatment on dyeability of polypropylene*. In: *Dyes and Pigments*, 2004, vol. 63, pp. 95-100
- [6] Nourmohammadian, F., Gholami, M. D. *An Investigation of dyeability of acrylic fiber via microwave irradiation*. In: *Progress in Color, Colorants and Coatings*, 2008, vol. 1, pp. 57-63
- [7] Yoshimura, Y., Ohe, T., Ueda, M., Kurokawa, T., Mori, F. *Effect of microwave on diffusion behaviour of dye molecules*. In: *Sen'i Gakkaishi*, 2009, vol. 65, issue 9, pp. 241-245
- [8] Mirabedini, S. M., Rahimi, H., Hamedifar, S., Mohseni, S. M. *Microwave irradiation of polypropylene surface: a study on wettability and adhesion*. In: *International Journal of Adhesion and Adhesives*, 2004, vol. 24, issue 2, pp. 163-170
- [9] Purwar, R., Joshi, M. *Effect of microwave curing on easy care finishing of cotton using glyoxal/glycol*. In: *AATCC Review*, 2005, pp. 40-44
- [10] Fouda, M. G. M., El Shafei, A., Sharaf, S., Hebeish, A. *Microwave curing for producing cotton fabrics with easy care and antibacterial properties*. In: *Carbohydrate Polymers*, 2009, vol. 77, issue 3, pp. 651-655
- [11] Mirabedini, S. M., Rahimi, H., Hamedifar, S., Mohseni, S. M. *Microwave irradiation of polypropylene surface: a study on wettability and adhesion*. In: *International Journal of Adhesion and Adhesives*, 2004, vol. 24, issue 2, pp. 163-170
- [12] Hou, A., Wang, X., Wu, L. *Effect of microwave irradiation on the physical properties and morphological structures of cotton cellulose*. In: *Carbohydrate Polymers*, 2008, vol. 74, pp. 934-937
- [13] Tsukada, M., Islam, S., Arai, T., Boschi, A., Freddi, G. *Microwave irradiating technique to enhance protein fibre properties*. In: *AUTEX Research Journal*, 2005, vol. 5, issue 1, pp. 40-47
- [14] Ozerdem, A., Tarakcioglu, I., Ozguney, A. *The use of microwave energy for the fixation of reactive printed cotton fabrics*. In: *Tekstil ve Konfeksiyon*, 2008, vol. 4, pp. 289-296
- [15] Büyükakıncı, B. Y., Sökmen, N., Öner, E. *Investigation dyeing properties of regenerated bamboo materials dyed with reactive and direct dyes*. In: *Industria Textilă*, 2011, vol. 62, issue 2, pp. 72-76
- [16] Büyükakıncı, Y. *Dyeing of PP fibers with special methods*. In: MSc Thesis, Marmara University, Institute of Applied Sciences, Supervised by Assoc.Prof.Dr. Nihal Sökmen, 2005
- [17] Büyükakıncı, Y., Öner, E., Sökmen, N. *Microwave assisted exhaust dyeing of polypropylene*. In: 4th Central European Conference, Lieberec, Czech Republic, 2005, pp. 173-174
- [18] Öner, E., Büyükakıncı, Y., Sökmen, N. *Microwave-assisted dyeing of poly(butylene terephthalate) fabrics with disperse dyes*. In: *Coloration Technology*, 2013, vol. 129, issue 2, pp. 125-130
- [19] Hasanbeigi, A., Price, L. *A review of energy use and energy efficiency technologies for the textile industry*. In: *Renewable and Sustainable Energy Reviews*, 2012, vol. 16, issue 6, pp. 3 648-3 665
- [20] Haghi, A. K. *Application of microwave techniques in textile chemistry* In: *Asian Journal of Chemistry*, 2005, vol. 17, issue 2, pp. 639-654

Authors:

B. YEŞİM BÜYÜKAKINCI
 İstanbul Aydın University
 Faculty of Engineering
 Department of Textile Engineering
 İstanbul, Turkey
 e-mail: byesimb2@gmail.com

NİHAL SÖKMEN
 ERHAN ÖNER
 Marmara University
 Faculty of Technology
 Department of Textile Engineering
 İstanbul, Turkey

REZUMAT – ABSTRACT

Vopsirea cu coloranți acizi și cationici a amestecului fibros din nailon și nailon modificat chimic

Pentru vopsirea amestecului fibros din nailon și nailon modificat chimic s-au folosit coloranți acizi și cationici. Au fost studiate: viteza de vopsire, influența pH-ului și a temperaturii de vopsire, proprietățile de absorbție a coloranților, cedarea culorii între două fibre și rezistența vopsirii. Valoarea pH-ului a avut o influență mai mare în cazul vopsirii cu coloranți acizi, decât în vopsirea cu coloranți cationici. Viteza inițială de absorbție a coloranților cationici a fost mai mare decât cea a coloranților acizi. Proprietățile de absorbție a coloranților acizi și cationici, utilizați pentru acest amestec, au fost bune. Folosirea unor coloranți acizi premetalizați și a unui pH mai scăzut al băii de vopsire ar putea determina reducerea cedării culorii. Rezistența slabă a vopsirii constituie un dezavantaj pentru amestecul vopsit cu coloranți cationici, aceasta trebuind îmbunătățită prin metode eficiente.

Cuvinte-cheie: nailon modificat chimic, nailon, vopsire, coloranți cationici, coloranți acizi

Acid and cationic dyeing of nylon/cationic dyeable nylon mixture

Acid and cationic dyes were respectively used to dye the nylon/cationic dyeable nylon (CD-nylon) mixture. The dyeing rates, the pH and temperature dependence of dyeing, the building-up properties of dyes, the cross-staining of two fibres and the colour fastness of dyeings were discussed. The dyeing of acid dyes was more greatly affected by pH than that of cationic dyes. The initial uptake rate of cationic dyes was faster than that of acid dyes. The building-up properties of acid and cationic dyes on the mixture were both good. Applying the lower pH of dyebath and pre-metallised acid dyes could reduce cross-staining. The poor colour fastness would be a shortcoming of the mixture dyed with cationic dyes and should be improved through effective methods.

Key-words: cationic dyeable nylon, nylon, dyeing, cationic dyes, acid dyes

Cationic dyeable nylon (CD-nylon) fibre contains a sufficient amount of sulphonate groups or carboxyl groups within the polymer structure to render the nylon fibre dyeable with cationic dyes [1], [2]. Such CD-nylon fabric with enhanced drapeability, lustre and softness can be used in women clothing, casual and sportswear, in addition to being used as stain resistant carpet material. New style fabrics can be produced by interweaving CD-nylon with conventional nylon, and two-colour effect or differential dyeing effect can be achieved by dyeing this mixture with cationic and acid dyes in one bath under appropriate conditions.

The CD-nylon dyed with cationic dyes can exhibit unusual brilliancy. However, during the dyeing and finishing process, it is subjected to two main problems: poor colour fastness and colour loss at high temperature and wet state [1]. In earlier work [1], anionic and cationic fixing agents, acrylic binders and N-hydroxymethyl resin were applied to treat the dyed CD-nylon yarn with the aim of improving the wet fastness of cationic dyes on CD-nylon. The applications of binders and an anionic fixing agent were found to have no improvement in washing fastness, while resin finishing as well as the application of a cationic fixing agent gave a slight improvement in washing fastness. However, some other reports stated that the syntans used as anionic fixing agents were

moderately effective in improving wet fastness on CD-nylon [3].

When the acid and cationic dyeing of the nylon/CD-nylon mixture is simultaneously carried out in one bath, the cross-staining deserves great attention. Although the dyeing properties of CD-nylon may be changed by chemical modifications and the substantivity of CD-nylon for acid dyes is very low [2], [4], [5], the cross-staining is still difficult to be avoided when the nylon/CD-nylon mixture is dyed with acid dyes, because the amino groups in CD-nylon are susceptible to the staining of acid dyes. On the other hand, cationic dyes are also acceptable by the anionic carboxyl groups in conventional nylon, so the nylon fibre can also be stained by cationic dyes. The cross-staining is likely to reduce the accuracy of colour matching and colour fastness of dyeings [3]. For the one-bath dyeing of the nylon/CD-nylon mixture with acid and cationic dyes, another problem is that the interactions between cationic and acid dyes possibly give rise to the reduced wet fastness and brilliancy of dyeings. This problem should be solved through the application of non-ionic anti-precipitants and the selection of dyes [3].

Although the problems mentioned above are faced by some industrial enterprises, relatively few publications have treated the dyeing behaviours of CD-nylon and the nylon/CD-nylon mixture [1], [3], [6]. Thus a fundamental and detailed study of the dyeing

behaviours of this mixture is necessary. In this work, the properties of the respective dyeing of the nylon/CD-nylon mixture with acid and cationic dyes were investigated in terms of dyeing rates, pH and temperature dependence of dyeing, building-up properties of dyes, and factors affecting staining. Also the fastness properties of acid and cationic dyes on the mixture were preliminarily discussed.

EXPERIMENTAL PART

Materials used

The woven and scoured nylon 6 (warp)/CD nylon (weft) mixture (40:60) was kindly supplied by Wujiang Sanlian Printing and Dyeing Co. Ltd., China. Commercial dyes used in this paper were used as received and listed in table 1. Acid and pre-metallised acid dyes were supplied by Everlight Chemical Industrial Co. – Taiwan. Maxilon cationic dyes were provided by Huntsman International LLC – USA, and other cationic dyes were obtained from Shanghai Qingcheng Dyestuff Chemical Co. Ltd. and Jiangsu Xinmin Textile Science and Technology Co. Ltd. – China. Glacial acetic acid, sodium acetate, sodium hydroxide, phosphoric acid and boric acid were of analytical reagent grade. Levelling agent O (a non-ionic surfactant, polyoxyethylene alkyl ether) was provided by Jiangsu Hai'an Petrochemical Plant – China. A commercial syntan of Mesitol NBS used as fixing agent was supplied by Tanatex Chemicals B. V. – Netherlands.

Table 1

DYES USED	
Commercial name	C.I. generic name
<i>Non-metallised acid dyes</i>	
Everacid Yellow N-MR	Acid Yellow 42
Everacid Yellow N-3R	Acid Orange 67
Everacid Orange N-G	Acid Orange 56
Everacid Red N-RFL	-
Everacid Red N-B	Acid Red 249
Everacid Blue A-2G	Acid Blue 40
Everacid Blue N-RL	Acid Blue 260
Everacid Cyanine N-5R	Acid Blue 113
<i>Pre-metallised acid dyes</i>	
Everset Yellow M-2R	-
Everset Red M-G	-
Everset Navy M-R	-
<i>Cationic dyes</i>	
Cationic Yellow X-5GL	Basic Yellow 51
Maxilon Red SL	Basic Red 51
Cationic Brilliant Red X-5GN	Basic Red 14
Cationic Pink X-FG	Basic Red 13
Cationic Red X-GRL	Basic Red 46
Cationic Red X-6B	Basic Violet 7
Maxilon Blue SL	-

Dyeing methods

All dyeing experiments were carried out in sealed and conical flasks immersed in a XW-ZDR low-noise oscillating dyeing machine (Jingjiang Xinwang Dyeing and Finishing Co. Ltd. – China), using a 50:1 liquor ratio. Both the acid and the cationic dyebaths contained Levelling Agent O (0.5 g/L). Unless otherwise stated, the dyeing experiments were performed according to the following method: the pH was adjusted to 5 with HAC–NaAc buffer; the fabric was introduced into the dyebath at 30°C and the temperature was raised to 95°C over 65 minutes, and the dyeing was continued at 95°C for 60 minutes; at the end of dyeing, the dyed samples were removed, rinsed thoroughly in distilled water, and allowed to dry in the open air.

To assess the effect of pH on dyeing, the fabrics were dyed at pH values of 3.04, 3.89, 4.15, 4.88, 5.80 and 6.90 using Britton-Robinson buffer (H₃PO₄-HOAc-H₃BO₃/NaOH). In the experiment of the temperature dependence of dyeing, in order to ensure the same dyeing time, the fabrics were immersed into the dye solutions at 30°C, and then the temperatures were raised to 90, 95, 100, 105 and 110°C at 1°C/minute and maintained for 65, 60, 55, 50 and 45 minutes, respectively. For the studies of the pH and temperature dependence of dyeing, and the dyeing rates, the dye amount was 0.8% owf for acid dyes and 0.3% owf for cationic dyes while 1.2% owf acid dyes and 0.8% owf cationic dyes were used to assess the staining of different dyes and the colour fastness of dyeings.

Measurements

The absorbance of dye solution was measured using a Shimadzu 1800 UV-vis spectrophotometer. The percentage of dyebath exhaustion (%E) was calculated by the following equation (1):

$$\%E = 100 \times \frac{A_0 - A_1}{A_0} \quad (1)$$

where:

A₀ and A₁ are the absorbance of the dyebath before and after dyeing, respectively.

The concentration of dyes on fibres (C_f, mg/g) was calculated according to the following equation (2):

$$C_f = \frac{C_0 \cdot (\%E) \cdot V}{W} \quad (2)$$

where:

C₀, g/L and V, mL are the concentration and volume of the initial dye solution, respectively;

W, g – the dry weight of the fabric.

The dyed fabric was taken apart as warp and weft yarns, which were arranged evenly and fixed on the uniform whiteboard, respectively. The CIE L*, a*, b* colour coordinates (lightness L*, redness-greenness value a*, yellowness-blueness value b*) and the apparent colour depth (K/S value) were measured using a HunterLab UltraScan PRO reflectance spectrophotometer (illuminant D65; 10° standard observer).

The colour difference, dE , between stained and undyed samples was calculated using equation (3), and the staining of fibre samples was characterized by colour difference:

$$dE = [(L_2^* - L_1^*)^2 + (a_2^* - a_1^*)^2 + (b_2^* - b_1^*)^2]^{1/2} \quad (3)$$

where:

L_2^* , a_2^* , b_2^* and L_1^* , a_1^* , b_1^* are the CIE colour coordinates of stained and undyed samples.

Colour fastness to rubbing, washing, and light were tested according to ISO 105-X12, ISO 105-C01, and ISO 105-B02, respectively. All the dyed samples prepared for colour fastness tests were subjected to fixation treatment with 3% owf *Mesitol NBS* at 70°C for 15 minutes using a 50:1 liquor ratio.

RESULTS AND DISCUSSIONS

Effect of pH on acid and cationic dyeing

The uptake of acid and cationic dyes by the nylon/CD-nylon mixture at different pH values is shown in figure 1. The exhaustion of acid dyes increased significantly with decreasing pH in the range of 3.04 – 6.90. This indicates that the electrostatic interaction between the amino groups in nylon and the sulphonate groups in acid dyes plays a major role in the adsorption of acid dyes on nylon. The higher exhaustion of

acid dyes at lower pH is due to the correspondingly greater protonated amino groups which lead to ion-ion interaction. Conversely, the uptake of cationic dyes decreased slightly with decreasing pH. CD-nylon contains sulphonate and carboxyl groups, the former of which are mainly receptive to cationic dyes [6], [7]. The ionization of strongly acidic sulphonate groups is less affected by pH while the dissociation of carboxyl groups is greatly dependent on pH. Thus the pH dependence of the exhaustion of cationic dyes is less than that of acid dyes.

Figure 2 reveals that the K/S value of nylon increased clearly with decreasing pH, which was in accordance with the results shown in figure 1. The staining (dE) of CD-nylon by acid dyes reduced a lot with decreasing pH in the range of 3.04-4.88, and reached a high value when pH was above 4.88. Theoretically speaking, the staining of CD-nylon by acid dyes depends on the ion-ion interaction between the sulphonate groups in acid dyes and the amino groups in CD-nylon, and lower pH can cause the increased amount of the protonated amino groups in CD-nylon, and result in more staining. However, figure 2 displays the opposite result. This can be explained by the fact that more dyes adsorbed by conventional nylon at lower pH lead to less staining of CD-nylon.

In the case of the cationic dyeing of the mixture, the staining of nylon by cationic dyes was found to decrease with decreasing pH, as shown in figure 3. The electrostatic interaction between the negatively charged carboxyl groups in nylon and cationic dyes contributes to this staining. At low pH, the decreased ionization extent of the carboxyl groups in nylon weakens the interaction between nylon and cationic dyes, and consequently reduces the staining of nylon by cationic dyes. As shown in figure 3, the K/S value of CD-nylon increased slightly with decreasing pH, which was not completely consistent with the exhaustion of cationic dyes shown in figure 1. This might be explained by the fact that the reduced staining of nylon by cationic dyes with decreasing pH gives rise to a slightly increased adsorption of cationic dyes by CD-nylon.

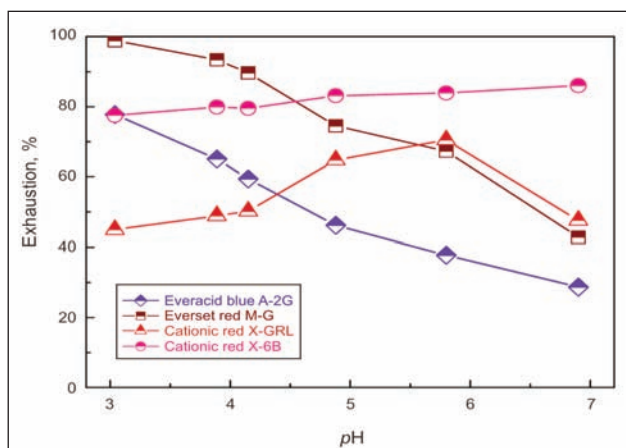


Fig. 1. Effect of pH on the uptake of acid and cationic dyes by nylon/CD-nylon mixture

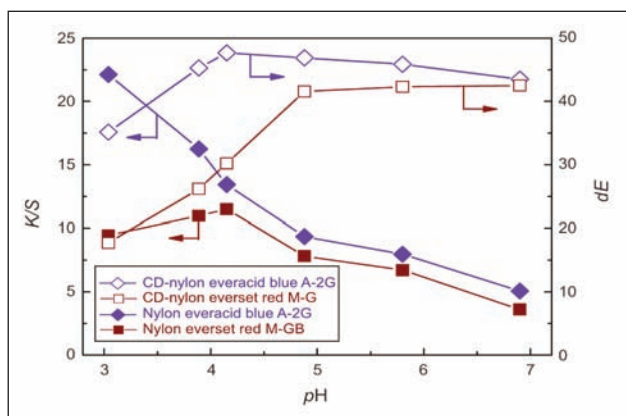


Fig. 2. Effect of pH on the apparent colour depth of nylon and the staining of CD-nylon by acid dyes

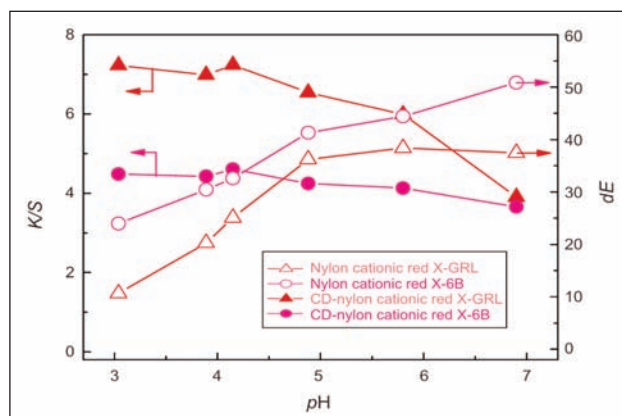


Fig. 3. Effect of pH on the apparent colour depth of CD-nylon and the staining of nylon by cationic dyes

From figures 1-3, it may be concluded that the pH of dyebath greatly affects the exhaustion of acid and cationic dyes, and the apparent colour depth and the extent of staining of dyed nylon and CD-nylon. In practical dyeing, pH would have a great impact on dyeing levelness. Therefore a reasonable pH control is very important when the nylon/CD-nylon combination is dyed.

Effect of temperature on acid and cationic dyeing

In the experiment of the temperature dependence of dyeing, in order to ensure the same dyeing time, the dyeing system was held at 90°C, 95°C, 100°C, 105°C and 110°C for 65, 60, 55, 50 and 45 minutes, respectively. Figure 4 shows that the exhaustion of acid and cationic dyes decreased slightly with increasing temperature, which can be attributed to the decreased affinity of dyes to fibres with increasing temperature. As shown in figure 5, the apparent colour depth and staining of nylon and CD-nylon fibres changed a little with increasing temperature. In general, the dyeing temperature of nylon is about 100°C. Sometimes, a higher temperature of dyeing is applied with the aim of covering the physical irregularities in nylon, and improving the levelness and colour fastness of dyeings due to the increased migration and diffusion

powers of dyes [8]. However, in this work, the touch of dyed samples became hard when the dyeing temperature exceeded 100°C, indicating that nylon/CD-nylon mixture cannot be dyed at temperatures higher than 100°C.

Dyeing rates of acid and cationic dyes

Figure 6 clearly shows that the initial dyeing rate of cationic dyes was faster than that of acid dyes, this being attributed to the strong interaction between cationic dyes and negatively charged CD-nylon. The apparent colour depth and staining of nylon and CD-nylon at different times and temperatures are shown in figure 7. The *K/S* of CD-nylon dyed with cationic dyes reached a very high value in a short time, then decreased a little as the time and temperature increased. And the *K/S* of nylon dyed with acid dyes increased gradually with increasing time and temperature. At the initial dyeing stage, the staining of CD-nylon by acid dyes was more serious on account of the low adsorption of acid dyes on nylon; however, as the temperature increased further, decreased staining occurred, which was accompanied by an increased uptake of acid dyes. In contrast, the change in the staining of nylon by cationic dyes was not so obvious throughout the dyeing process.

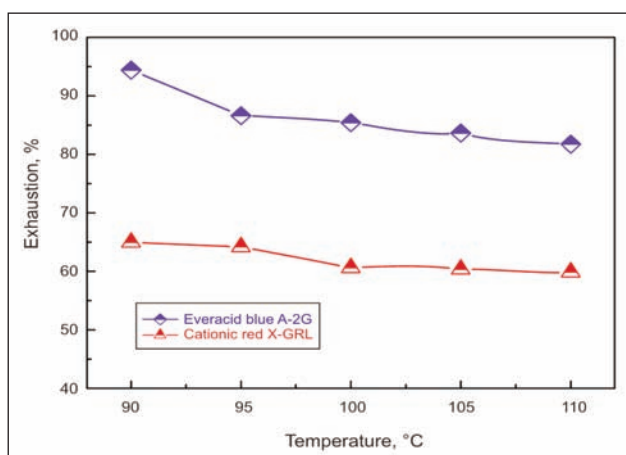


Fig. 4. Effect of temperature on the uptake of acid and cationic dyes by nylon/CD-nylon mixture

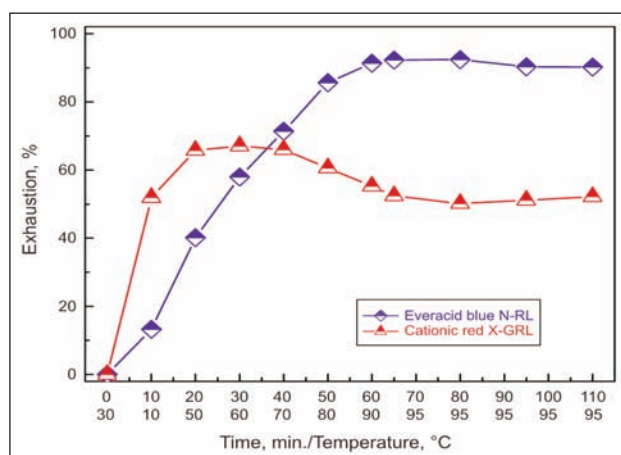


Fig. 6. Dyeing rates of acid and cationic dyes

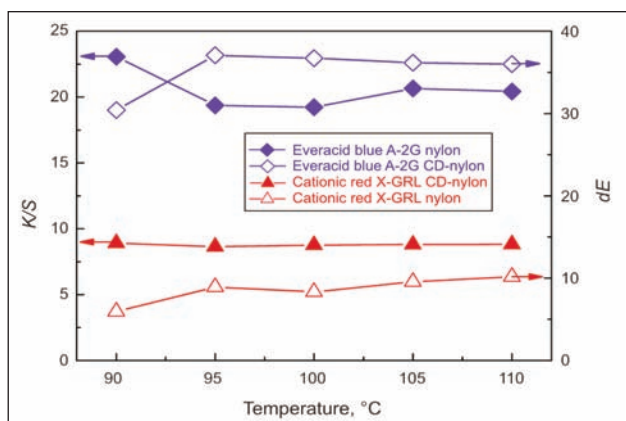


Fig. 5. Effect of temperature on the apparent colour depth and staining of nylon and CD-nylon

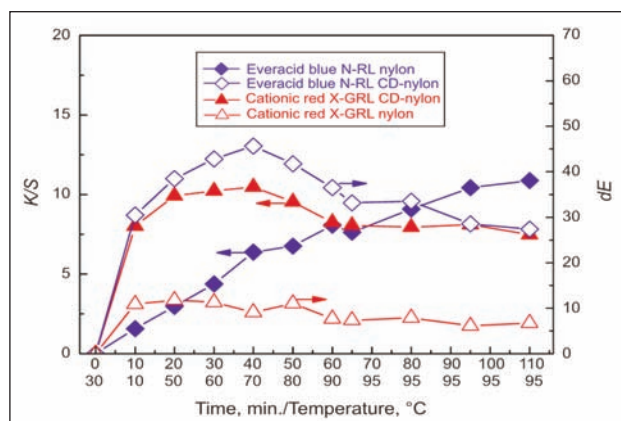


Fig. 7. Apparent colour depth and staining of nylon and CD-nylon at different times and temperatures

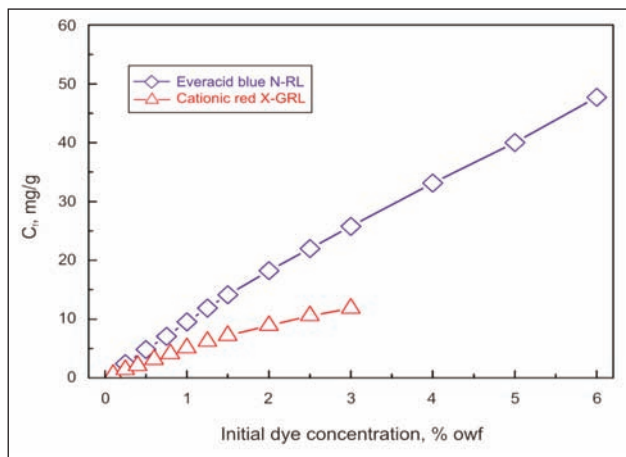


Fig. 8. Building-up properties of Everacid Blue N-RL and Cationic Red X-GRL

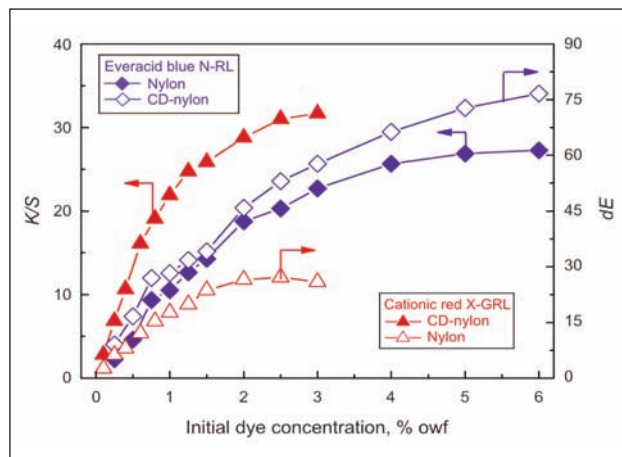


Fig. 9. Effect of initial dye concentrations on the apparent colour depth and staining of nylon and CD-nylon

Building-up properties of acid and cationic dyes

Everacid Blue N-RL and Cationic Red X-GRL were employed to evaluate the influence of the initial dye concentrations on the total amount of adsorbed dyes and the apparent colour depth of dyed nylon and CD-nylon fibres. As shown in figure 8 and figure 9, the adsorption quantities of two dyes linearly increased, and the apparent colour depth of the corresponding dyed nylon and CD-nylon also gradually increased with an increase in the initial concentrations of dyes in solution. This implies that the building-up properties of both acid and cationic dyes on the mixture are good.

However, from figure 9, it is worthwhile to note that the more serious staining of nylon by cationic dyes and that of CD-nylon by acid dyes were difficult to be avoided when the initial concentrations of acid and cationic dyes were high.

Staining of different acid and cationic dyes on the mixture

In order to discuss the staining properties of different acid and cationic dyes, ten acid dyes (1.2% owf initial concentration) and seven cationic dyes (0.8% owf initial concentration) were chosen to dye the mixture. From table 2 and table 3, it is evident that the exhaustion of dyes as well as the apparent colour depth and staining of nylon and CD-nylon varied according to dye categories. Table 2 shows that pre-metallised acid dyes exhibited higher exhaustion, and lower staining on CD-nylon than non-metallised acid dyes. This suggests that the dyeing of nylon with pre-metallised acid dyes can help to reduce the staining of CD-nylon when the dark shades are required. As shown in table 3, in comparison with the staining of acid dyes on CD-nylon, the staining of cationic dyes on nylon was relatively low although cationic dyes had low exhaustion. Overall, non-metallised acid dyes had the serious problem of staining.

Colour fastness of dyeings

All the dyed samples prepared for colour fastness tests were subjected to fixation treatment with syntan

(3% owf Mesitol NBS), and the testing results are given in table 4. For cationic dyes, the colour change in the washing process, and the colour fastness to wet rubbing and light were unsatisfactory; the adjacent fabrics were also stained - seriously by cationic

Table 2

EXHAUSTION AND STAINING OF TEN ACID DYES		
Dyes	Exhaustion, %	dE, staining of CD-nylon
<i>Non-metallised acid dyes</i>		
Everacid Yellow N-MR	90.71	33.06
Everacid Yellow N-3R	86.76	50.58
Everacid Orange N-G	65.33	63.81
Everacid Red N-RFL	97.40	17.46
Everacid Red N-B	84.32	37.16
Everacid Cyanine N-5R	92.06	50.11
Everacid Blue N-RL	94.52	30.33
<i>Pre-metallised acid dyes</i>		
Everset Yellow M-2R	96.81	26.24
Everset Red M-G	98.61	24.41
Everset Navy M-R	97.90	22.01

Table 3

EXHAUSTION AND STAINING OF SEVEN CATIONIC DYES		
Dyes	Exhaustion, %	dE, staining of nylon
Cationic Yellow X-5GL	56.10	19.39
Maxilon Red SL	28.80	17.29
Cationic Brilliant Red X-5GN	67.45	26.36
Cationic Pink X-FG	75.00	34.32
Cationic Red X-GRL	52.36	14.43
Cationic Red X-6B	77.84	39.21
Maxilon Blue SL	79.74	22.77

COLOUR FASTNESS OF ACID AND CATIONIC DYES ON NYLON/CD-NYLON MIXTURE										
Dyes	Washing							Rubbing		Light
	Colour change	Staining of adjacent						Dry	Wet	
		Wool	Acrylic	Polyester	Nylon	Cotton	Acetate			
<i>Acid dyes</i>										
Yellow N-3R	5	5	5	4	3	4-5	3-4	5	5	4-5
Red N-B	5	5	5	5	4	3-4	5	5	5	5
Cyanine N-5R	5	5	5	5	4	5	5	5	5	5
<i>Cationic dyes</i>										
Yellow X-5GL	3-4	3	4	4	2-3	2	2	5	4	3-4
Red X-GRL	3	3	3	3	2-3	2	2	5	3	2
Blue SL	3-4	3	3	3	3	2-3	3	5	3-4	3

dyes. The colour fastness of acid dyes on the mixture was better than that of cationic dyes. Therefore, the poor colour fastness would become a shortcoming of the dyed nylon/CD-nylon mixture, and should be improved through effective methods.

CONCLUSIONS

The main purpose of this work was to study the respective acidic and cationic dyeing properties of the nylon/CD-nylon mixture, and to provide the fundamental references for the practical one-bath dyeing of this mixture.

The pH dependence of the cationic dyeing of CD-nylon was less than that of the acid dyeing of nylon due to the existence of the strongly acidic sulphonate groups in CD-nylon. The strong ion-ion interaction between cationic dyes and negatively charged CD-nylon caused the dyeing rate of cationic dyes for CD-nylon faster than the acid dyeing of nylon. The

building-up properties of acid and cationic dyes on the mixture were both good. The high temperature dyeing resulted in a stiff hand of the mixture, indicating that it could not be used to cover the physical irregularities in nylon and CD-nylon. The staining of CD-nylon by non-metallised acid dyes was more serious than that by pre-metallised acid dyes, and that of nylon by cationic dyes.

According to the results obtained in this study, the reasonable pH control and dye selection are two important measures which should be taken for the purposes of reducing cross-staining. The poor colour fastness would be a shortcoming of the nylon/CD-nylon mixture dyed with cationic dyes and should be improved through effective methods.

ACKNOWLEDGEMENTS

This work was funded by the Priority Academic Program Development of Jiangsu Higher Education Institution (China).

BIBLIOGRAPHY

- [1] Joshi, H. D., Joshi, D. H., Patel, M. G., Naik, S. R. *Application of cationic dyes to anionically modified nylon and their performance evaluation with cationic dyeable polyester with special reference to fastness properties*. In: Colourage, 2008, issue 11, p. 71
- [2] Sun, Y. (E. I. du Pont de Nemours and Company). US 005662716A, 1997
- [3] Shore, J. *Blends dyeing*. In: Society of Dyers and Colourists, Bradford, 1998, p. 61
- [4] Jenkins, W. G. (Burlington Industries Inc.). US 005085667A, 1992
- [5] Sun, Y. (E. I. du Pont de Nemours and Company). US 006312805B1, 2001
- [6] Müller, H., Rossbach, V. *Dyeing of anionically-modified polyamide fibres with cationic dyestuffs*. Part I. *Uptake of the dyestuff and its binding*. In: Textile Research Journal, 1977, vol. 47, issue 1, p. 44
- [7] Huffman, A. M. (American Colour and Chemical Co.). US 4043749, 1977
- [8] Datye, K. V., Vaidya, A. A. *Chemical processing of synthetic fibres and blends*. In: John Wiley and Sons Inc., New York, 1984, p. 255

Authors:

PEI CHU
REN-CHENG TANG
National Engineering Laboratory for Modern Silk
College of Textile and Clothing Engineering
Soochow University

Suzhou 215123, P. R. China

Corresponding author:

REN-CHENG TANG
e-mail: tangrencheng@suda.edu.cn